EXPERIMENTAL AND NUMERICAL INVESTIGATION OF NATURAL CONVECTION HEAT TRANSFER OF SEMICIRCULAR-FINNED RADIAL HEAT SINK AT VARIOUS MOUNTING ANGLES

2024
PHD THESIS
MECHANICAL ENGINEERING

Yousif Hashim HUSSEIN

Thesis Advisors
Assist.Prof.Dr. Abdulrazzak Ahmed Saleh AKROOT
Prof. Dr. Tahseen Ahmad TAHSEEN

EXPERIMENTAL AND NUMERICAL INVESTIGATION OF NATURAL CONVECTION HEAT TRANSFER OF SEMICIRCULAR-FINNED RADIAL HEAT SINK AT VARIOUS MOUNTING ANGLES

Yousif Hashim HUSSEIN

Thesis Advisors
Assist. Prof. Dr. Abdulrazzak Ahmed Saleh AKROOT
Prof .Dr. Tahseen Ahmad TAHSEEN

T.C.
Karabük University
Institute of Graduate Programs
Department of Mechanical Engineering
Prepared as
PhD Thesis

KARABÜK
December 2024

I certify that in my opinion the thesis submitted by Yousef Hashim HUSSEİN titled "DESIGN AND NUMERICAL İNVESTIGATIONS OF NATURAL CONVECTION HEAT TRANSFER OF RADIAL HEAT SINK WITH SEMICIRCULAR FINS AT VARIOUS INSTALLATION ANGLES" is fully adequate in scope and in quality as a thesis for the degree of PhD

Assist. Prof. Dr. Abdulrazzak Ahmed Saleh AKROOT .....
Thesis Advisor, Department of Mechanical Engineering
Prof. Dr. Tahseen Ahmad TAHSEEN .....
CO- Advisor, Department of Mechanical Engineering of Iraq University of Kirkuk

This thesis has been accepted by the Examination Committee by unanimous vote in the Department of Mechanical Engineering as a PhD 27/12/2024

Examining Committee Members (Institutions) Signature

Chairman: Prof. Dr. Muhammet KAYFECİ (KBU) .....

Member: Prof. Dr. Mehmet OZKAYMAK (KBU) .....

Member: Prof. Dr. Kamil ARSLAN (KBU) .....

Member: Assist Prof. Dr. Saeed Abdullah ALQAED (NU) .....

Member: Assist. Prof. Dr. Ali CAN (KBU) .....

Member: Prof. Dr. Mustafa Wahby Kanbar JABER(KU) .....

Member: Assist. Prof. Dr. Abdulrazak A. Saleh AKROOT (KBU) .....

Member: Prof. Dr. Tahseen Ahmad TAHSEEN (KU) .....

The degree of PhD by the thesis submitted is approved by the Administrative Board of the Institute of Graduate Programs, Karabuk University

Assoc. Prof. Dr. Zeynep ÖZCAN .....

Director of the Institute of Graduate Programs

"I declare that all the information within this thesis has been gathered and presented in accordance with academic regulations and ethical principles and I have according to the requirements of these regulations and principles cited all those which do not originate in this work as well"

Yousif Hashim HUSSEIN

ABSTRACT

Phd. Thesis

EXPERIMENTAL AND NUMERICAL INVESTIGATION OF NATURAL CONVECTION HEAT TRANSFER OF SEMICIRCULAR-FINNED RADIAL HEAT SINK AT VARIOUS MOUNTING ANGLES

Yousif Hashim HUSSEIN

Karabük University
Institute of Graduate Programs
Department of Mechanical Engineering

Thesis Advisors:
Assist. Prof. Dr. Abdulrazzak Ahmed Saleh AKROOT
Prof. Dr. Tahseen Ahmad TAHSEEN
December 2024, 114 pages

The effect of fin shapes in heat sinks under free convection was investigated both numerically and experimentally. The thermofluid characteristics of semicircular fin heat sinks were analyzed using three-dimensional numerical simulations. Parametric studies were conducted to examine the effects of geometrical parameters, particularly orientation angles (0°, 15°, and 30°) and input heat rates. A structured, non-uniform computational mesh was employed, and numerical simulations were performed using ANSYS Fluent 2021R2, based on the Finite Volume Method (FVM). A 210-mm diameter semicircular fin was used in the CFD simulations. Experimentally, three heat sink models (SC-0, SC-40, and SC-50) were compared to identify the optimal reference model. The study investigated the impact of fin shape, fin number, and heat flow on thermal resistance and the overall heat transfer coefficient.

The parametric study applied a design of experiments (DOE) approach, including the design and execution of 18 experiments, empirical model analysis, and factor optimization. Optimization followed a general factorial design (GFD) framework, where factor ranges were coded between +1 and -1, with adjustments for unit variability across independent variables. Using GFD, regression analysis was applied to derive a new model, incorporating Nusselt number and thermal resistance. Experimental data from the literature on semicircular radial fins under natural convection were included. Key determinants for the best transfer function were R^2, adjusted R^2, predicted R^2, coefficient of variation (C.V.), and parameter proximity to optimal values.

Results showed that airflow velocity was higher at a 0° orientation angle. However, airflow parallel to the fins at this angle caused minimal obstruction, resulting in a heat transfer coefficient 3.9% to 7.3% lower than those at 15° and 30°, respectively. The Nusselt number was highest at the 30° orientation. Experimentally, the heat transfer coefficient increased by up to 30% between SC-0 and SC-40, and 27% between SC-0 and SC-50, while thermal resistance was 17% lower for SC-40 and 19% lower for SC-50 compared to SC. A larger number of fins enhanced heat dissipation under natural convection. CFD simulation results closely matched experimental data, with temperature differences within ±4.9%, indicating strong qualitative agreement.

DOE results revealed the best performance for the Nusselt number with R^2 (98.15%), predicted R^2 (97.08%), adjusted R^2 (94.87%), and C.V. (2.44%). For thermal resistance, the corresponding values were R^2 (97.91%), predicted R^2 (96.70%), adjusted R^2 (94.21%), and C.V. (3.33%). These findings demonstrate that the proposed model accurately predicts the performance of semicircular radial heat sinks and holds promise for future designs.

Keywords **:** Free convection, Vertical cylinder, Fins number, Semicircular fins, General factorial design, Design expert, Optimization. CFD

Science Code : 91439

ÖZET

Doktora Tezi

ÇEŞİTLİ MONTAJ AÇILARINDA YARIM DAİRESEL KANATLI RADYAL ISI EMİCİNİN DOĞAL KONVEKSİYON ISI TRANSFERİNİN DENEYSEL VE SAYISAL ARAŞTIRMASI

Yousif Hashim HUSSEIN

Karabük Üniversitesi
Lisansüstü Eğitim Enstitüsü
Makine Mühendisliği Anabilim Dalı

Tez Danışmanları:
Assist. Prof. Dr. Abdulrazzak Ahmed Saleh AKROOT
Prof. Dr. Tahseen Ahmad Tahseen
Aralık 2024, 114 sayfa

Kanatçık şeklinin serbest konveksiyon altındaki ısı alıcılar üzerindeki etkisi hem sayısal hem de deneysel olarak araştırılmıştır. Yarı dairesel kanatçık ısı alıcılarının termoakışkan özellikleri üç boyutlu sayısal simülasyonlar kullanılarak analiz edilmiştir. Parametrik çalışmalar, geometrik parametrelerin (özellikle yönlendirme açıları: 0°, 15° ve 30°) ve giriş ısı yüklerinin etkilerini incelemek amacıyla gerçekleştirilmiştir. Yapısal, gayri-uniform bir hesaplama ağı kullanılmış ve simülasyonlar Finite Volume Method (FVM) temel alınarak ANSYS Fluent 2021R2 yazılımında gerçekleştirilmiştir. Sayısal simülasyonlarda 210 mm çapında yarı dairesel bir kanatçık kullanılmıştır. Deneysel olarak, en iyi referans modelini belirlemek için üç farklı ısı alıcı modeli (SC-0, SC-40 ve SC-50) karşılaştırılmıştır.

Çalışmada, kanatçık şeklinin, sayısının ve ısı akışının termal direnç ve toplam ısı transfer katsayısı üzerindeki etkisi incelenmiştir.

Parametrik çalışma, deney tasarımı (DOE) yaklaşımını kullanarak 18 deneyin tasarımı ve uygulanması, ampirik model analizi ve faktör optimizasyonunu içermiştir. Optimizasyon, faktör aralıklarının +1 ve -1 arasında kodlandığı ve bağımsız değişkenlerin birimleri arasında değişkenlik olduğu genel faktöriyel tasarım (GFD) çerçevesinde gerçekleştirilmiştir. GFD kullanılarak, Nusselt sayısı ve termal direnç dahil edilmiş ve yeni bir model türetmek için regresyon analizi uygulanmıştır. Literatürdeki doğal konveksiyon altındaki yarı dairesel radyal kanatçıklarla ilgili deneysel veriler de çalışmaya dahil edilmiştir. En iyi transfer fonksiyonunu belirlemek için temel faktörler R^2, düzeltilmiş R^2, tahmin edilen R^2, değişim katsayısı (C.V.) ve parametrelerin optimum değerlere yakınlığıdır.

Sonuçlar, hava akış hızının 0° yönlendirme açısında daha yüksek olduğunu göstermiştir. Ancak bu açıda hava akışı kanatçıklara paralel hareket ettiğinden, kanatçıklardan minimum engelleme oluşmuş ve bu durum ısı transfer katsayısının 15° ve 30°'lik açılara göre sırasıyla %3,9 ila %7,3 daha düşük olmasına neden olmuştur. Nusselt sayısının en yüksek değeri 30° yönlendirme açısında gözlemlenmiştir. Deneysel olarak, ısı transfer katsayısının SC-0 ile SC-40 arasında %30'a, SC-0 ile SC-50 arasında ise %27'ye kadar arttığı belirlenmiştir. Ayrıca, SC-40 için termal direncin %17, SC-50 için ise %19 daha düşük olduğu görülmüştür. Daha fazla sayıda kanatçık, doğal konveksiyon altında daha etkili bir ısı dağılımı sağlamıştır. CFD simülasyon sonuçları ile deneysel veriler arasında ±%4,9 içinde bir sıcaklık farkı ile güçlü bir uyum gözlemlenmiştir.

DOE sonuçları, Nusselt sayısı için en iyi performansın R^2 (%98,15), tahmin edilen R^2 (%97,08), düzeltilmiş R^2 (%94,87) ve C.V. (%2,44) ile elde edildiğini göstermiştir. Termal direnç için ise karşılık gelen değerler R^2 (%97,91), tahmin edilen R^2 (%96,70), düzeltilmiş R^2 (%94,21) ve C.V. (%3,33) olarak bulunmuştur. Bu bulgular, önerilen modelin yarı dairesel radyal ısı alıcılarının performansını doğru bir şekilde tahmin ettiğini ve gelecekteki tasarımlar için umut vadettiğini göstermektedir.

Anahtar Kelimeler : Serbest konveksiyon, Dikey silindir, Kanatçık sayısı, Yarım dairesel kanatçıklar, Genel faktöriyel tasarım, Tasarım uzmanı, Optimizasyon. CFD.

Bilim Kodu **:** 91439

ACKNOWLEDGEMENT

To the one who planted the seeds of ambition in me, and watered me from the river of his sincere prayers, to the one who supported me on my path, to my dear father, may God protect him. To the fountain of tenderness, who spared no effort in supporting and encouraging me, to my beloved mother, may God prolong her life.

To my partner on the path, who was patient and understanding of all my busy moments, to my dear wife.

To my honorable professors, who were a light that illuminated the path of knowledge and learning for me.

To everyone who supported me and stood by my side in my academic career, I dedicate this humble work, hoping that God will make it a building block in the construction of knowledge and learning.

To those who were my best helpers and one hand in this world, my brothers and my support after Allah, who supported me and accompanied me throughout the period of study and gave everything they could to complete this work. I do not forget to pray and have mercy on my deceased brothers who waited for this day but Allah's mercy came before my study journey ended and Allah is the Most Merciful of the merciful. I also extend my gratitude to my country and my companion on the road, my beloved wife.

To my distinguished professors and teachers, Assistant Professor Dr. Abdul Razzaq Ahmed Saleh AKROOT and Professor Dr. Tahseen Ahmed TAHSEEN, who had a great role in educating me and providing advice, guidance, and opinions throughout the study period and scientific advice and are my best reference. I also thank the Head of the Department of Mechanical Engineering, Prof. Dr. Engin GEDİK.

I also dedicate my accomplishments to my beloved homeland of Iraq, my supervisor's country, and my second country, Yemen, to all those who helped and encouraged me. I also extend my sincere thanks to both my university, Kirkuk University, as well as my university, which opened the doors of study for me and embraced me with all love and high appreciation, Karabuk University, represented by its country that hosted me throughout my study period, the sisterly Republic of Turkey.

CONTENTS

Page

Page

Page

LIST OF FIGURE

Page

Page

Page

LIST OF TABLES

Page

SYMBOLS AND ABBREVITIONS INDEX

SYMBOL

A- : Area-m^2

c_p- : Specific Heat Capacity-j/(kg K)

R- : Fin Radius-m

D- : Cylinder Diameter-m

G- : Gravitational Constant-m/s^2

H- : Heat Transfer Coefficient -w/m^2k

$\dot{Q}$- : Heat Flux-W/m

k- : Thermal Conductivity-w/(mk)

L- : Fin Length-m

I- : Current-A

M- : Mass-kg

N- : Number Of Holes--

N- : Fins Number--

Q- : İnput Heat-W

R_{th}- : Thermal Resistance-k/w

t- : Fin Thickness-m

T- : Temperature-℃

NONDIMENSIONAL SYMBOLS

El- : Elenbaas--

Ra- : Rayleigh Number--

Nu- : Nusselt Number--

GREEK SYMBOLS

α- : Thermal Diffusivity-m^2/s

β- : Expansion Coefficient-1/k

Ɛ- : Emissivity

μ- : Dynamic Viscosity-Kg/(ms)

ν- : Kinematic Viscosity-m^2/s

ρ- : Density-Kg/m^3

σ- : Stefan-Boltzmann Constant $5.670*10^{-8}$-w/m^2k^4

ϕ- : İnput Voltage-V

Al- : Aluminum--

B- : Fin Base--

Act.- : Actual--

φ- : Air--

∞- : Ambient --

CHAPTER ONE

INTRODUCTION

1.1. GENERAL

The development of fins as an adaptation during the Jurassic period, approximately 150 million years ago, constituted a significant evolutionary milestone. The Stegosaurus is notable for its unique characteristic: two rows of parallel bony plates extending along its back. Initially, these bony plates were believed to serve as armor for predator protection; however, current findings suggest their potential role as heat-dissipating fins. Researchers have discovered evidence indicating that substantial volumes of blood traversed these structures. This circular pattern indicates a function that extends beyond just protection. The plates may have operated similarly to a vehicle's radiator. This analogy depicts the heart as a pump that circulates blood via the veins within the plates, while the plates function to disperse heat, ing in the regulation of the blood's temperature. This recent study underscores the intricacy of dinosaur physiology and demonstrates that evolution is a remarkable mechanism for creatures to adapt to their surroundings.[1].

Thermal dissipation using expanded surfaces and fins is frequently used to improve heat conduction between a solid surface and another fluid, such as water or air. Fins augment the surface area available for heat transfer, facilitating more efficient cooling or heating as required by the situation. This technique is extensively employed in numerous engineering applications, such as heat exchangers, radiators, and electronic cooling systems. The use of fins for temperature management in biological systems, as exemplified by the plates of the Stegosaurus, illustrates how nature frequently adopts analogous tactics for thermal control [2].

Extended surfaces are utilized to enhance heat transfer rates, reduce temperature gradients, and optimize the efficiency of industrial heat exchangers, electronics, and various systems and devices, including electrical appliances [3]. Heat transfer by natural convection is considered a critical concern due to its extensive applications across various domains. Despite the absence of applied force or velocity to generate this load, the effects of buoyant force induce the formation of natural convection currents within the fluid. Natural convection is essential for the proper functioning and construction of systems that employ multiple heat transfer processes. This significantly influences heat transfer rates and operational expenses, rendering forced convection generally advantageous. [4].

Figure 1.1. The picture shows the fins of a Stegosaurus dinosaur for cooling purpos.[1].

Radiating surfaces with tubular sheets and radially annular fins were standard design elements for spacecraft heat dissipation systems starting in the early 1960s. The finned heat sink has demonstrated efficacy in dispersing heat from electronic systems over the last three decades, guaranteeing steady performance even in the face of substantial heat generation. As extended surface technology advances, novel design concepts emerge, including porous media-based fins and distinctive composites, as well as slotted plates [5, 6].

A multitude of engineering specialties is increasingly focused on energy conversions, necessitating rapid heat transport. The need for heat transfer materials that perform

better while being suitably scaled, weighted, economical, and shaped is therefore increasing. The transfer of heat between sources and sinks is enhanced by employing basic forms and materials in the planning and building of heat transfer devices, including cylinders, fluid-exposed tubes, and plates. They provide renowned surfaces for thermal absorption or dissipation, termed prime surfaces. Increasing the number of surfaces enhances the surface area, lowering the issue of high load resistance between the fluid surrounding the base surface and the base surface, which helps to lower the neighboring fluid's total heat transfer coefficient about the base surface [7].

The Direct Simulation Monte Carlo (DSMC) algorithm was used in order to understand fluid dynamics and gas transport in porous microchannels. We have shown that up to 40% porosity in DSMC can be used to simulate porous medium. The researcher in this work distributed circular barriers randomly across the microchannel to generate the porous geometry and guarantee that there was no interference between the obstacles. to investigate how apparent permeability is affected by form, permeability, and gas type. The impacts of porosity, solid particle diameter, and specific surface area are also taken into account in this study. The findings showed that an increase in Knudsen numbers causes a drop in torsion because of flow slippage at the solid-material interfaces, but a decrease in porosity increases torsion in the forward flow field. Additionally, the study showed that slippage and perceived gas permeability are affected by using two different gas kinds. [8].

1.2. HEAT TRANSFER THROUGH EXTENDED SURFACES

To maintain extended surfaces within an acceptable temperature range, the heat transfer through the contacting coolant must be optimized. Extended surfaces are extensively utilized across numerous industrial applications. This pertains to the processes and their behavior in diverse thermal environments, namely as a component of high-efficiency heat transfer across extended surfaces. The surface area of heat transfer systems can be augmented by employing fins or extended roof fins. A variety of fin configurations are commonly utilized, including loop, wedge, triangular, flat-wall, and straight (rectangular) fins. These ubiquitous components are utilized in several applications, including aerospace, aviation, and terrestrial vehicles. A

multitude of further uses encompasses gas turbines, convection ovens, electrical and electronic refrigeration, and chemical processes, among others. Toroidal fins are commonly used in heat exchanger tubes for fluid cooling, whereas straight fins are commonly used to enhance cooling in electrical transformers and automotive engines. Heat exchangers consist of many tubes equipped with fins and fans that circulate a substantial volume of air through the fins to dissipate heat from the tubes containing the heated fluidThe fins significantly expand the surface area for heat transfer, which positively affects the overall efficiency of the cooling process. Additional factors, such as fluid properties, production expenses, and ambient air circulation, influence the optimal design of finned tube heat exchangers. Each fin possesses a primary surface utilized for heat absorption or dissipation; these surfaces are augmented by appendages that are intricately linked, such as metal bands or grooves within the tube. Extended surfaces or fins in engineering applications are frequently employed to improve the transfer of heat from surfaces to the cooling waters that come into contact with them, keeping the surfaces at an acceptable temperature. Heat exchangers in large industrial systems and transistors, along with other electronic components, are merely two instances of these applications. Historically, heat exchangers, compressors, control systems, and internal combustion engines have included radial fins, commonly known as toroidal or round fins [9].

1.3. IMPROVE HEAT TRANSFER

From a thermal engineering point of view, thermal systems should be properly sized and equipped to generate and discharge the required amount of heat. The safe operation of thermal units depends on several variables, including the heating or cooling of system components and barriers. The heat generated in electrical systems can cause problems such as burning and overheating, potentially damaging components, raising costs, and diminishing their lifespan. Consequently, in several applications, heat dissipation analysis and testing must focus on providing an efficient cooling system that minimizes the risk of machinery overheating to the maximum extent possible [10]. Thermal systems that are poorly designed frequently overheat surfaces that fail to dissipate the requisite amount of excess heat, resulting in permanent overheating and detrimental effects on the system. A requisite amount of heat must be efficiently

dissipated from these surfaces to avert adverse consequences of overheating. Heat transfer performance can typically be improved by the following methods [11, 12]:

1.4. HEAT SINK

The buoyancy effects alone are often inadequate for modern electronic circuits to cool components by the density of the convection approach. Therefore, engineering design, such as the implementation of heat sinks, is necessary to improve heat transfer.Therefore, the heat sink has a lower thermal resistance, allowing it to halve the surface area needed to dissipate heat to the environment. In terms of terminology, "a device or equipment for dissipating heat from the surface of hot air" refers to a textural dissipator, while the cooling element or medium represents the recipient of the generated heat. The air-solid interface constitutes the primary impediment to heat dissipation, as heat transfer across this boundary is frequently the least efficient within the system regarding the interaction between the solid surface and cooled air. Heat sinks primarily reduce this barrier by augmenting the contact area with the cooling water. This can reduce the operational temperature of the gadget by facilitating greater heat dissipation. Heat sinks are mostly employed to keep a device's temperature beneath the manufacturer's specified maximum limit.

Heat sinks increase the surface area for heat transfer from a semiconductor device to the cooling medium, often air, and are affixed directly to the device's housing. Heat sinks use a variety of types of fins increase the area of the surface that can be used to transport heat [13]. Numerous factors influencing both heat sinks and the entire system performance must be considered when choosing a suitable heat sink which meets the necessary thermal criteria.

The allowable thermal budget of the heat sink and adjacent environmental variables significantly influence the selection of the heat sink type. A heat sink's resistance to heat changes according to external cooling conditions and cannot be considered a fixed value. Airflow must be classified as normal heat transmission, mixed low flow, or high flow heat transfer when choosing a heat sink. Natural convection is what happens when there is no local flow in the system and heat transfer is solely dependent on the

buoyancy effect of the air surrounding the heat sink. Forced convection occurs when airflow is generated mechanically, typically by a fan or blower. The disparity in flow velocity between forced convection and mixed flow is, nonetheless, not readily apparent [14]. While natural convection is cost-effective and remarkably simple to implement, it is typically restricted to low-power applications. Moreover, forced convection requires a greater volumetric flow rate than natural convection; however, it incurs higher costs. Liquid-cooled heat sinks are the most costly and provide superior thermal performance per unit volume.

1.5.THE FIN SHAPE

Fins can be strategically placed on a surface, and their surface area can be augmented to significantly enhance the dissipation of collected heat. These fins exhibit many geometric configurations. Figure 1.2 illustrates a range of fin configurations. The elongated surfaces of straight rectangular fins are affixed to flat walls. The cross-sectional area may be either constant or variable, contingent upon the fin's length. Plate fin surfaces exhibit several configurations, including regular, strip, wave, wedge, and ring, with the fins circumferentially affixed to a cylinder or tube, and their cross-sectional area varying with the cylinder's radius from its centerline. Wedge fins are elongated structures characterized by consistent or inconsistent cross-sectional areas and circular profiles

The optimal fin design has been the subject of extensive investigation, including rectangular, triangular, wedge-shaped, wavy, and serrated designs. Some studies rely on the ideal partitioning of certain fin dimensions, based on the premise that the total volume of fin material remains unchanged. Fins can be made by removing material from the fin body to create slots, grooves, holes, and cavities that increase the coefficient of thermal transfer and effective thermal transfer area. Fins are generally located in arrays or clusters rather than in isolation. Radiation and convection transfer heat from these groupings to the ambient air. Nonetheless, fin design can always be enhanced based on many considerations, as discussed in the subsequent sections [16].

- Temperature distribution on the collector base and along the fin.

- The geometric configuration of fins.
- Airflow velocity.
- Direction of fin assembly.

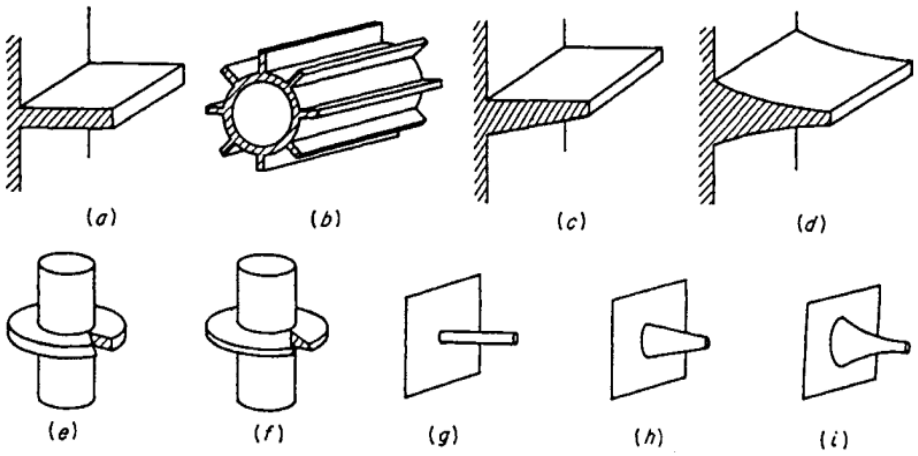

Figure 1.2. The figure shows several common examples of extended fin surfaces that can be arranged in different directions [15].

1.6. DESIGN OF THE FIN

The surface area of an object is a characteristic that influences the heat transfer coefficient to an adjacent fluid. In engineering, it is standard procedure to augment the surface area to enhance the coefficient of heat transfer between the object and the surrounding fluid. An example is the utilization of fins as auxiliary components to enhance heat dissipation due to the transmitter's substantial electrical consumption [17].

Specific formulas must be employed for each type of fin in heat exchange systems linked to extended surfaces. These represent simplified formulations of general heat transfer equations, each incorporating various boundary conditions. The fin design requires further development and is contingent upon various factors that must be taken into account, including the following [18]:

Fins functioning as extension surfaces augment the weight, dimensions, and manufacturing expenses of a system. Consequently, recent endeavors have focused on optimizing fin geometry, a process that necessitates advanced technology and efficient heat transfer systems. There exist two categories of heat transfer optimization processes: inefficient and active [19].

In order to improve or speed up the heat transfer process, active methods need an external energy or power source, whereas passive ones don't. Fins are a common example of a passive technique that is employed in many industrial applications to enhance heat transfer from the base surface and the surrounding fluid [20].

Fins are becoming prevalent as heat transfer enhancement devices due to advancements in extended surface technology, with innovative designs emerging, including hanging panels, porous media, fins composed of different materials, and perforated fins. A multitude of inquiries and studies have been conducted to improve fin geometry. To improve the heat transfer coefficient and area, additional research has modified the fin body design by using slots, cavities, holes, grooves, and channels [15].

1.7. RADIAL FINS AND MODERN APPLICATIONS

Radial fins are used in a variety of applications in modern engineering to enhance heat dissipation efficiency. They are characterized by a layout emanating from a center point that extends outward. Computer central processing units and graphics processing units are two examples of electrical devices that employ cooling systems. Radial fin heat sinks enhance the surface area available for convective heat transfer, resulting in superior thermal performance. Efficient cooling is essential to maintain electrical equipment at optimal temperatures and to avert overheating-related problems [22, 23].

Light-emitting diodes (LEDs) are prevalent in contemporary use. These are semiconductor light sources that emit light of a specific wavelength when a forward voltage is supplied to a p-n junction. LEDs possess an extended lifespan, function at elevated power levels, and exhibit commendable energy efficiency [24]. This lighting

technology is always evolving. LEDs are employed across various industries because to their safety and availability in multiple colors. They also lack any deleterious substances, including mercury. The industry has significantly expanded recently due to increased energy-efficient lighting and decreased electricity use. Nonetheless, these lamps emit heat after utilizing approximately 70% of their total energy [25].

To satisfy the escalating thermal performance demands of LEDs, The size and weight of heat sinks are increasing, hence jeopardizing the integrity of lighting devices and elevating production costs. Consequently, techniques are necessary to enhance heat sink efficiency while reducing heat sink mass [26, 27]. Radial heat sinks are the optimal choice since LEDs are often round. Figure 1.3 depicts several commercial LED variations.

The field of automotive engineering has an additional important application. Radial fins are used in the design of heat exchange mechanisms, such as radiators and oil coolers, to improve the overall efficiency of the heat transfer process [28]. The radial shape increases the fins' surface area exposed to airflow, enhancing the cooling of engine and gearbox fluids [29]. Extending the longevity and efficacy of vehicle systems is particularly crucial. Additionally, radial fins enhance the energy efficiency of solar collectors [30]. Manufacturers can enhance the surface area for solar radiation absorption on solar collectors by using radial fins. This enhances heat absorption and transfer in several solar thermal applications [31].

Radial fins enhance the efficiency of industrial heat exchangers in the heat transfer process. Radial fins are extensively utilized in various applications, including air conditioners and chemical processing facilities, highlighting their adaptability and importance in improving thermal management.

Figure 1.3. Three instances: radial and rectangular fins [28].

1.8. STUDY OBJECTİVES

This study aims to design a new heat sink with semicircular fins of different shapes, as in the design described in Chapter 3 (SC-0 SC-40 SC-50). This design can contribute to enhancing the heat dissipation process through natural convection. The main objectives of this study are:

- To investigate how the unique fin geometry affects the heat transfer coefficient
- To investigate the effect of several properties, geometric parameters, fin number and Rayleigh number on the thermal transfer coefficient. It is also analyzed using Design-Expert-v.11 software (DOE).
- To develop a mathematical model that accurately describes the heat transfer characteristics of a semicircular fin heat sink The equation will consider not only the Rayleigh number, but also the variation of geometric properties such as fin length, thickness, and height. Theoretical studies are also carried out using the program (ANSYS FLUENT 2021R2) to compare the experimental and theoretical results.

CHAPTER TWO

LITERATURE REVIEW

2.1. INTRODUCTION

The majority of engineering systems generate heat during operation. For equipment to operate efficiently and prevent overheating or, in the worst cases, system failure, system heat control is crucial. Prior research on heat transfer through free convection from the fin surface has concentrated on modeling the fin surface and resolving the energy, momentum, and continuity governing equations (Lienhard et al. [32]).

By improving the transfer of heat, radial fins are crucial for raising energy efficiency and encouraging environmentally friendly industrial practices, both of which help to meet the Sustainable Development Goals (SDGs). They are frequently used to efficiently control heat dissipation in devices including electronic cooling systems, LED lights, and heat exchangers. Developing more sustainable and effective cooling solutions can be aided by examining the performance, composition, and design of radial fins in different conditions (M. Arqam et al [33]).

$$Nu = \frac{1}{24} Ra^{*} \left[1 - e^{\left(\frac{-35}{Ra^{*}}\right)}\right]^{0.75} \quad (2\text{-}1)$$

In electronic systems, heat sinks are passive components used to dissipate heat from devices into the surrounding air, helping to cool high-power semiconductors and optoelectronic devices, such as lasers and light-emitting diodes (LEDs). LED lamps, in particular, have gained significant attention in the lighting industry due to their low power consumption, long lifespan, compact size, and robust construction compared to other lighting sources. However, LEDs face thermal management challenges, as approximately 70% of the energy they consume is emitted as heat (Hussein et al [34]).

To address this issue, the design of efficient heat sinks is crucial. Natural convection heat sinks are particularly suitable for LED lighting due to their inherent advantages, including simplicity and reliability. However, a common mismatch arises while most natural convection heat sinks have a rectangular base, LED lighting systems typically have a circular shape. This discrepancy necessitates innovative design approaches to ensure optimal thermal performance (M. Bdaiwi et al [35]). Furthermore, electronic systems' highly efficient thermal management is essential to reduce greenhouse gas emissions and enhance overall system efficiency (J.B. Khaleel et al [36]. Since lighting accounts for 20% of global electrical energy consumption (Almeida et al [37]), replacing conventional lighting with more energy-efficient alternatives is crucial. Light-emitting diodes (LEDs) have gained significant traction in electronics due to their superior luminous efficiency. However, a major challenge arises from LEDs converting approximately 70% of their total energy into heat, presenting a thermal management issue (Elenbaas et al [38]; Schuepp [39] . While radial fins significantly improve heat transfer, challenges remain in tailoring their design for specific applications. Further research is essential to address these challenges, striking a balance between material usage, cost, and performance to advance sustainable and efficient cooling technologies in alignment with the SDGs (Ojuro et al [40]; M.H. Mousa et al [41]).

2.2. COMPREHENSIVE REVIEW

If the heat generated by LEDs is not effectively dissipated, it will negatively impact both their performance and lifespan. Therefore, despite the numerous advantages of LED lighting, addressing the issue of heat dissipation is crucial for successful market adoption. Natural convection heat sinks have been identified as a suitable solution for this purpose (Lee et al [42]; Assaf et al [43]). Since natural convection does not require additional equipment, it has been recommended as an efficient method for cooling LED lighting systems (Karimi et al [44]). However, if the heat sink is not properly designed, LEDs can reach excessive temperatures, reducing their lifespan (Xiang et al [45]). Furthermore, the angle at which LED lighting is mounted differs based on its application and location, which significantly influences the effectiveness of natural convection cooling. Consequently, it is crucial to assess the impact of system

orientation on gravity on the cooling performance of a heat sink (Chiang et al [46]).Tahseen et al. [47] reviewed plain fin-and-tube heat exchangers and compared their thermal-hydraulic performance to that of un-finned tube banks. Wiriyasart and Naphon [48] investigated the effects of three fin designs-rectangular, conical, and circular-employing both statistical and experimental methods. Tang et al. [49] conducted an experimental investigation into the hydrothermal performance of heat sinks featuring conical fins, revealing that circular fins exhibited enhanced thermal performance relative to alternative fin geometries. The investigation also examined how parameters of conical geometry, including the conical angle and base diameter, influenced the Nusselt number. The results demonstrated that conical heat sinks exhibited superior hydrothermal performance compared to conventional smooth plate heat sinks. Additionally, a correlation was proposed to predict the radial heat sink's average Nusselt number, which can be expressed as follows (Elshafei [50]):

$$Nu = 0.195(Ra^*)^{0.263}\left(\frac{nb_{avg}}{H}\right)^{1.35}\left(\frac{r_o}{L}\right)^{0.444}\left(\frac{r_o}{b_{avg}}\right)^{-0.142}\left(\frac{r_o}{H}\right)^{-1.4} \quad (2\text{-}2)$$

Where:

$$Ra^* = \frac{\rho^2 g\beta C_P \pi(r_o^2 - r_i^2)\dot{q}L^3}{\mu L k^2}$$

$$b_{avg} = \frac{1}{2}\left\{\left(\frac{2\pi r_o}{n} - t\right) + \left(2\pi\frac{(r_o - L)}{n} - t\right)\right\}$$

Within the following bounds and with an error rate of less than 10%, the expected values from this equation match the theoretical values:

$$\mathrm{t} = 2\ \mathrm{mm}, 20 \le \mathrm{n} \le 26, 21.3\mathrm{mm} \le \mathrm{H} \le 63.9\mathrm{mm}, 75\mathrm{mm} \le \mathrm{r_o} \le 102\mathrm{mm}$$

$$40\mathrm{mm} \le \mathrm{L} \le 80\mathrm{mm},\ \ 300\mathrm{W/m^2} \le \dot{\mathrm{q}} \le 1100\mathrm{W/m^2}$$

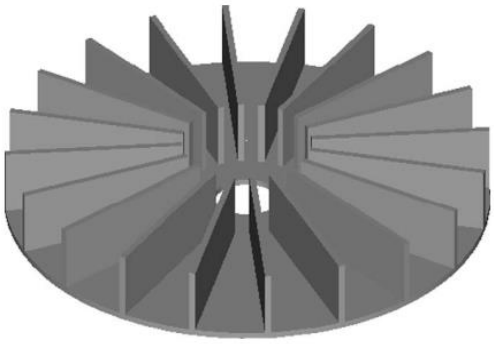

Figure 2.1. The radial heat sink's rectangular fins and circular base [50].

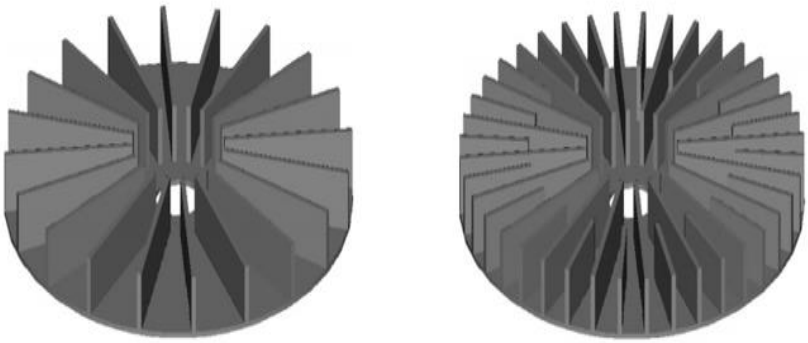

Figure 2.2. Fins used in the investigation and their configuration [50].

An optimal radial heat sink design has been proposed by researchers (see Figure 2.3) that decreases bulk by more than 30% while maintaining cooling efficiency comparable to the finned heat sink (Yu et al. [51]).

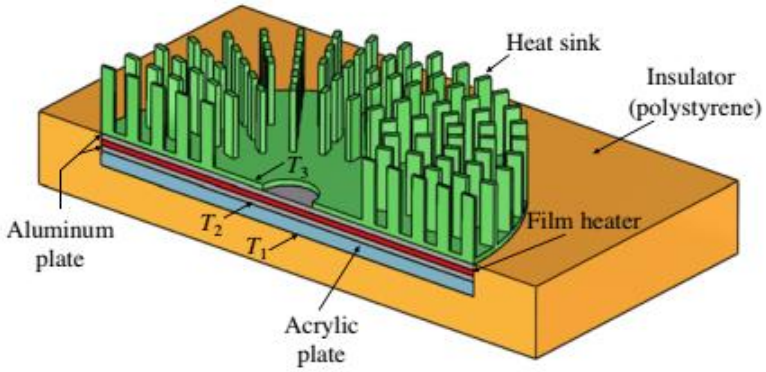

Figure 2.3. Pin-fin radial heat sink experimental setup diagram [51].

Freegah et al [52] performed a quantitative analysis examining the impact of incorporating semicircular pins into plate fins arranged in both orthogonal and parallel orientations. These pins were made from material removed from the base of the fins. The study revealed that heat sinks with vertically oriented semicircular hollow pins exposed to shock flow exhibited the best thermal performance when compared to other configurations. Tahseen and Mohamed [53] performed experiments to investigate the impact of novel fin designs on the thermal performance of a circular-base radial heat sink under free convection. Heat inputs ranging from 136 to 808 W were tested, focusing on fin shape, number, and heat flow. Results indicate that increasing the number of fins from 8 to 16 and 24 enhanced Nusselt numbers by 22% and 88%, respectively, at higher heat inputs. A greater number of fins proved more effective for heat dissipation.

Heat transmission was measured in studies by Kim and Kim [54] at different fin heights, fin angles, and cylinder wall temperatures. Finding the heat transfer coefficient between the finned cylinder and the ambient air was the main goal of these studies. According to the findings, a vertically finned cylinder with forked fins was 20% less heat resistant than a standard vertically finned cylinder. Furthermore, for each unit of fin volume, the forked finned cylinder's heat resistance decreased by 40%. Additionally, the study found a link between the Nusselt number and the computed thermal resistance. The experimental data's margin of error revealed a correlation of 0.05%. A numerical investigation of free convection in heat sinks composed of different aluminum alloys was carried out by Nazzal et al. [55].

The thermal and fluid characteristics of airflow in an in-line flat tube bundle were quantitatively examined by Tahseen et al. [56]. They made predictions about the pressure drop and heat transfer coefficient using the neuro-fuzzy inference system (ANFIS) model. For Reynolds numbers between 10 and 320, they looked at longitudinal pitches of 3, 4, and 6 as well as transverse pitches between 1.5 and 4.5 (interval 1.0). The results, which were displayed as temperature contours, streamlines, dimensionless pressure drop, and average Nusselt number, revealed an average difference between the ANFIS and numerical forecasts of 2.97% for the pressure drop and 1.9% for the Nusselt number.

Nano-enhanced PCMs (NePCMs) address this limitation by improving thermal conductivity, reducing system temperatures, and extending device operating times. This study experimentally analyzed three heat sink configurations-simple (SHS), square pin-fin (SpfHS), and Cu foam integrated (CufmHS)-using NePCMs with alumina nanoparticles (0.15, 0.20, 0.25 wt%) under heat flux conditions ranging from 0.98 to 2.94 kW/m². The CufmHS demonstrated superior performance, reducing base temperature by 36.95% and increasing working time by 288%. NePCMs are highly effective for electronic cooling applications (Zahid et al [57]). Thermal error critically affects the machining accuracy of gear-grinding machine tools, necessitating effective control. A novel method was introduced to directly cool the moving heat source, replacing the conventional hollow screw cooling system. A multi-objective topology optimization approach was employed to design a new cooling element. The optimized channel offered significantly improved heat transfer and reduced pressure drop by 2–3 times compared to traditional serpentine channels. Integrating this cooling element reduced the moving nut's temperature rise by over 3 K, decreased the screw shaft's thermal elongation by 10%, enhanced repetitive positioning accuracy by 29.03% to 92.59%, and improved grinding accuracy by approximately 65% (Yang et al [58]). The solar-powered thermoelectric refrigerator (SPTR) uses solar energy for cooling, with its performance influenced by solar insolation and a dual-axis solar tracking system (STS) that optimizes energy capture (Qamar et al [59]) . (see Figure 2.4).

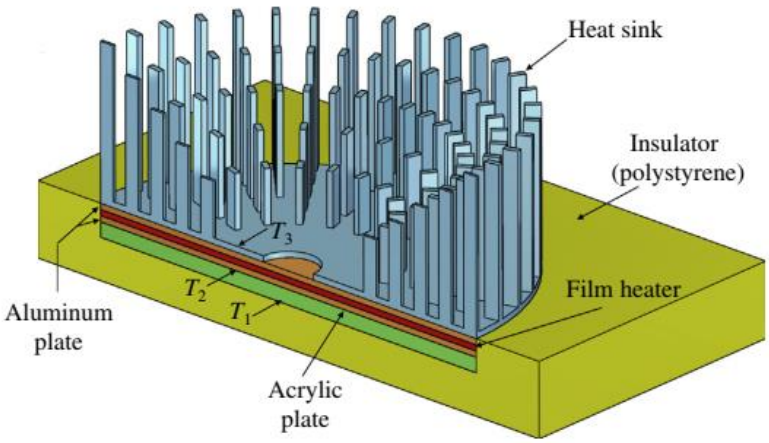

Figure 2.4. Platform schematic for the experiment.[60]

Selecting specific dimensions and orientation angles for heat sinks in free convection is critical for optimizing thermal performance. Studies show that varying these parameters significantly affects heat transfer efficiency, which is vital for ensuring the operational stability of electronic devices (Kurkute et al [61]). Studies have examined orientations from 0^o to 90^o, showing that vertical positions typically achieve better thermal performance due to enhanced natural convection currents (Baldry et al [62]). Increasing the angle from horizontal to vertical significantly raises the Nusselt number, indicating improved heat transfer rates. While optimizing dimensions and angles enhances performance, it is crucial to consider the specific application and device constraints. Excessive modifications can result in diminishing returns or increased manufacturing complexity (Elsaid et al [63]). The study focuses on a heat sink with vertically oriented semicircular fins operating under natural convection. Aluminum alloy 195 was chosen as the cooling material due to its excellent thermal conductivity.

In free convection studies, selecting inlet velocities and applied heat flux is vital for understanding thermal performance, especially in applications like electronic cooling. These parameters impact heat transfer rates and fluid dynamics, which are key to optimizing cooling systems (Almuzaiqer et al [64]). Inlet velocities influence the thermal boundary layer thickness, a key factor in free convection scenarios (Daghab et al [65]). Lee and Kim [66] conducted an analytical and experimental analysis. The applied heat flux sets the temperature gradient, which drives buoyancy forces responsible for fluid motion in free convection.

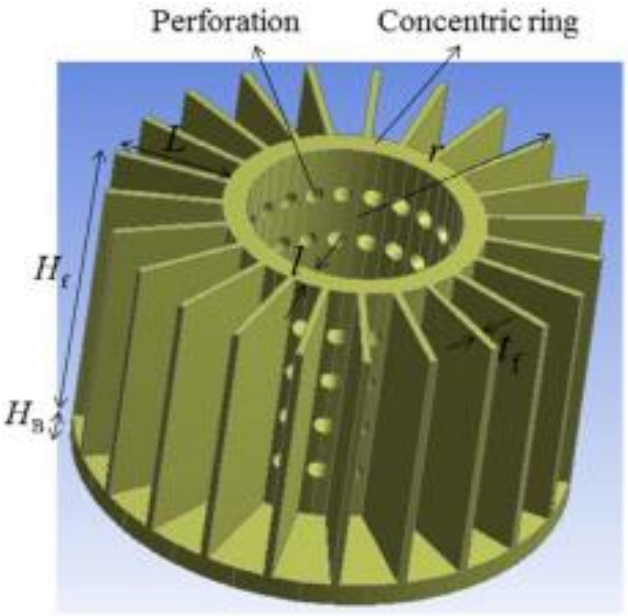

Figure 2.5. Radial heat sink with four holes [67].

$$n_{opt} = 1.24\left(\frac{r_r}{H}\right)^{0.3}\left(\frac{L}{H}\right)^{0.3}\left(P^*_{pumo}\right)^{0.2} \quad (2\text{-}3)$$

$$L_{opt}/L = 0.0878\left(\frac{r_r}{H}\right)^{0.3}\left(\frac{L}{H}\right)^{-0.45}(k^*)^{-0.4} \quad (2\text{-}4)$$

where

$$P^*_{pumo} = \frac{P_{pump}}{\mu^3\rho^{-2}H^{-1}} \quad (2\text{-}5)$$

$$k^* = \frac{k_s}{k_a} \quad (2\text{-}6)$$

Where:

H: is the fin height.

L: is the fin length.

r_r: is the radius of the rigid cylinder.

The impacts of various fin forms as well as rectangular plate fins (Figure 2.7), on overall thermal/fluid performance were investigated by (Khan et al. [68]). The dimensionless entropy production rate was formulated using several dimensionless variables, including the drag coefficient, Reynolds number, Nusselt number, and aspect ratio. A few chosen fin shapes' heat transfers, fluid friction, and minimal entropy production rate were investigated about several variables, such as the Reynolds

number, axial ratio, and aspect ratio. The findings show how important these factors are for the desired fin profile.

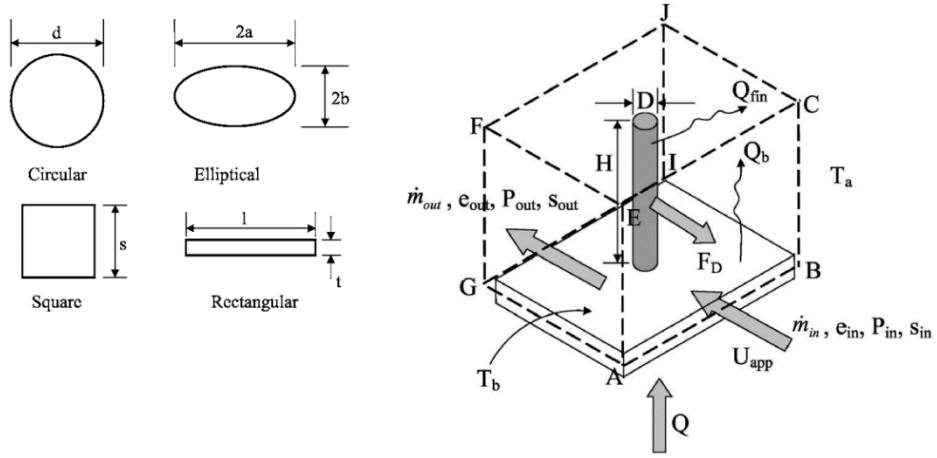

Figure 2.6. Rectangular plate fins, elliptical pin fins, square fins, and round fins [69].

Changes in heat flux can alter flow patterns and heat transfer rates, affecting the overall thermal performance of systems such as electronic devices. While these parameters are essential for optimizing cooling, they can also add complexity to system design, necessitating careful consideration of trade-offs between efficiency and operational stability (Sundar et al [70]).

The cooling potential of a radial heat sink with triangular fins mounted on a circular base was investigated theoretically and practically by (Kwak et al. [71]). Free convection circumstances with varying inclination degrees were used for the study. The researchers discovered that the heat resistance was affected by the circular base diameter, inclination angle, fin density factor, finning factor, and Rayleigh number. They discovered that there was good agreement between theoretical and experimental studies. The researchers developed a correlation equation to ascertain the degree of cooling performance enhancement. According to (Kwak et al. [72]), this formula can be used to calculate heat sinks' thermal resistance for LED lighting even if fins aren't present. With a mean error ratio of less than 10% and a maximum error ratio of 11.8%, the data obtained from the equation showed good agreement with numerical results.

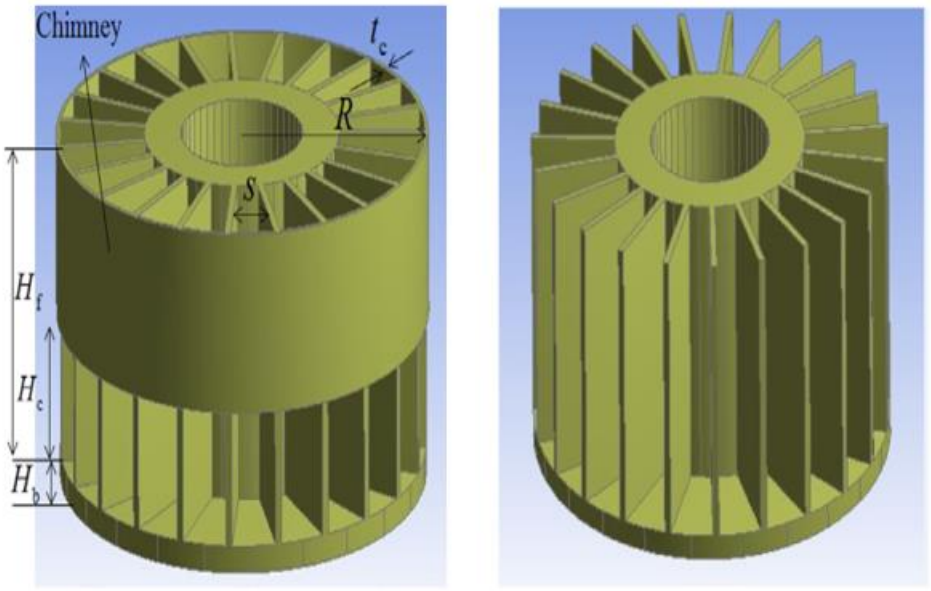

(a) (b)

Figure 2.7. Heat sink diagrammatic depiction (a) with and (b) without [73].

Three relationships pressure drop, average Nusselt number, and heat sink efficiency are used to determine the ideal number and thickness of heat sink fins under different pump power levels. These relations serve as a reference for designing radially coupled plates and fin heat sinks. Therefore, engineers can use these equations as a tool to design heat sinks that are optimized and have higher thermal performance under a variety of operating conditions (El Ghandouri [74]).

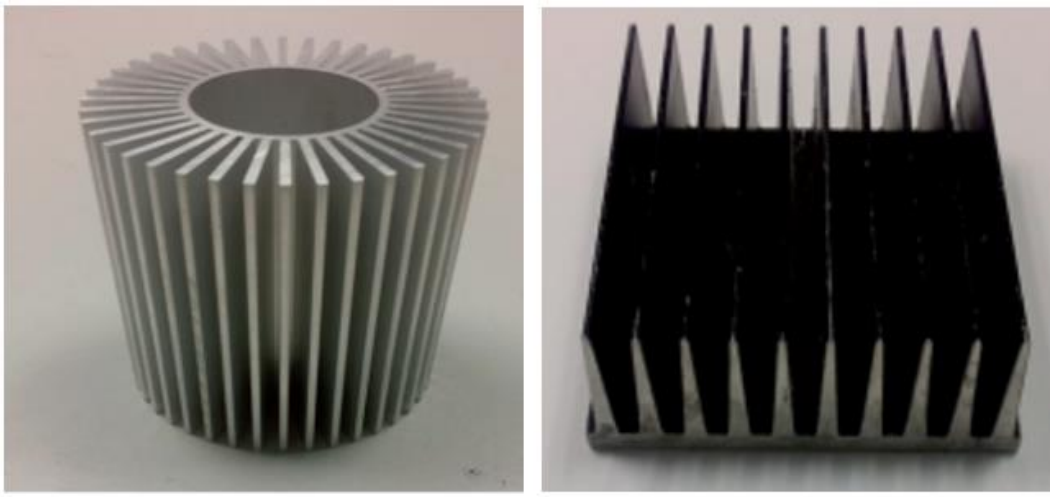

Figure 2.8. In this investigation, a photograph of the heat sink was employed. [75].

As anticipated, the results indicated that the additional heat raised the heating surface temperature. Furthermore, upon cooling under free convection circumstances, the surface temperature increased. The horizontal plate-fin heat sinks displayed higher surface temperatures than the vertical plate-fin heat sinks (BP type) at high heat flux. The plate-fin heat sinks (PFHs) outperformed the other conditions when cooled by free convection. To find the coefficient of heat transfer reflected by the Nusselt numbers (Yıldız and Yüncü [76]).

$$Nu_L = 0.68 + \frac{0.670\ Ra_L^{1/4}}{[1 + (0.492/Pr)^{9/16}]^{4/9}} \quad Ra_L \leq 10^9 \tag{2-7}$$

LED lights will overheat and shorten their lifespan if heat sinks are not built correctly. Additionally, there are many different applications for LED lights, and the installation angle might change depending on the location and usage. One of the most crucial elements affecting the natural convection cooling of LED lights is the installation angle. Assessing the variation in heat sink cooling efficiency with the mounting angle of gravity is therefore essential (Walunj et al. [77]). In an experiment, Sparrow and Bahrami [78] measured the rate of heat transfer from vertical square fins installed on a horizontal tube using the naphthalene sublimation process. The natural convection heat transfer of heated finned and unfinned cylinders has long been important in both study and industry. The goal of Churchill and Chu [79] was to establish a fundamental empirical relationship for a cylinder's mean Nusselt number. In order to verify that their association held throughout a broad range of Prandtl and Rayleigh values, they thus examined data from numerous previous investigations. This recipe can be used to create consistent heating and wall temperatures. When air is taken into consideration as the working fluid, Morgan [80] examined a sizable collection of experimental data and discovered that there might be a relationship between the Nusselt and Rayleigh values for smooth horizontal cylinders. Semicircular fins have not been the focus of as many studies as plate fins or pin fins. Figure 2.6 shows a schematic depiction of the model under study.

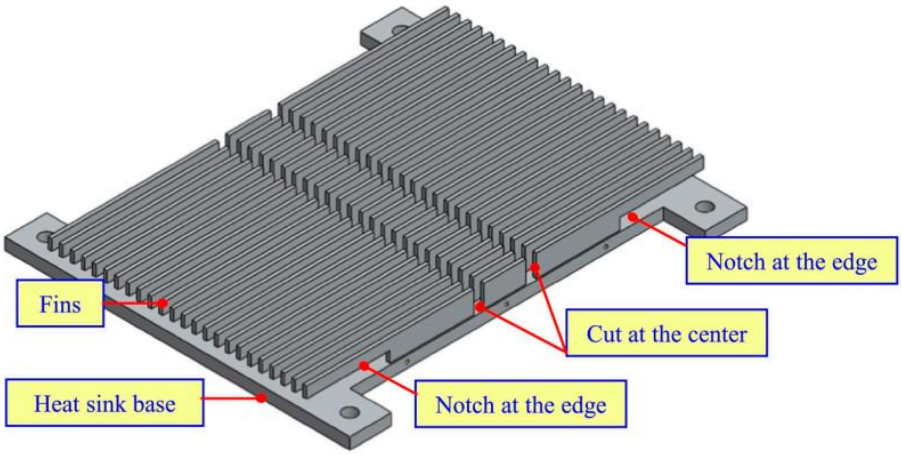

Figure 2.9. The use of notched fins for dissipating heat [81].

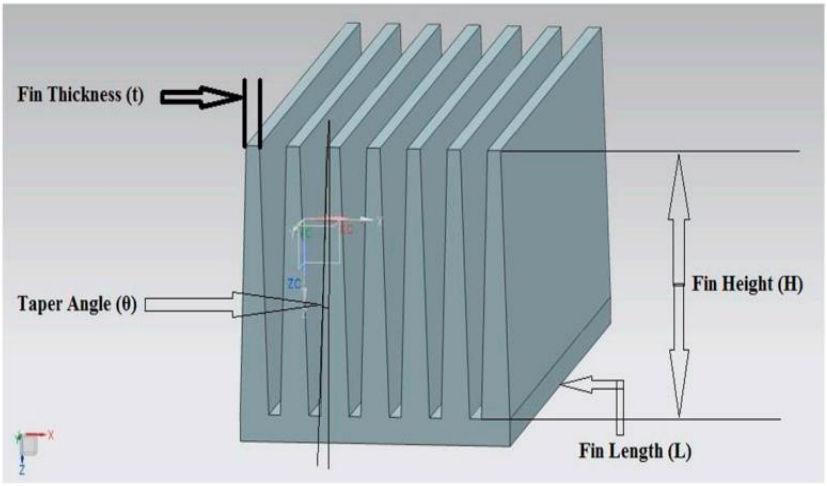

Figure 2.10. A tapered fin shape was employed to optimize heat transmission [82].

Dhumne and Farkade [83] conducted tests to look at the phenomenon of heat transfer from vertical cylinders with branched pin fins by natural convection. To determine the rates of heat transmission from finned cylinders to the surrounding air, experiments are conducted at different cylinder wall temperatures, fin pitch angles, and fin heights.. The results show that the thermal resistance of typical vertical cylinders with plate fins is 20% higher than that of vertical cylinders with branched pin fins. The former's heat resistance is 40% less per unit volume than that of traditional finned cylinders. Additionally, a correlation between the Nusselt number and the calculated thermal resistance values is discovered. Less than 20% of the discrepancy between the experimental and anticipated data may be explained by the correlation. The

experimental thermal performance of radial heat sinks with triangular fins was investigated by Hassan et al. [84], who looked at both non-perforated and perforated models. A numerical simulation model and experimental investigation of a wavy fin heat exchanger in a negative gauge pressure condition are developed. The effects of fin size parameters (fin height, fin pitch, and fin amplitude) on the temperature field and flow field distribution of wavy fins are investigated. 336 groups of numerical simulations have been used to generate empirical correlations between the friction factor and the Colburn-j factor. Comparing the air side to atmospheric pressure, the friction factor rises by 61.5% and the heat transfer coefficient falls by an average of 34% at -44 kPa negative pressure. According to Dhanadhya et al. [85], the average deviations of correlation for the friction factor and the Colburn-j factor are 2.7% and 2.3%, respectively.

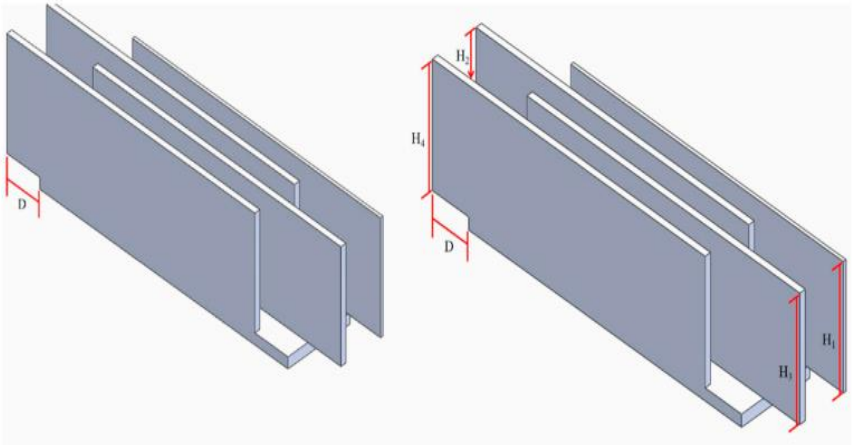

Figure 2.11. Employing the fins' inter-fin thermal barrier layers [86].

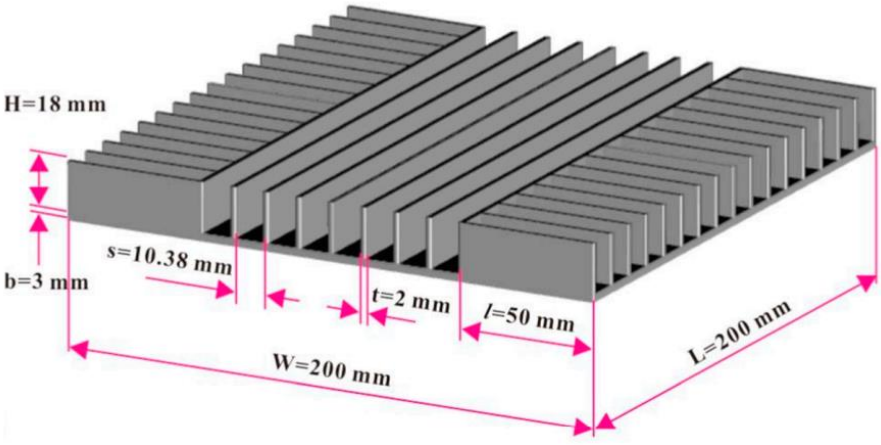

Figure 2.12. The cross-fin heat sink's design [86].

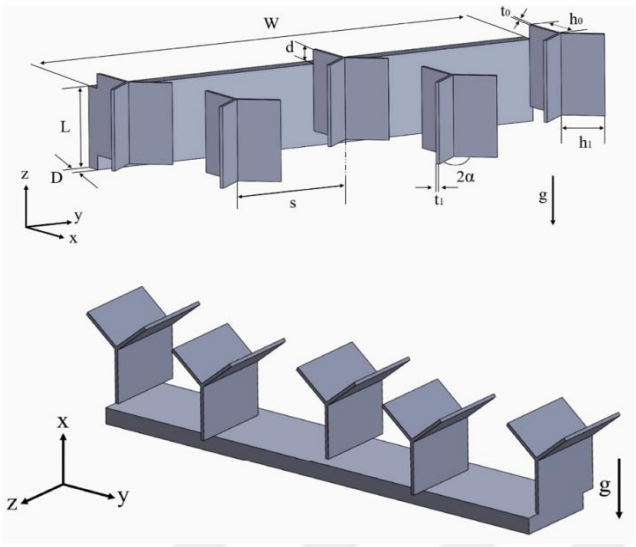

Figure 2.13. The heat sink's Y-shaped design [87].

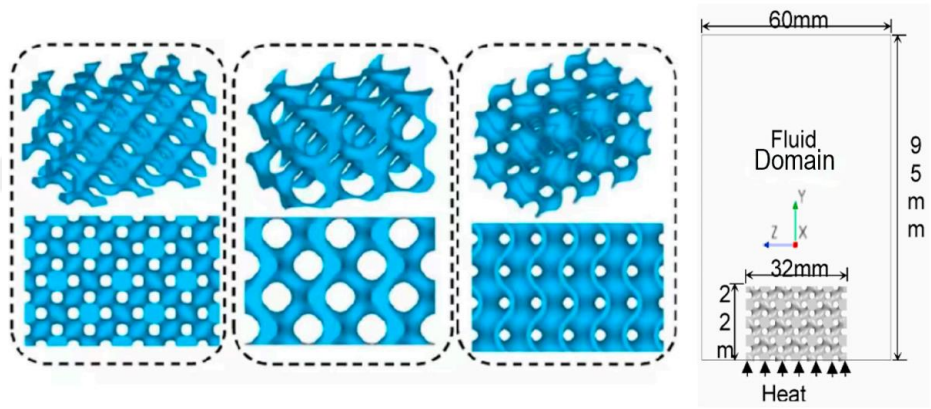

Figure 2.14. The three heat sink types with TPMS bases were designed [87].

Feng et al. [88] investigated a novel cross-finned heat sink design that took radiation heat transfer into account and enhanced heat transmission by natural convection using a relatively simple structure. According to their article, the newly developed cross-fin heat sink is a suitable alternative to conventional plate-fin heat sinks. They carried out several trials as part of their inquiry.

The optimal configuration for an L-shaped operational radial plate-fin heat sink (RPFHS) was determined by Noda et al. [89]. Four RPFHS prototypes were made; they differed in the amount of fins but all had the same box size. Out of the four PFHSs,

they chose the most efficient heat sink form to lower thermal resistance. Finding an ideal shape often requires time-consuming calculations and tedious laboratory work, even though computational and experimental methods are commonly used for optimizations. To the best of the author's knowledge, no link involving PFHSs has been proposed. The thermal efficiency of heat sinks with vertically oriented plate fins, triangle fins, or pin fins attached to a rectangular base has been investigated by Iyengar and Bar-Cohen [90] using a method called least-material optimization, with a focus on natural convection. In the end, they discovered that a heat sink with triangle fins was more thermally efficient than one with pin and plate fins in specific circumstances.

Natural convection is characterized by a low heat transfer coefficient, with air temperature often representing the average atmospheric temperature. To prevent overheating electrical components, experiments used heating powers under 80 W. These studies showed a median heat transfer coefficient of less than 15 $W/m^2 \cdot K$. Additionally, several investigations have explored forced convection heat dissipation, examining the correlation between Nusselt and Reynolds numbers under different heat transfer conditions. (Zhang and Aziz [91]).

In conclusion, not much research has been done on the thermal performance of heat sink forms like the vertical cylinder base and semicircular fin heat sink that work with the majority of LED light bulbs.Examining the thermal performance of a radial heat sink with semicircular fins on a circular base at varying heat fluxes, fin numbers, and forms is the goal of the current paper products. The Nusselt number connection is the second section of this investigation.

2.3. SUBJECT OF THE CURRENT STUDY

After reviewing the latest research literature on radial heat sinks, especially those with semicircular fins, despite their potential importance in modern applications such as LEDs. In this sense, our current research aims to fill this gap by focusing on experimental investigations of radial heat sinks with semicircular fins. We are not only interested in changing the number of fins, but we are also looking at the effect of changing the shape of the fins. Our research, conducted under free convection

conditions, aims to demonstrate the potential benefits and advantages of using semicircular fin shapes in radial heat sink configurations. By analyzing these aspects, we aspire to provide valuable insights that can contribute to the design and development of more efficient thermal management solutions, especially in the context of modern LED lighting applications.

CHAPTER THREE

EXPERIMENTAL SETUP AND CFD SIMULATION

3.1. INTRODUCTION

This chapter contains the details of this study in terms of preparing requirements for the production of experimental testing facilities, measuring devices, and raw materials required to manufacture this facility. The calibration of measuring devices that require before starting the measurement. In addition, the strategies required to conduct the tests completed in this study. To develop a practical plan to conduct the necessary tests according to a successive approach. The CFD simulations using the ANSYS 2021R2 software. The finite volume method was used to solve the governing equations. The governing equations of the airflow, which are believed to be incompressible, stable, and laminar, can be expressed as follows using the Boussinesq method for the buoyancy term.

3.2. CURRENT RESEARCH STRATEGY

Scheme 3.1 clearly defines the guidelines for this present work from the moment is approved until the end. They conduct a comprehensive review of previous studies, as well as studies conducted in close or somewhat similar systems in this work to find research gaps and move on. Then after proving the work vision, we will prepare the equipment and preparation for the research part, which is an experimental facility, to provide the raw materials, tools, and equipment to complete this work. Finally, they organize and prepare the cases and conditions of the experimental work. After completing the required measurements through pre-defined cases, experimental data is collected. After completing this stage, the data is analyzed, and the calculations are performed. Finally, the result is displayed with a curve or a graph form and tables.

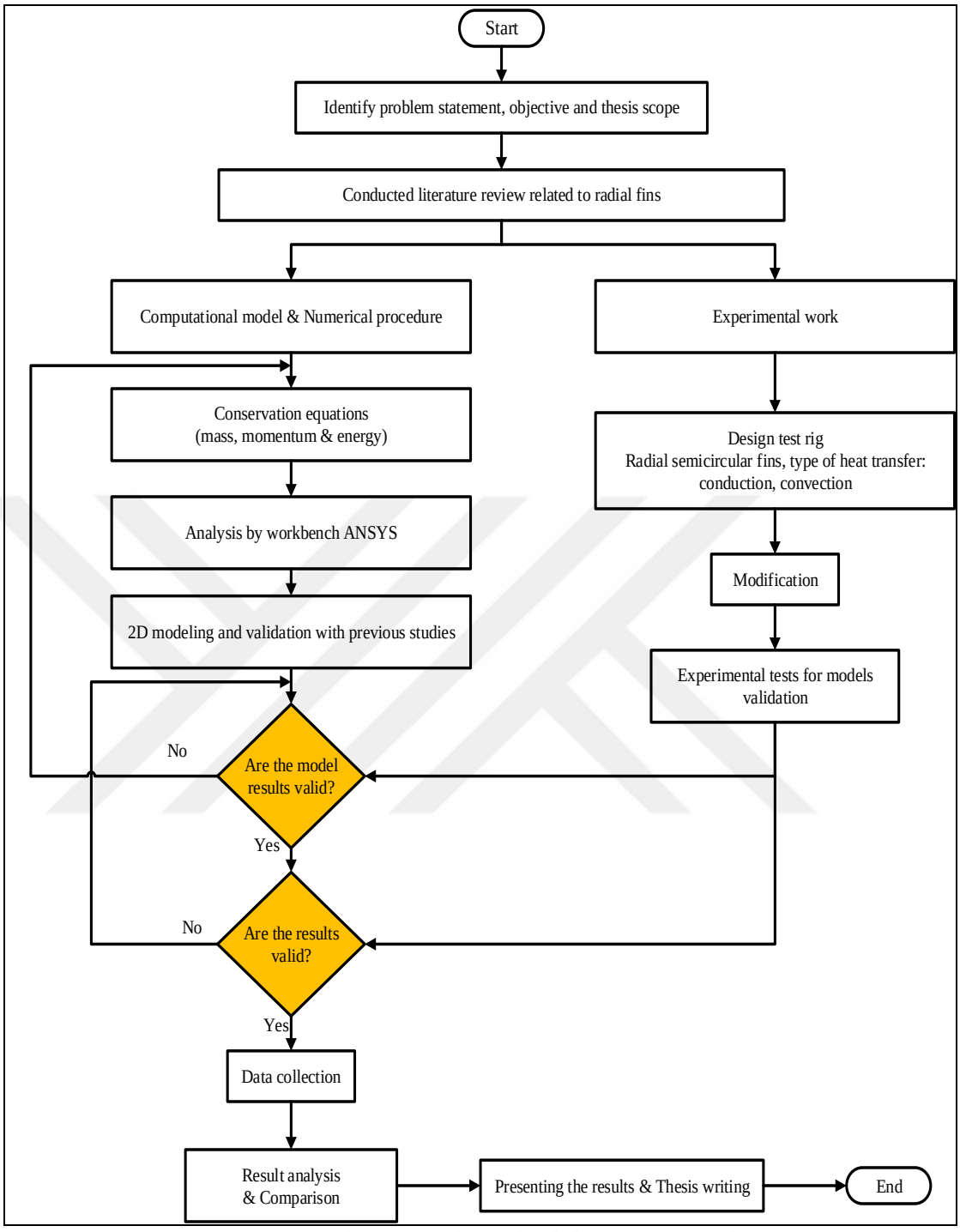

Figure 3.1. The research methodology's approach.

3.3. EXPERIMENTAL SETUP

In the experimental setup, heat transfer due to airflow and thermal energy generation in the electric heater will be calculated and measured. The heat will be transferred through radiation, conduction, and natural convection. Key factors, including Rayleigh

number (Ra), Nusselt number (Nu), thermal resistance (Rth), and heat transfer performance, will be used to analyze the process. Further details on the components and equipment involved will be provided in the following sections to explain how each part influences the heat transfer process and the performance of the electric heater.

The experimental setup shown in Figure 3.1 has the following elements.. Figure 3.2 shows a photograph of the schematic diagram and experimental setup.

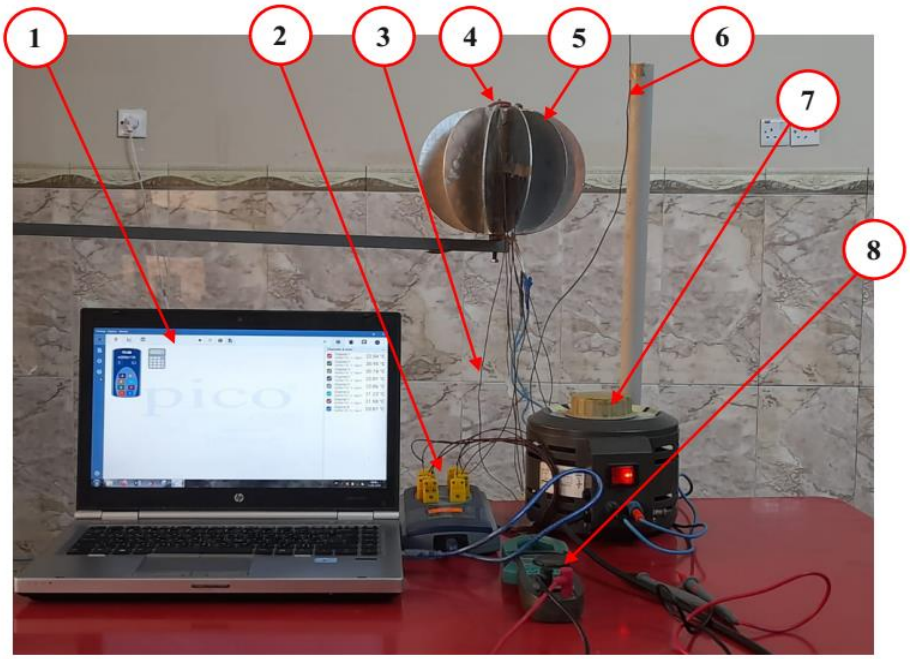

Figure 3.2. The setup for the experiment.

No.	Part Name	No.	Part Name	No.	Part Name
1	Laptop	**4**	Cartridge heater	**7**	Power supply
2	Data logger	**5**	Test rig	**8**	Voltage and current measure.
3	Thermocouples	**6**	Air Temp. Thermocouple		

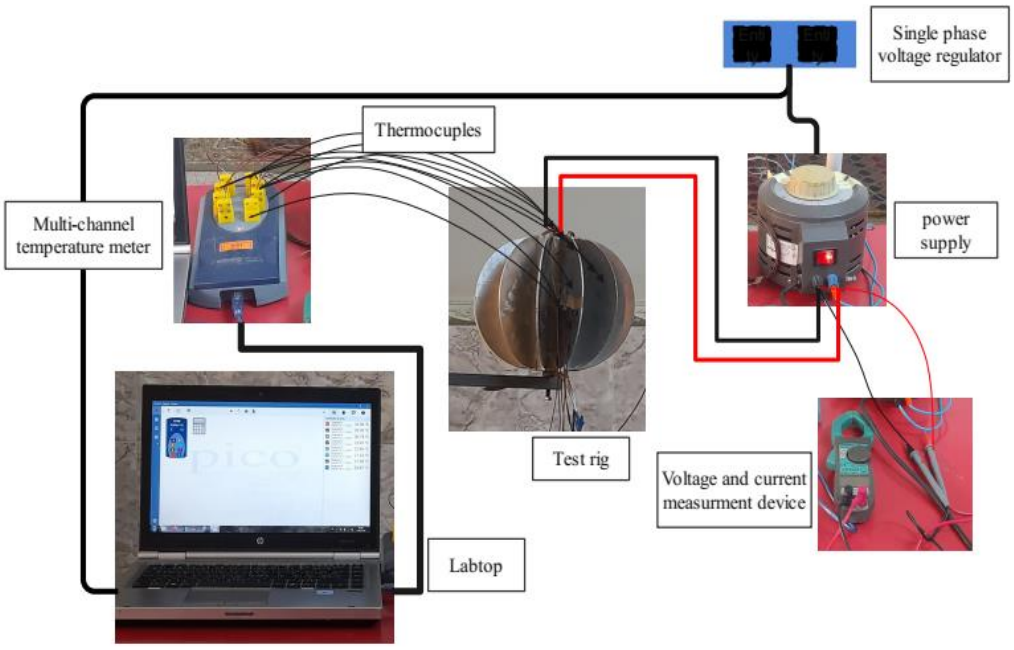

Figure 3.3. Diagrammatic representation of the experimental configuration

3.4. MATERIALS

The components and apparatus of the system are described as follows:

3.4.1. Cylinder

A solid cylinder made of aluminum alloy 195 (the heat transfer properties see in Table 3.2) with a diameter of 70 mm and a length of 210 mm, was designed. On the cylinder's upper surface, five holes measuring 8 mm in diameter and 200 mm in depth were drilled. These holes are impermeable as shown in Figure 3.3, and a schematic diagram of the cylinder with dimensions is shown in Figure 3.4 .After figuring in the cylinder's center (R = 35 mm) to punch the first hole, the fin base's punching procedure was carried out. The locations of the remaining four holes were then established by establishing a distance of 17.5 mm from the cylinder's center and an angle of 90º. As seen in Figure 3.5, electric heaters were positioned within these openings. Twelve longitudinal incisions were made in the form of a channel with a thickness of (3 mm), a depth of 3 mm, and a length of (210 mm) to include the fins on the outside of the cylinder. The adjacent to slot was 30º from the others.

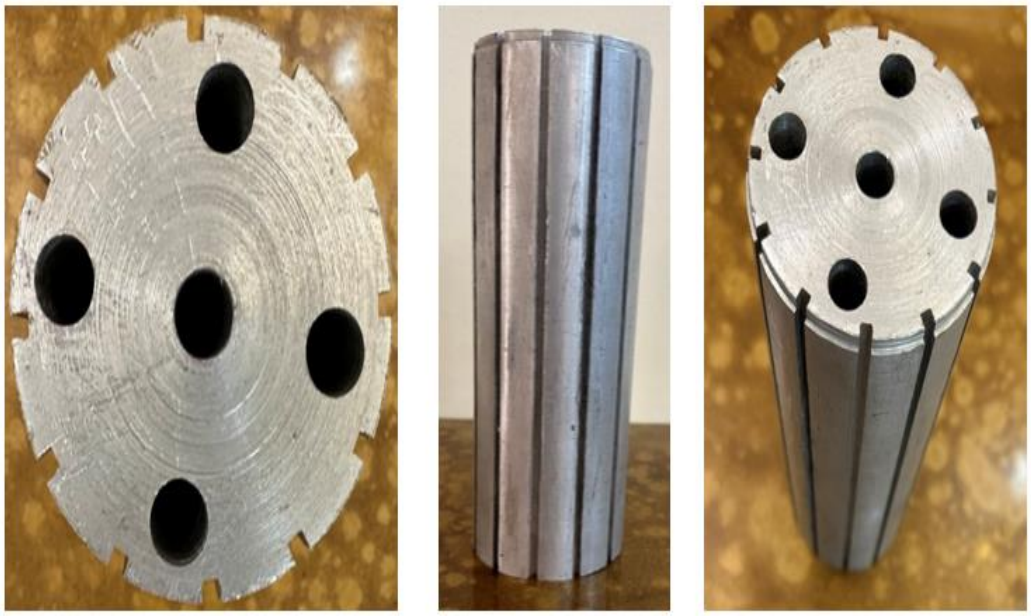

Figure 3.4. A photograph of a base cylinder with holes.

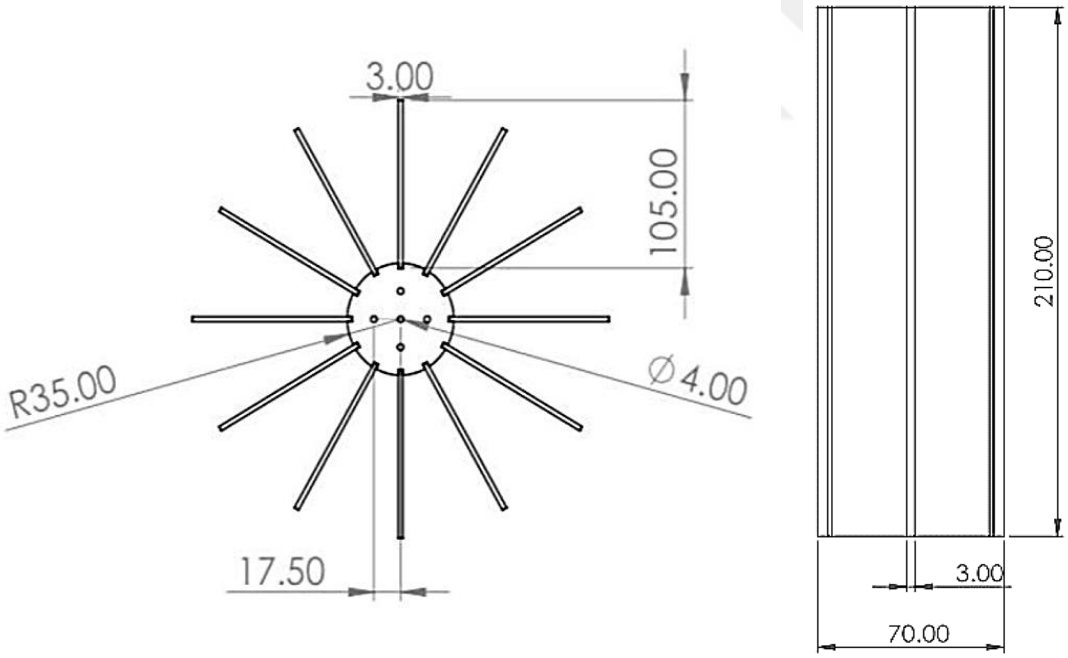

Figure 3.5. The drawing of the base cylinder (all dimensions in mm).

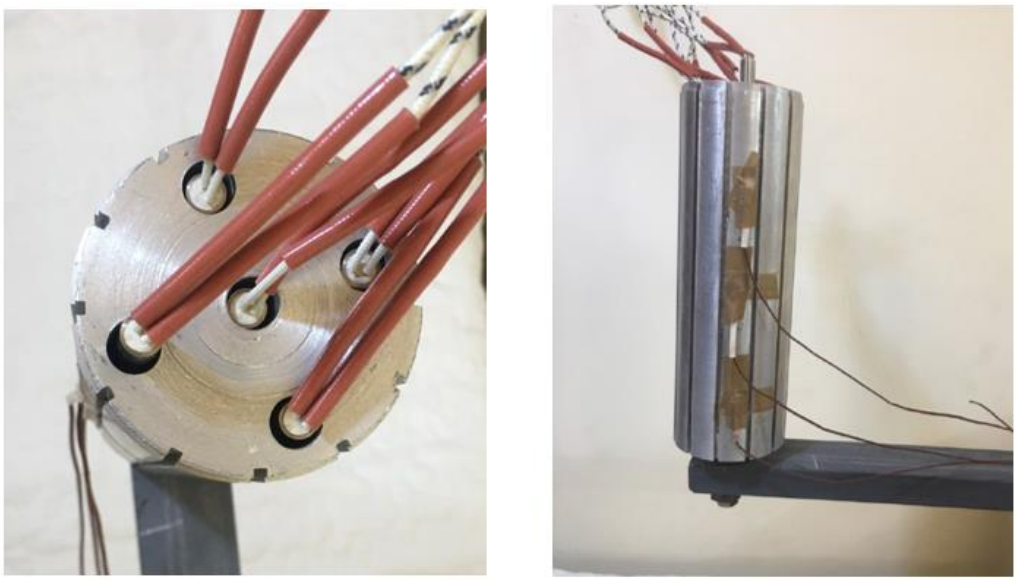

Figure 3.6. Photographs of the electric heater assembly and base cylinder with thermocouples fixed.

3.4.2. Fins

Three cases of semicircular fins were taken in this study: semicircular fins in the order (SC-0), SC-40, and SC 50) made of aluminum alloy 195 with a thickness of (3 mm) and a height equal to the cylinder length is (210 mm). The semicircular fin radius is (105 mm). 36 models of semicircular fins of different shapes were manufactured. The three cases are (SC-0, SC-40, and SC 50) for each case are 12 types, the cases are shown in Figure 3.6(a),(b) and details are presented in Table 3.1. The diagram in Figure 3.7. shows how the fins are installed on the cylinder body.

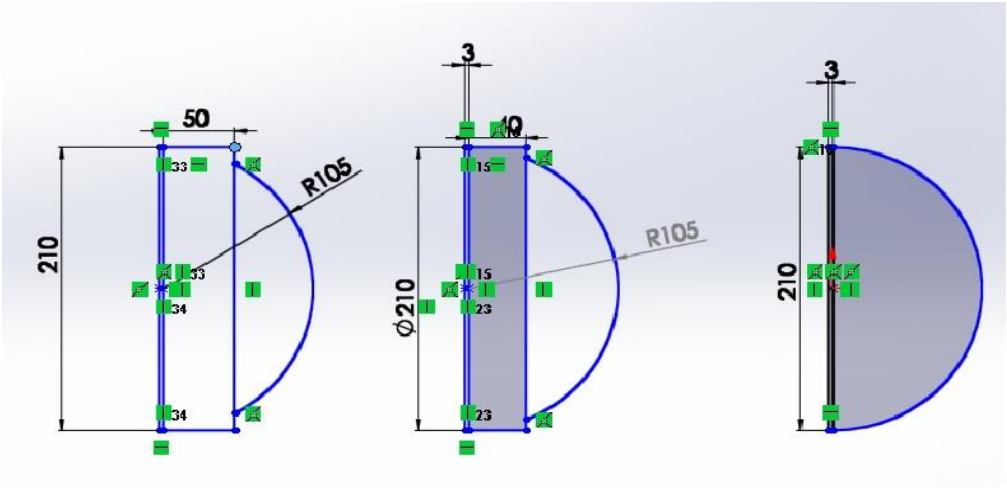

(a)

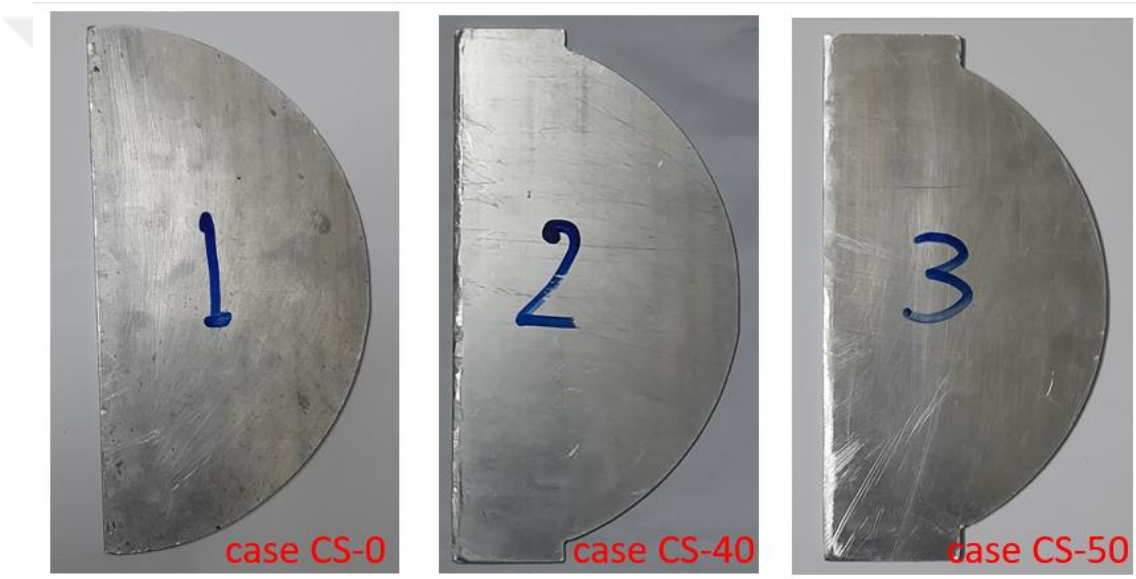

(b)

Figure 3.7. Cross-section of semicircular fins (a) Schematic diagram and (b) a photograph.

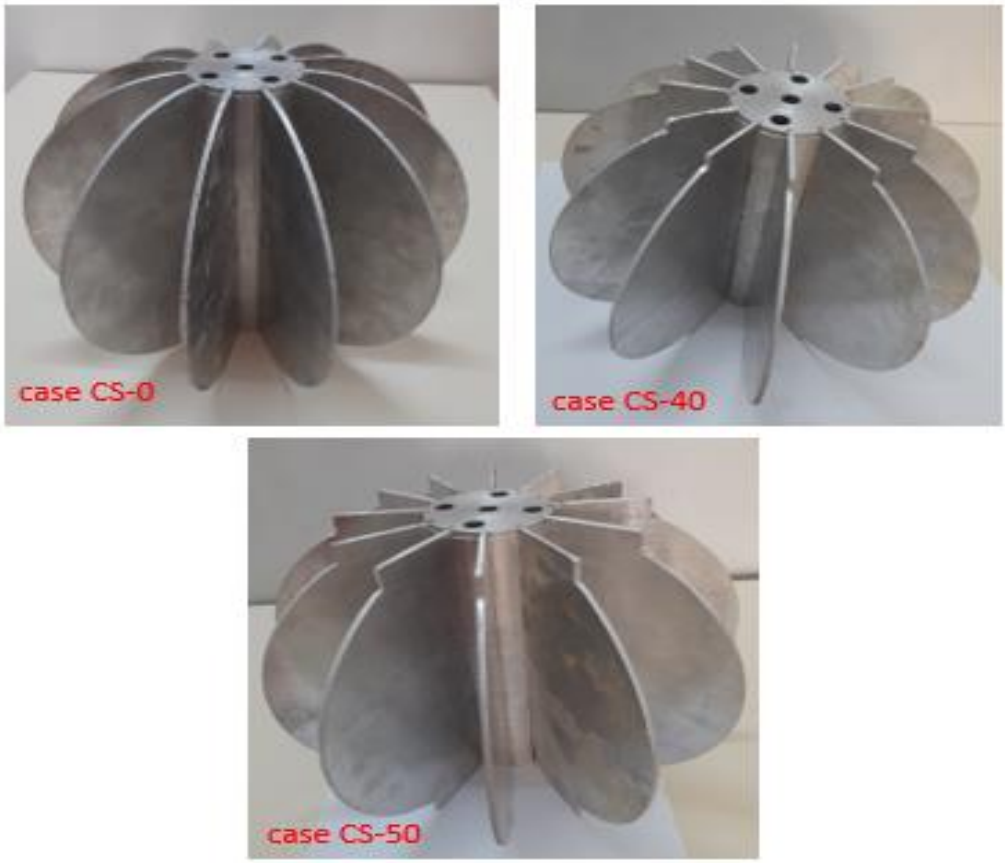

Figure 3.8. A photograph of the three cases used in this work.

3.4.3. Thermocouple

Type K thermocouples with a diameter of (1.2 mm) and a length of (1850 mm) were used, as shown in Figure 3.8. The temperature is measured using eight precisely calibrated thermocouples. Use three of the above-mentioned thermocouples at the base of the cylinder, while three of them are attached to the fin wall. One independent K-type thermocouple is also used to measure the temperature of the air surrounding the system outside the heat sink. The thermocouple locations mounted on the cylinder wall and fin surface are shown in Figure 3.9. If the core temperatures of these thermocouples on the cylinder are approximately uniform in the vertical direction of the cylinder.

Figure 3.9. The K-type thermocouple.

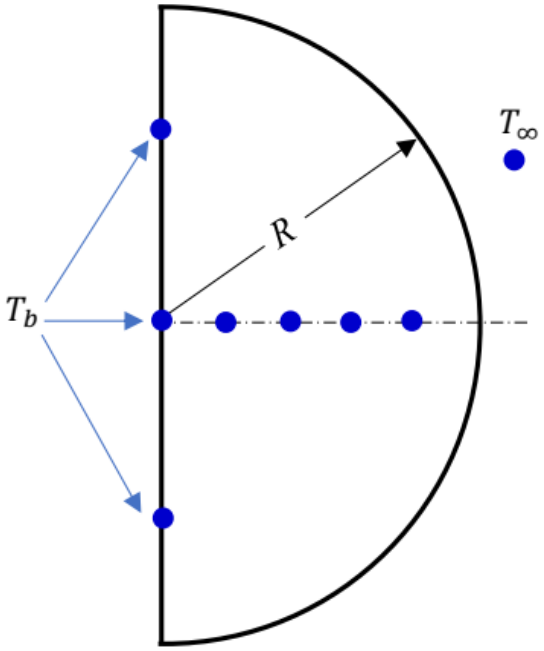

Figure 3.10. The thermocouples locations.

3.4.4. Electrical Heaters

A cylindrical electric heater (cartridge heater) was employed, measuring 200 mm in length and 8 mm in diameter. The power consumption range when operating at 220V is 50 to 850 W. Figure 3.10 shows the cartridge heater.

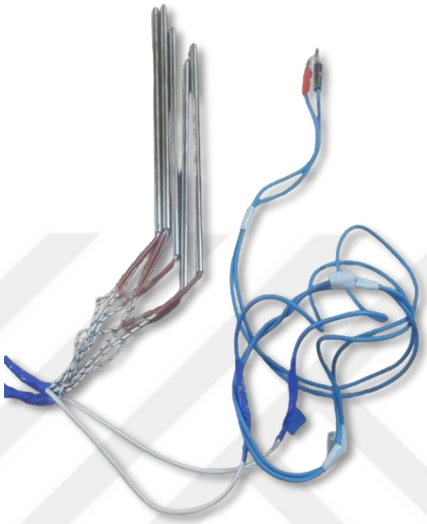

Figure 3.11. Electrical resistors.

3.4.5. Temperature Measurement

Offer use of the eight-channel, LCD-screened Pico Technology USB TC-08 temperature meter (see Figure 3.11). The data recorder has an accuracy of 0.2%±1 °C and measures between -200 °C and 1300 °C. The mechanism of the device is to install the tips of the thermocouple on the channel of the device, then turn on the device to ensure that the thermocouple is working before attaching it to the site to know the temperature by exposing the thermocouple to heat, and monitor the device screen to indicate whether the thermocouple responds to temperature changes Make sure all thermocouples are working. (8) thermocouples were used in this investigation to measure temperature; (3) of these were placed on the cylinder, (4) on the fins at various points, and (1) was used to assess the temperature of the air around the test platform.

(a)

(b)

Figure 3.12. The Pico Technology USB TC-08 (a) the device and (b) the software interface.

3.4.6. Power Supply Regulator

A single-phase voltage regulator and a variable transformer of the type HSN 0103 220V PLUG were utilized to regulate the amount of electricity transferred to the electric heater. The voltage regulator is used to control the supplied voltage and achieve the heat flux necessary to heat the test cylinder and be within the range (0-250 V), as shown in Figure 3.12.

Figure 3.13. Voltage controller.

3.4.7. Devices for Measuring Current and Electrical Voltage

The device used to measure the electric current that passes through the voltage difference from the power microscope to the electric heaters is a multi-meter (Clamp meter model MT-3102). The reading accuracy for the current is (0.4-20A) with a range of (3). %+15) As for the voltage (200-2V), the range is (1.2%±5). Figure 3.11 shows a photograph of the device used.

Figure 3.14. Multi-reading device for reading current and voltage.

3.5. CALIBRATION OF THERMOCOUPLE

The thermocouples were calibrated before use to measure experimental temperatures compared with a mercury thermometer under three different conditions. The first reading was taken for the thermocouples in the open air. At the same time, they were placed in the shade, and the second reading was taken for the heaters inside the laboratory, while the last reading was by exposing the mercury thermometer used for calibration and the thermocouples together to the heat of the sun. It was done by relying on the readings through the special relationship to find the error rate in the thermocouple readings, as shown in Figure 3.14, by obtaining equation 3.1 through which we find the true reading by the thermocouple.

$$T_{\text{Thermocouple}} = 1.041 \times T_{\text{Thermometer}} - 0.351 \qquad (3\text{-}1)$$

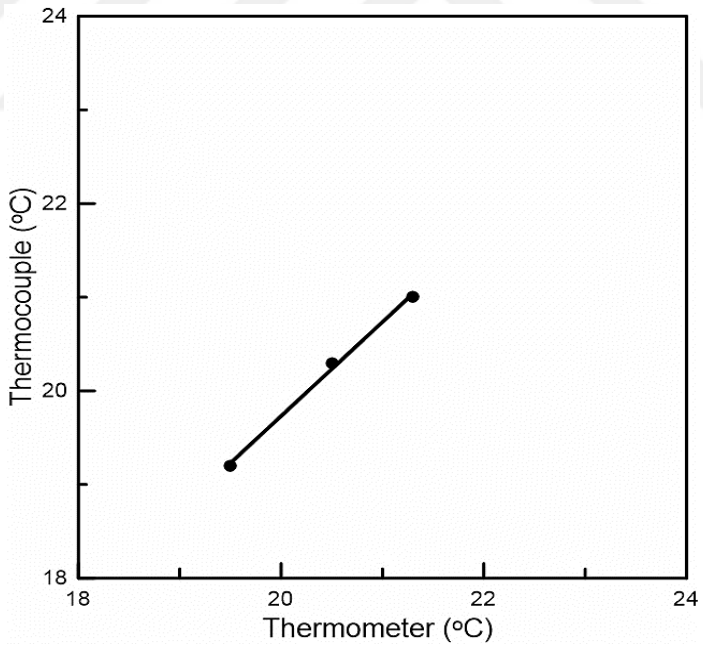

Figure 3.15. Thermocouple calibration.

3.6. STAGES OF THE TEST SAMPLE PREPARATION PROCESS

Before each test, some important steps must be followed. For example, the three fin shapes in the test, are:

- The fins, in terms of the shape and number required for testing, are installed on the drum hall by placing them and fixing them in the slot made along the length of the news drum, maintaining the design intact using a flexible plastic hammer of the structure and without causing any damage to both the fins and the drum.
- Place the five electric heaters inside the cylinder within the holes that were specially made for them, and you must ensure that each heater is working before each test.
- The cylinder base (fins) is installed after the fins are installed on it on the steel arm.
- The thermocouples are numbered before being mounted on the body of the structure and the temperature recorder.
- Installing the electrical wire that connects the electrical power supply base to the voltage regulator device
- Install a thermocouple for the ambient temperature measurement.
- The thermocouples are numbered before being mounted on the body of the structure and the temperature recorder.
- As shown in Figure 3.9, place the (3) thermometers on the surface of the cylinder.
- One of the test fins is chosen to plan it and determine the locations for installing the thermocouples. There are four thermocouples along the semicircular fin surface, as shown in Figure (3.15). A horizontal line is drawn along the fin surface. The thermocouple No. (4) is placed at a distance of (35 mm) from the fin root, then the thermocouple No. (5) is placed at a distance of (20 mm) from No. (4), and the thermocouple No. (6) is placed at a distance of (20 mm) from No. (5) and then the final thermocouple (7) are at a distance of (20 mm) from No. (6).
- After starting the operation system took about 1.5 hr to 2 hr for the system to arrive steady state and to started the recorded the current, voltage, and temperature for all locations above.
- After completing the first input heat flow, change the input heat flow and record the above.

- After completing the first test change the number of fins and repeat the (10) and (11).
- Change the orientation angle and repeat the (10), (11) and (12).

3.7. COMPUTATIONAL MODEL AND NUMERICAL ANALYSIS

3.7.1. The Issue's Description

The heat sink with semicircle fins orientated vertically and under natural convection topic. The cylinder base of heat sinks measures 70 mm in diameter and 210 mm in length, respectively. Figure 3.15, illustrates the computational domain. Aluminum alloy 195 was selected as the material of cylinder and fins because of its high thermal conductivity. The computational domain of cooling air surrounds the heat sink across a measuring of diameter 360 mm and a height 6L, the L is the length of the heat sink. Table 3.1 summarizes the cases of heat sinks and geometrical parameters of semicircle fins. Table 3.2 summarizes the thermophysical characteristics of the aluminum alloy and air used in the simulation.

Table 3.1. The cases and geometrical parameters.

case	Angle (degree)	L (mm)	Rfin (mm)	No. of fins	t (mm)
A	0	210	105	12	3
B	15	210	105	12	3
C	30	210	105	12	3

Table 3.2. Thermophysical properties of air and aluminum alloy 195 [92].

	ρ (kg/m^3)	Cp (J/kg K)	k (W/m K)
Al	2270	875	168
Air	1.1614	1007	0.0263

3.7.2. Numerical Details

The computational fluid dynamics (CFD) models were created under identical conditions to the fabricated model and with the same dimensions. The vertical laminar

natural convection semicircle fins were computationally analyzed in this work. The heat was absorbed from the base of each fin at T_b and by convection heat transfer to the ambient air at T_∞. The ANSYS 2021R2 software for the carryout of the CFD simulations. The governing equations were solved using the finite volume method. Using the Bossiness approximation for the buoy term, the current air flows governing equations which are thought to be incompressible, steady and laminar. Numerical simulations take into consideration the following assumptions:

- At specific temperatures, air is utilized as a working fluid because of its stable characteristics.
- A three-dimensional with laminar flow.
- The heat input of 53.08, 128.21, and 322.40 W is taken into consideration in the base cylinder heat sink.
- The buoyancy is approximated using the Boussinesq approximation, and the reference temperature is equivalent to the ambient temperature shift from 15.8 °C to 17.2 °C.
- The sliding condition does not apply to walls.
- Radiation effect is neglected.

The governing equations are as follows: [93,94].

Continuity equation

$$\rho\nabla\left(\vec{V}\right) = 0 \tag{3-2}$$

Momentum equations are written as

$$\rho\nabla\cdot\left(u\vec{V}\right) = -\frac{\partial p}{\partial x} + \mu\nabla^2 u, \tag{3-3}$$

$$\rho\nabla\cdot\left(v\vec{V}\right) = -\frac{\partial p}{\partial y} + \mu\nabla^2 v + (\rho - \rho_a)g, \tag{3-4}$$

$$\rho\nabla\cdot\left(w\vec{V}\right)=-\frac{\partial p}{\partial z}+\mu\nabla^2 w \tag{3-5}$$

The fluid area's energy equation is written as

$$\rho\nabla\cdot\left(\vec{V}T\right)=\frac{k}{C_p}\nabla^2 T, \tag{3-6}$$

The solid area energy equation is written as

$$\nabla^2 T=0 \tag{3-7}$$

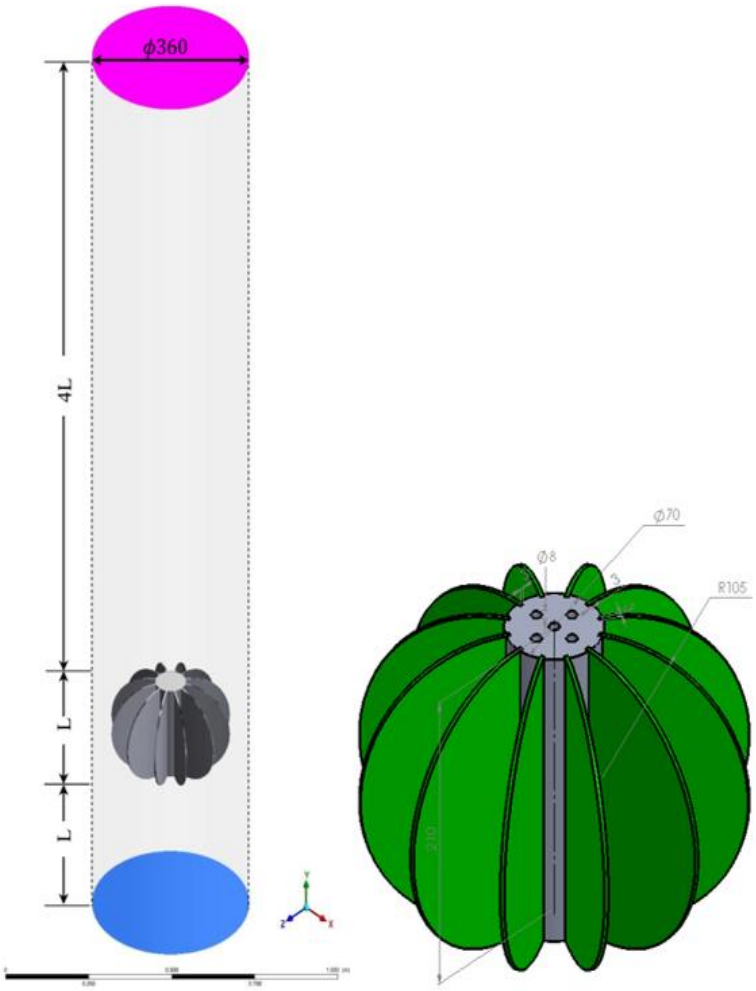

Figure 3.16. Heat sinks featuring semicircle fins in both computational domains and schematic diagrams.

In this case, the 2.5 million-element mesh was chosen. Figure 3.16 shows further details about it. Therefore, 0.4 mm and 1 mm represent the minimum and maximum fin element sizes in the regions close to the fin range, respectively.

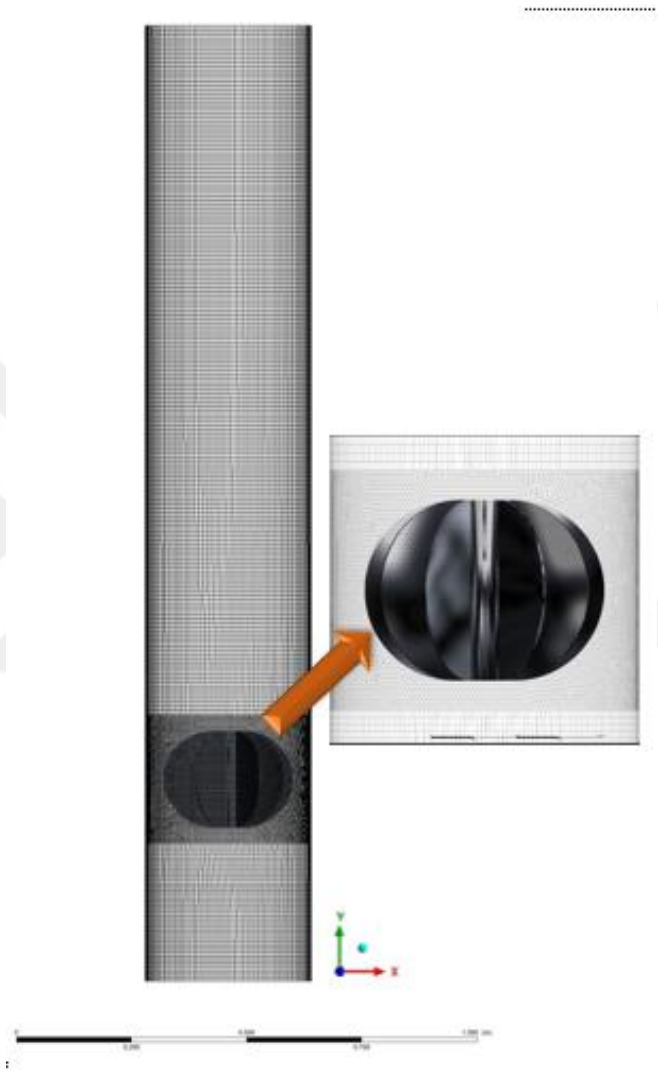

Figure 3.17. Configuration of the computational domain grids.

3.7.3. The Conditions at the Boundary

Table 3.3 shows the boundary conditions used in the numerical simulation.

Table 3.3. The boundary conditions for pressure, input heat flow, and temperature.

	p	Q (W)	Initial temperature (℃)
Inlet	0	-	25
Exit	$\frac{\partial p}{\partial y} = 0$	-	25
Cylinder surface	0	53.08, 128.21, 322.40	25

3.7.4. Analysis Of Heat Transfer Performance

The calculations and measurements related to the heat transfer process, if thermal energy is generated in the electric heater as a result of the passage of the electrical current supplied by the power supply, and this energy is dissipated in 3 ways. There are three primary ways that heat is transferred: convection, radiation, and conduction. The computation of the heat produced by electrical resistance is the fundamental component [95].

The electrical heat gain rate and uniform heat flux from the outside cylinder base surface can be calculated using the following equations:

$$q_{\text{in}} = \Phi \times I \tag{3-8}$$

The electrical heat test surface's steady-state heat balance can be expressed as follows:

$$q_{\text{convection}} = q_{\text{in}} - q_{\text{radiation}} \tag{3-9}$$

One way to get the average cylinder base temperature is to:

$$T_b = \frac{1}{3}\sum_{i=1}^{3} T_{b,\text{i}} \tag{3-10}$$

The calculated rate of radiation-induced heat transfer was [91]:

$$Q_{\text{radiation}} = F\sigma A\varepsilon(T_b^4 - T_\infty^4) \tag{3-11}$$

For a commercial aluminum tube that has an emissivity of 0.028 and a form factor of F = 0.1 [96]. the experimental error at base temperatures below 0.2°C on average. The rate of heat transmission through radiation is lowered by around 5% due to emissivity loss.

The following formula defines the heat flux as follows:

$$\dot{Q}_{\text{net}} = \frac{Q_{\text{convection}}}{A_b} \tag{3-12}$$

where (A_b) is the cylinder area is defined as:

$$A_b = 2\left(\frac{\pi}{4}D^2\right) + \pi DL - NLt - 5(\frac{\pi}{4}d^2_{\text{heater}}) \tag{3-13}$$

where (d_{heater}) diameter of the electric heater.

Figure 3.6 shows the fin area, which may be calculated as follows:

$$\left.\begin{aligned} A_{\text{fin}} &= \frac{\pi}{4}L^2 + \frac{1}{2}\pi Lt, && (\text{SC}-0\ \text{case}) \\ A_{\text{fin}} &= 2\left[A \times B + \pi\frac{\theta}{360}\left(\frac{L}{2}\right)^2 - \frac{1}{2}(L - 2\text{B} \times \text{A})\right] \\ &+ \left[2(A+B) + \pi\frac{\theta}{360}L\right]t, && (\text{SC}-40, \text{SC}-50\ \text{cases}) \end{aligned}\right\} \tag{3-14}$$

Consequently, one can determine the net heat transfer area by:

$$A_{\text{net}} = A_b + NA_{\text{fin}} \tag{3-15}$$

The free streams outer layer is the main focus of this investigation. The corresponding air characteristics from the following equations are used in the computations that follow. They are suitable for temperatures between $275\text{K} \leq 0.5(T_b + T_\infty) \leq 375\text{K}$ and are validated by data [97].

$$\left.\begin{aligned}
\rho_f &= 2.209 - 3.414 \times 10^{-3}\left(\frac{T_b + T_\infty}{2}\right), && \text{kg/m}^3 \\
C_{Pf} &= \left[9.8185 + 7.7 \times 10^{-4}\left(\frac{T_b + T_\infty}{2}\right)\right] \times 10^2, && \text{J/(kg K)} \\
k_f &= \left[3.74152 + 7.495 \times 10^{-2}\left(\frac{T_b + T_\infty}{2}\right)\right] \times 10^{-3}, && \text{W/(m K)} \\
\mu_f &= \left[4.99343 + 4.483 \times 10^{-2}\left(\frac{T_b + T_\infty}{2}\right)\right] \times 10^{-6}, && \text{kg/(m s)} \\
\nu_f &= \frac{\mu_f}{\rho_f}, && \text{m}^2/\text{s} \\
\alpha_f &= \frac{k_f}{\rho_f \times C_{Pf}}, && \text{m}^2/\text{s} \\
\beta_f &= \frac{2}{T_b + T_\infty}, && 1/\text{K}
\end{aligned}\right\} \quad (3\text{-}16)$$

An average free heat transfer coefficient is expressed as follows. [7].

$$h = \frac{Q_{\text{net}}}{A_{\text{net}}(T_b - T_\infty)} \quad (3\text{-}17)$$

The following is how to find the (Nu) number :

$$Nu = \frac{hL}{k_{\text{air}}} \quad (3\text{-}18)$$

The expression for the calculated Rayleigh number (Ra):

$$Ra = \frac{g\beta_{\text{air}}(T_b - T_\infty)L^3}{\nu_{\text{air}}\alpha_{\text{air}}} \quad (3\text{-}19)$$

We define the resistance to heat as [98] based on the experimental findings:

$$R_{th} = \frac{(T_b - T_\infty)}{Q_{net}} \quad (3\text{-}20)$$

The study of uncertainty is done to estimate a mistake in the experimental results. They consist of measuring mistakes, bias, and accuracy. The accuracy error of φ_T temperature measurement is calculated by.

$$\varphi_T = t_{(N_{data}-1),95\%} \times \frac{\sigma_T}{\sqrt{N_{data}}} \quad (3\text{-}21)$$

where σ_t, N_{data} and $t95\%$ are the temperature, number of data, and t distribution standard deviations at a 95 % confidence level, correspondingly [99], Based on data from the manufacturer, the instrument's temperature error in measurement for the Ω_T bias error is as follows.

$\Omega_T = 0.26℃$

One definition of the thermocouple uncertainty is:

$$\psi_T = \pm\sqrt{{\Omega_T}^2 + {\varphi_T}^2} \quad (3\text{-}22)$$

The uncertainty of the temperature measurement is computed. This expression represents the $\psi_{R_{th}}$ uncertainty in the thermal resistance measurement:

$$\frac{\psi_{R_{th}}}{R_{th}} = \pm\sqrt{\left(\frac{\psi_T}{T_b}\right)^2 + \left(\frac{\psi_T}{T_\infty}\right)^2 + \left(\frac{\psi_I}{I}\right)^2 + \left(\frac{\psi_\phi}{\phi}\right)^2} \quad (3\text{-}23)$$

The degree of error in the voltage and current measurements is represented by the symbols Ψϕ and ΨI, respectively. The investigation uses 0.03℃ precision thermocouples and a 0.1℃ resolution and ±(0.2%+0.1)℃ accuracy data collection equipment to calculate the temperatures at various locations.

The following is a description of the calculation of the thermal resistance error ΨRth:

$$\frac{\psi_{R_{th}}}{R_{th}} = \pm\sqrt{\left(\frac{\psi_T}{T_b}\right)^2 + \left(\frac{\psi_T}{T_\infty}\right)^2 + \left(\frac{\psi_I}{I}\right)^2 + \left(\frac{\psi_\phi}{\phi}\right)^2} \quad (3\text{-}24)$$

Consequently, the temperature measurement has a margin of error of ±0.05 °C. Table 3.4 shows the temperature measurement error, ΨT, as calculated and displayed.

Table 3.4. An overview of the levels of uncertainty.

Parameter	Uncertainty (%)
q_{in}	±0.1205
Ra	±8.07
Nu	±1.74
R_{th}	±1.22
I	± 11.625
ϕ	± 3.171

CHAPTER FOUR

RESULTS AND DISCUSSION

4.1. GENERAL

The performance of radial semicircular fins in heat transfer is examined in this work. Several input heat rates of 53, 128, and 322 W with fin numbers of 4, 8, and 12 were tested in the experimental investigation. In this work, three semicircular fin cases are investigated. In addition, the CFD simulation study for the same conditions of the experiment work and addition of the orientation angle for the first case. In many engineering applications, temperature distribution is essential to heat transfer [18]. Typically, the findings are displayed as graphs that illustrate the correlation between fin height and temperature distribution, as well as between Nusselt number and thermal resistance.

4.2. GRID INDEPENDENT TEST

A grid sensitivity test was conducted for case (a) with semicircular fins in order to verify the precision of the numerical results., calculating eight grid sets of 0.45, 0.7, 1.1, 1.5, 2.0, 2.5, 3.1, and 3.7 million cells. Figure 4.1 exhibits the findings. With a relative variation of less than 0.21%, the 2.5 million grid system provides results comparable to finer meshes with 3.1 million and 3.7 million elements

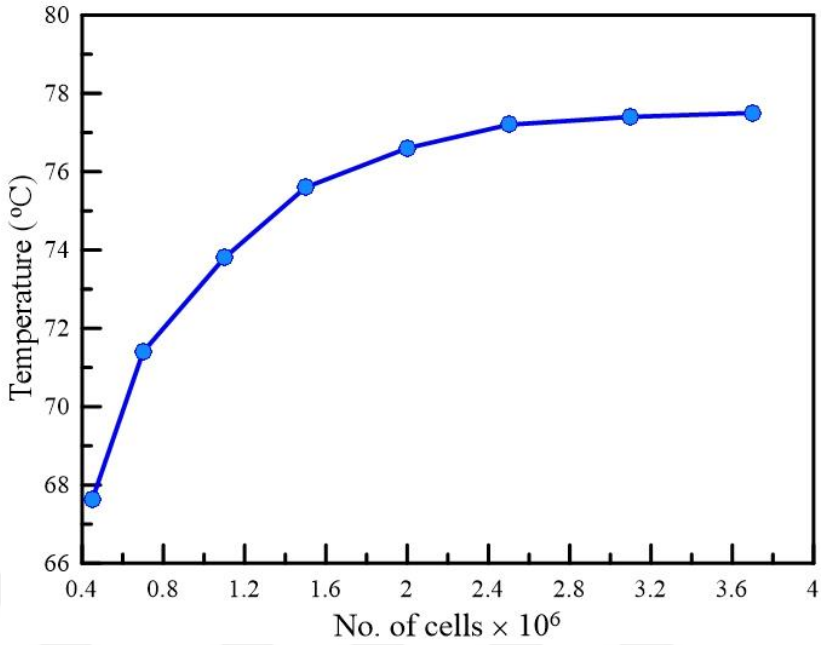

Figure 4.1. The mesh sensitivity investigation for case SC-0 (number of cells vs. temperature).

4.3. VALIDATION

For heat flows in the range of roughly 53 to 322 W. Figure 4.2 display the compared based cylinder temperatures between CFD simulation results and empirical data for zero-degree orientation. With an inaccuracy of less than ±4.9%, the temperatures predicted numerically and empirically agreed well. As a result, the study's numerical model indicated a good ability to predict the heat sink temperatures with accuracy.

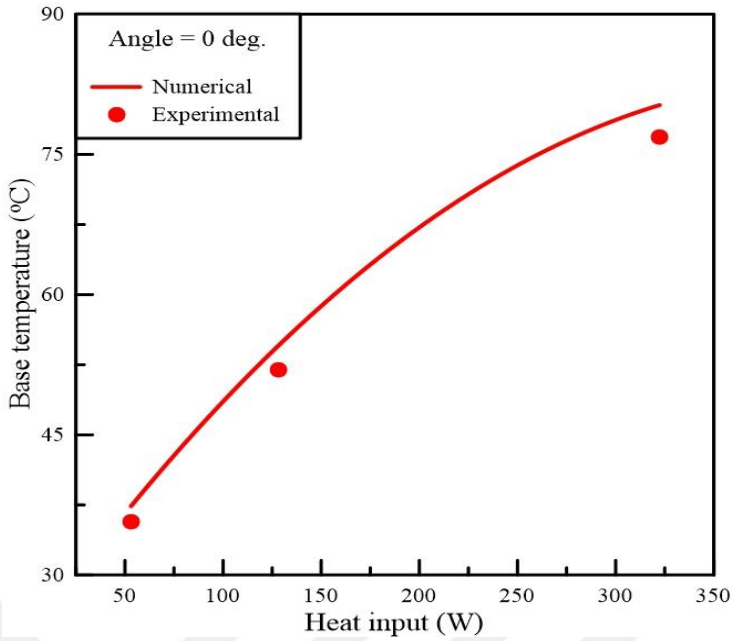

Figure 4.2. Using a comparison of experimental data and CFD simulation findings for heat sink tempera

4.4. HEAT TRANSFER

4.4.1. CFD Results

A typical plot of the Nu number against the Ra number with various orientation angles is displayed in Figure 4.3. For every examined case, this chart shows that the Nu number rises as the Ra number does. The 30-degree orientation angle showed a greater Nu number value. These phenomena may be caused by a reduction in the temperature differential between the surface and the surrounding environment.

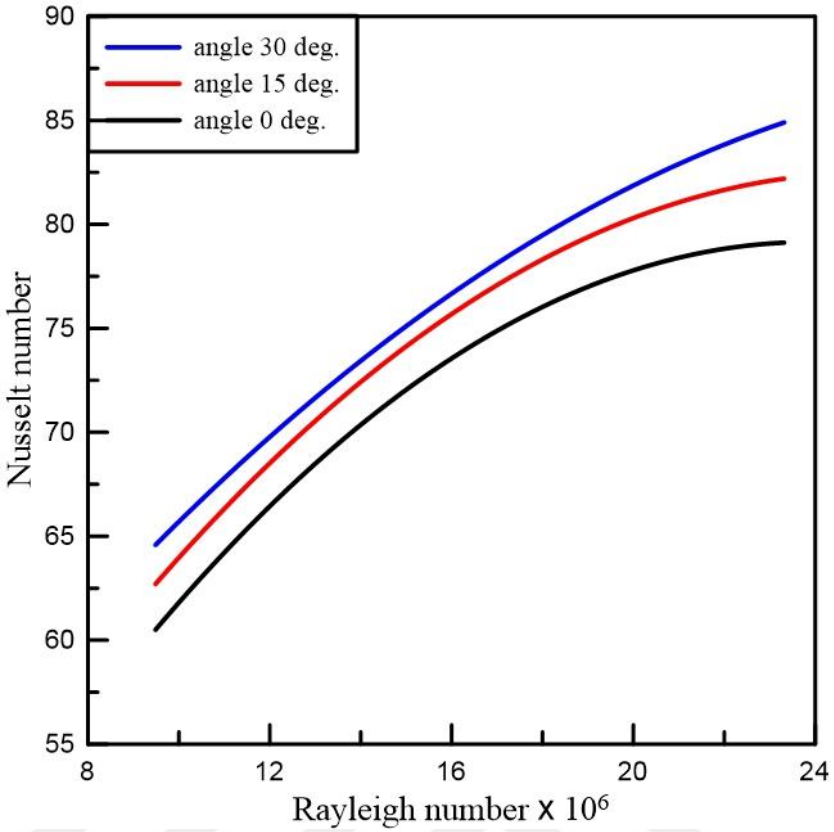

Figure 4.3. Orientation angle's impact on Nu number with varying Ra numbers.

4.4.2. Experimental Result

The impact of input heat flow on the base temperature of the heat sink relative to the surrounding air temperature for the three investigated instances is depicted in Figure 4.4. Temperature distributions from the heating elements were shown for different input heat rates. As the amount of heat input increases, the temperature gradient increases. On the other hand, the upper curve in the picture displays a decrease in temperature within the area of laminar flow. The second curve acts differently from other curves because of a severe drop because it is close to the transitional area.. The high temperature is reflected in the low fins number. The four fins have the highest temperature because of the air layers that come into contact with multiple fin surfaces. It is evident that the traditional fins (semicircular) in instances CS-40 and CS-50 have differing maximum temperatures. This is distinct due to the fins' expanded area.

Another significant element that was investigated in this study was fin height. Figure 4.5 illustrates how fin height affects heat sink temperature for different heat supplies using the CS-0 example. The numbers show the temperature of the surrounding air on various surfaces. Generally speaking, as fin height increases, the temperature drops.

The scenarios that were investigated for unrestricted airflow around and through four fins with a heat supply rate of 53.08 W are depicted in Figure 4.5a. It is evident that as the number of fins rose for all examined fin counts, the temperature distribution dwindled. A fin delays the anticipated heating of the air at constant heat rates by increasing the air around and through it. By doing this, the air-fin temperature differential is kept low enough to optimize the fin's heat-removal capabilities. Four high thermal value fins. The second and third heat input situations are depicted in Figures 4.5b and 4.5c. Figures 4.6 and 4.7 illustrate the correlation between fin height and temperature for the CS-40 and CS-50 examples.

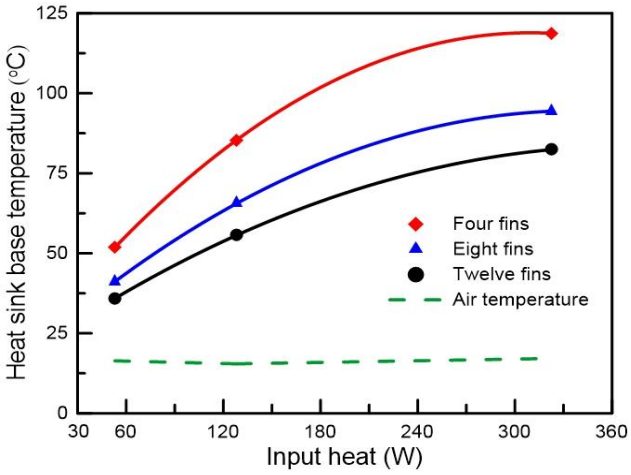

(a) case CS-0

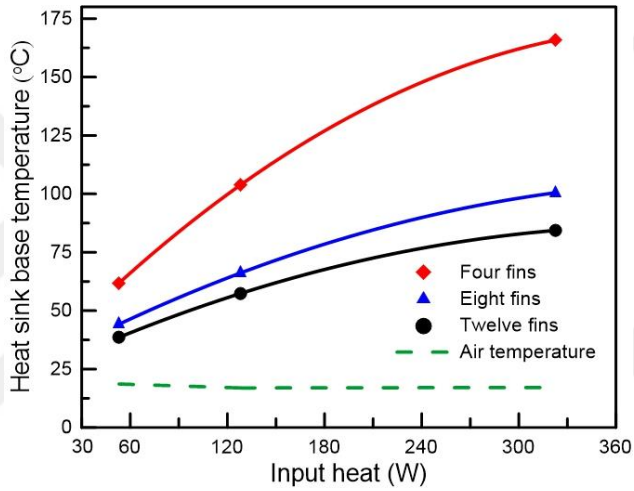

(b) case CS-40

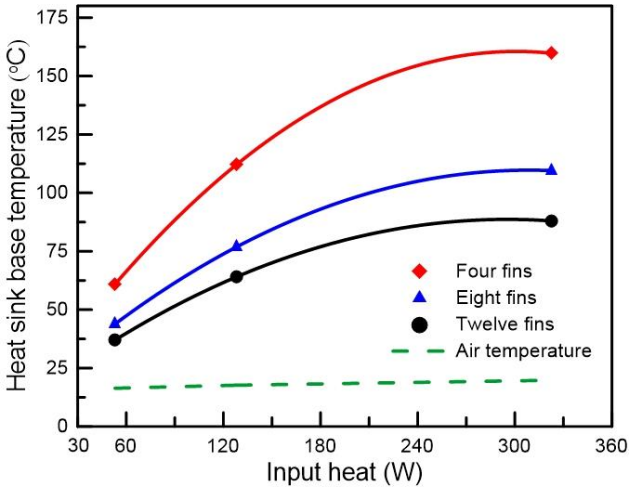

(c) case CS-50

Figure 4.4. The effect of fin count on the heat sink's baseline temperature

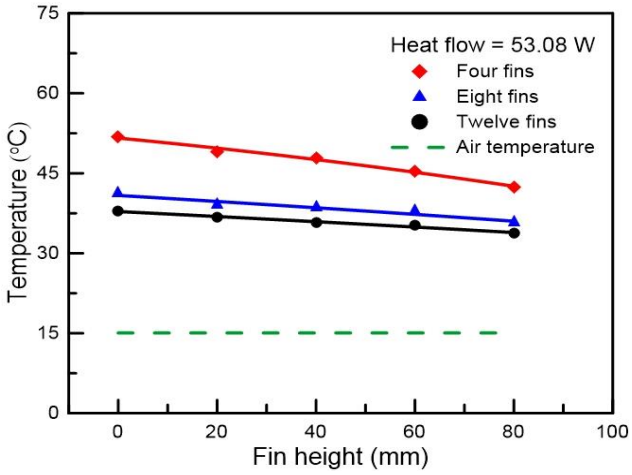

(a) Q = 53.08 W

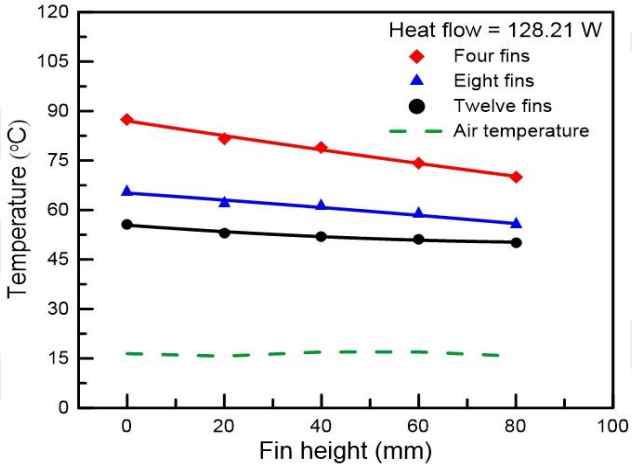

(b) Q = 128.21 W

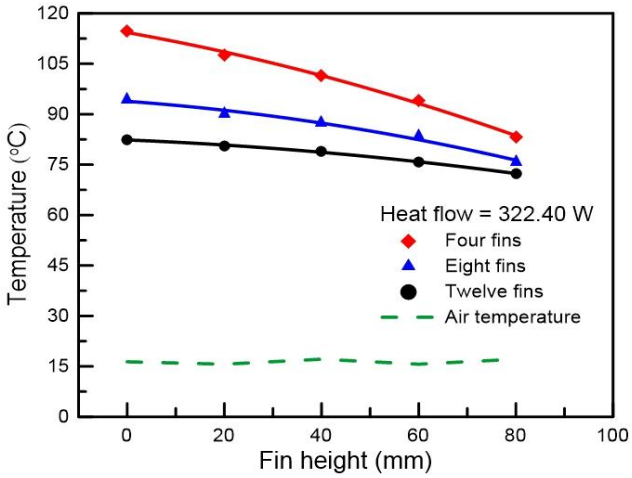

(c) Q = 322.40 W

Figure 4.5.The effect of fin height on the ambient temperature dispersion in the CS-0 example

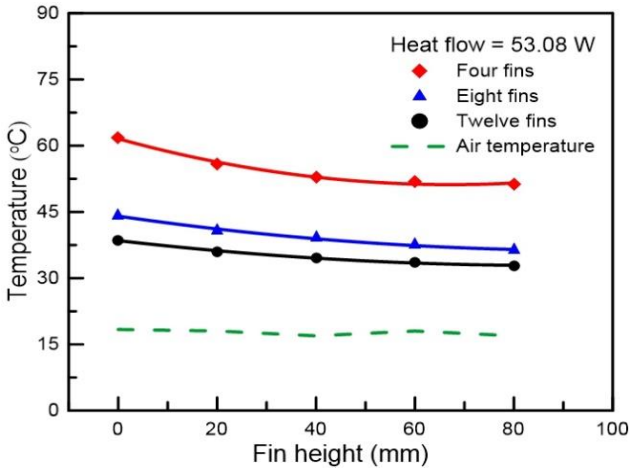

(a) Q = 53.08

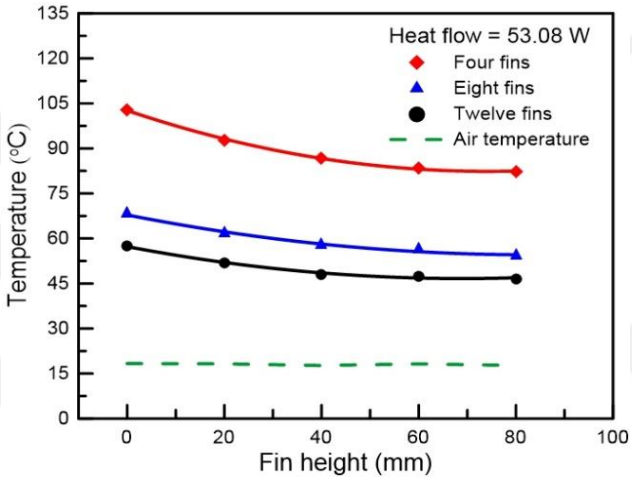

(b) Q = 128.21 W

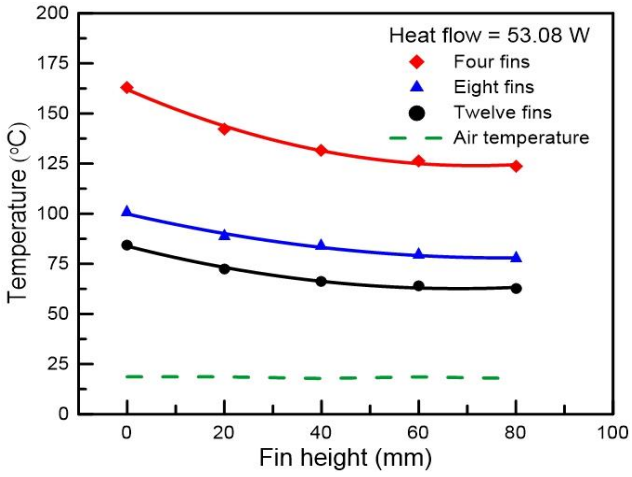

(c) Q = 322.40 W

Figure 4.6. Impact of raising the fin height on the SC-40 case's temperature distribution.

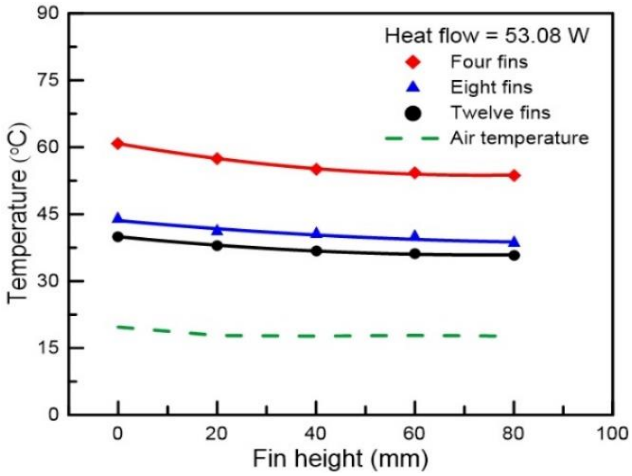

(a) Q = 53.08 W

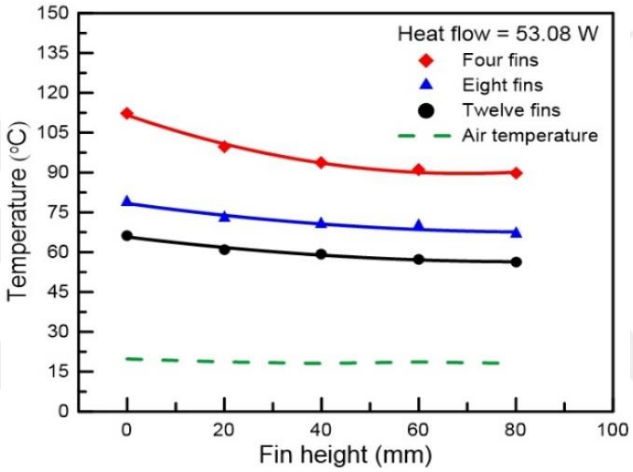

(b) Q = 128.21 W

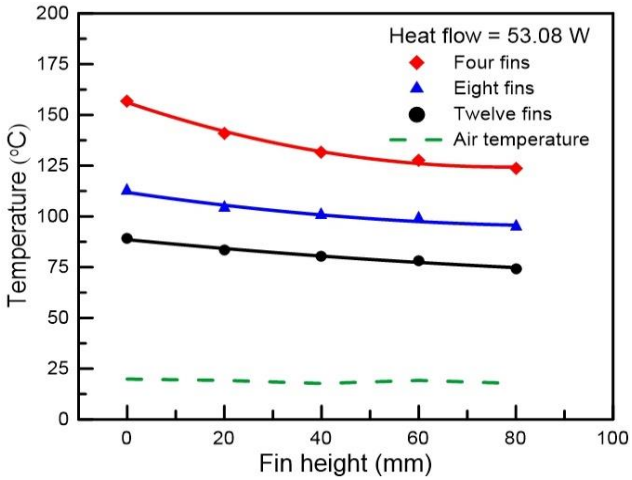

(c) Q = 322.40 W

Figure 4.7. The impact of fin height on the distribution temperature in the SC-50 case.

Using three research instances, Figure 4.8 illustrates how the Rayleigh number affects the heat transfer coefficient at different fin numbers. For every examined situation, the heat transfer coefficient invariably rises with the Rayleigh number. Remember that in all cases, the heat transmission coefficient increases nonlinearly with the Rayleigh number. The heat transfer coefficient is maximum when the heat sink has four fins. This pattern results from a decrease in the temperature differential between the base and the surrounding air as the number of fins decreases.

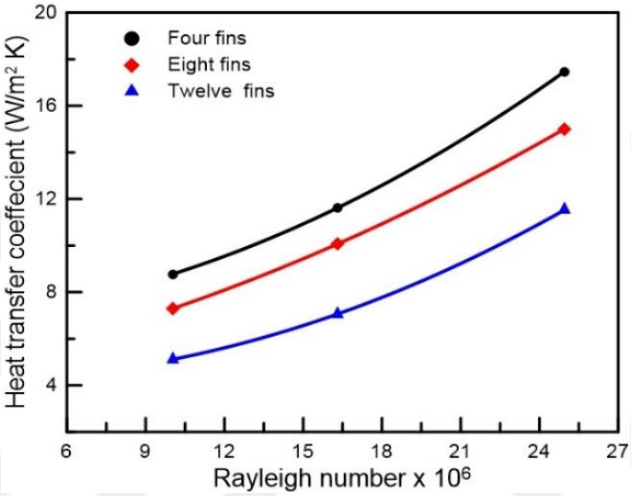

(a) case CS-0

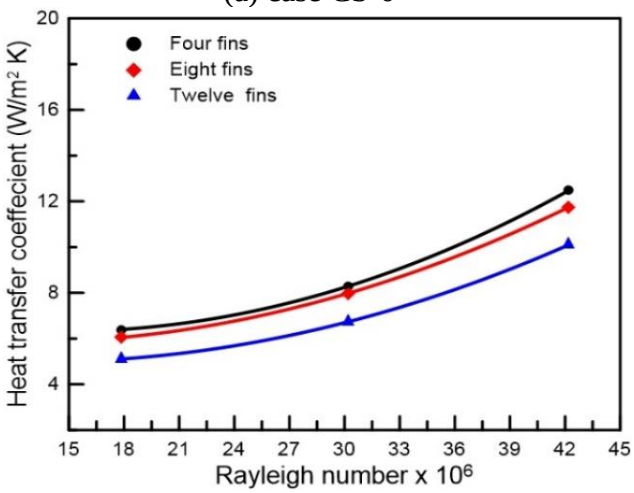

(b) case CS-40

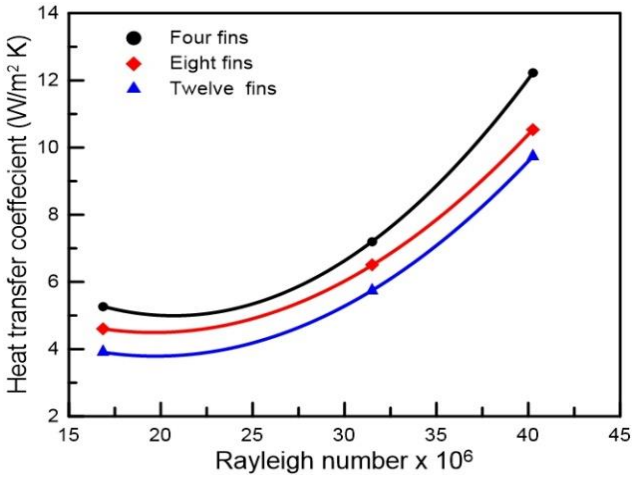

(c) case CS-50

Figure 4.8. Change in the heat transfer efficiency of the heat sink as a function of Rn at different fin counts.

Figure 4.9 displays a representative Nusselt number vs Rayleigh number at fins number. Additionally, it is observed that in every instance, the Nusselt number rises as the Ra number does. Additionally, it can be observed that the four fins have a higher Nusselt number because to the higher temperature differential between the ambient and bass heat sink and the heat transfer via free convection. The Nusselt number's peak value in the CS-0 scenario makes this clear from the numbers as well.

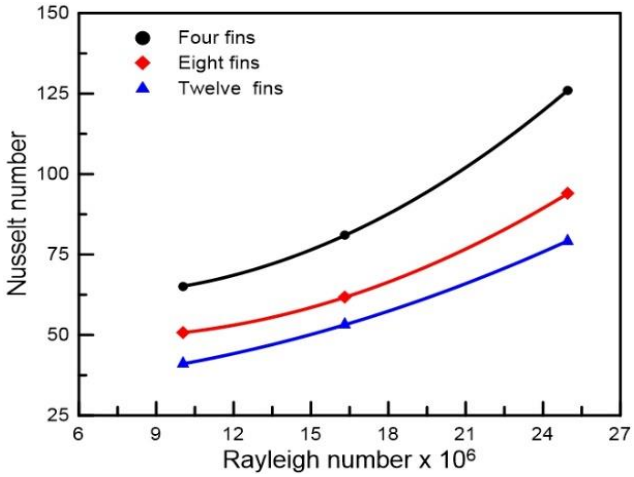

(a) case CS-0

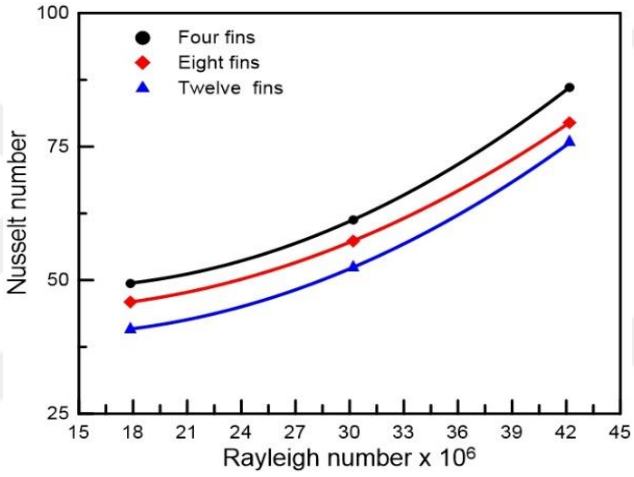

(b) case CS-40

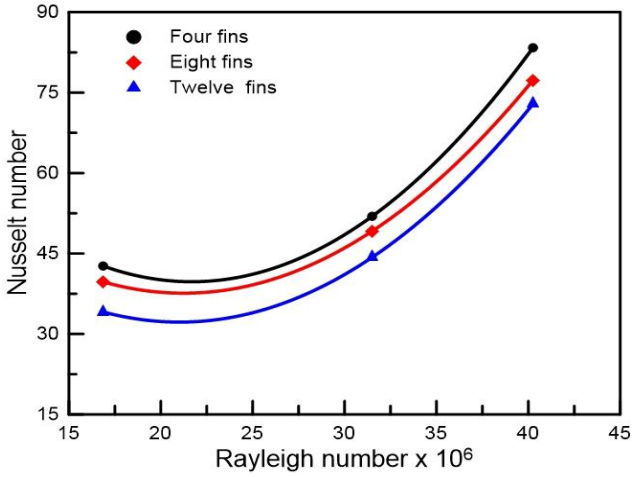

(c) case CS-50

Figure 4.9. Ra number's effect on the $Nu\ the$ number at various fin numbers.

Figure 4.10. depicts the variation of the Nusselt number with fins number at different inputs heat for the CS-0, CS-40, and CS-50. It is also noted that, the Nusselt number decreases with increased fins number for all heat inputs. The curves exhibit different behaviors in different ranges of heat input.

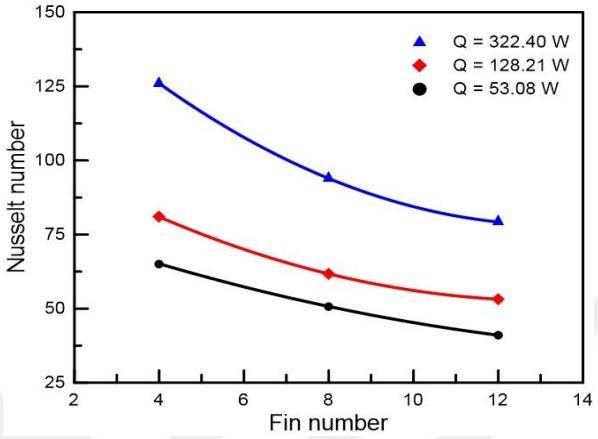

(a) case CS-0

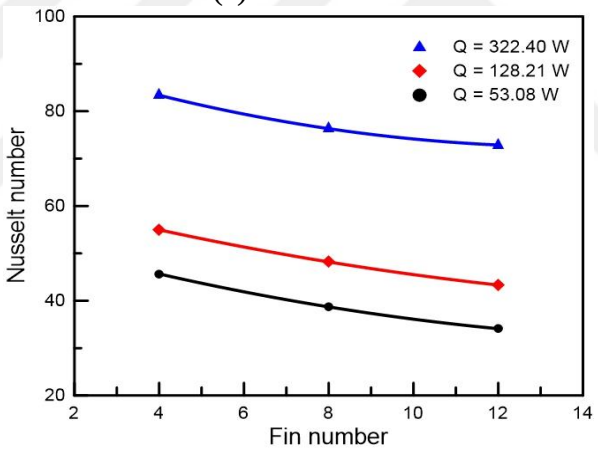

(b) case CS-40

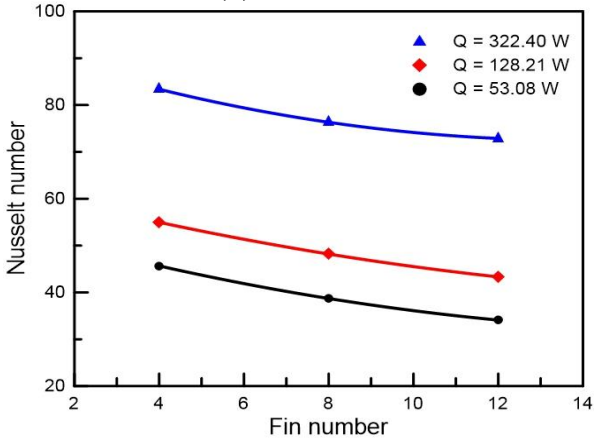

(c) case CS-50

Figure 4.10. The number of Nusselt. Fin number at various research cases and input temperatures.

The effects of heat input on thermal resistance at various fin numbers are shown in Figure 4.11. According to the figures, when the heat input rises, the thermal resistance falls. As the heat input rises, the thermal resistance falls nonlinearly, as the image shows. This is explained by the increased fluid flow. Adding more fins boosted the rate of heat transfer and reduced the thermal resistance of the heat sink by increasing the effective area of heat transfer. The results show that thermal resistance dramatically drops as fin number rises.

Figure 4.12 illustrates the thermal resistance relations that are developed for the number of fins of different inputs. The graphic shows that when the number of fins increases in all input heat, the thermal resistance decreases. In radial heat sinks, this increases the rate of heat transmission. Because of boundary layer overlap, the effective surface area grows as the overall surface area does. As a result, the low value of thermal resistance is caused by high input heat.

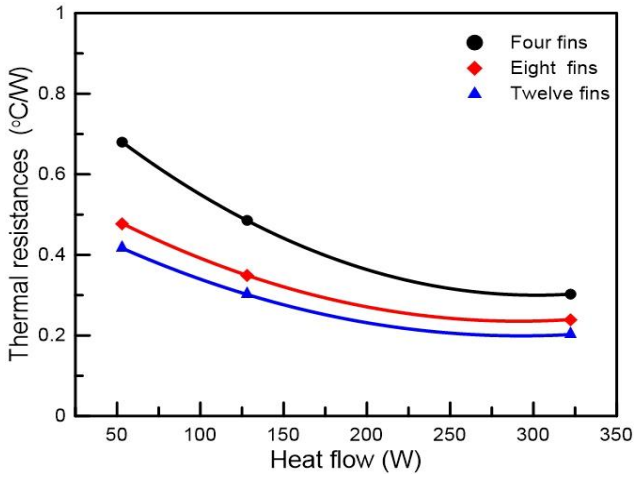

(a) case CS-0

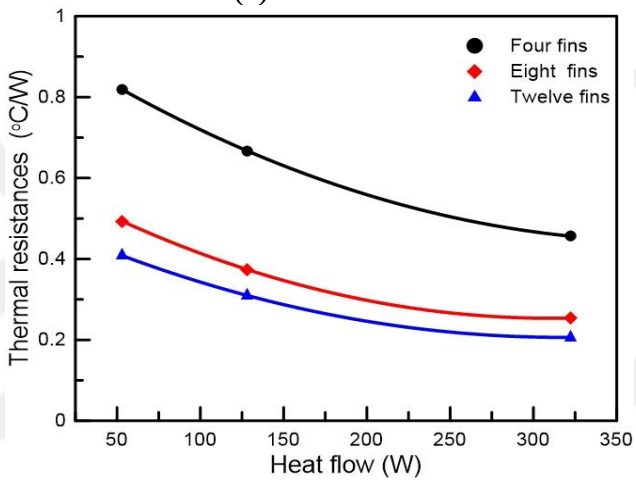

(b) case CS-40

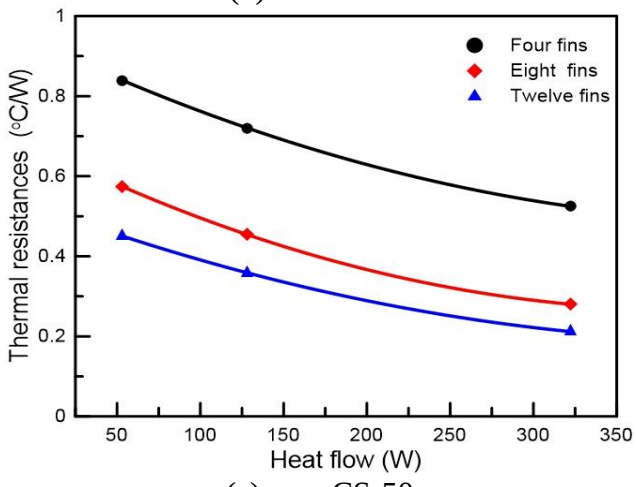

(c) case CS-50

Figure 4.11. Variation in thermal resistance at different fin counts and research scenarios as a function of heat flow.

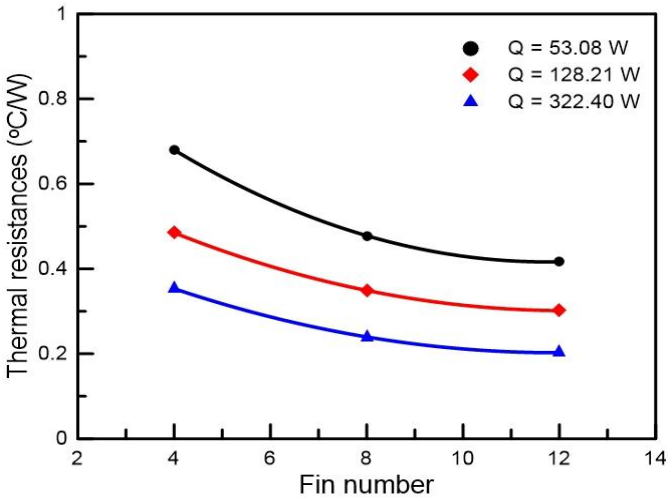

(a) case CS-0

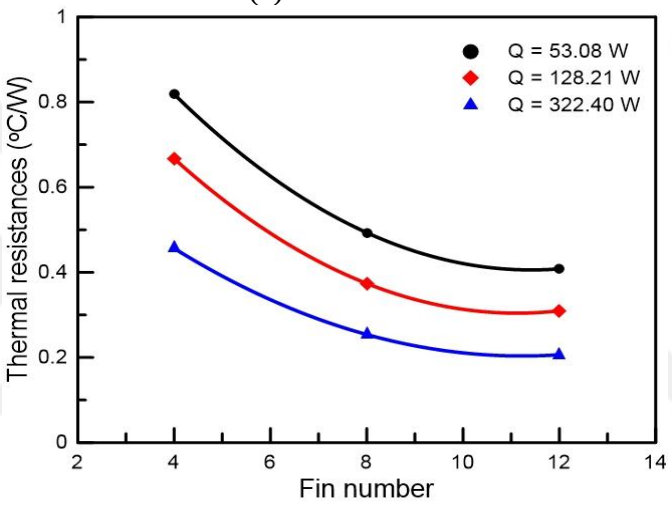

(b) case CS-40

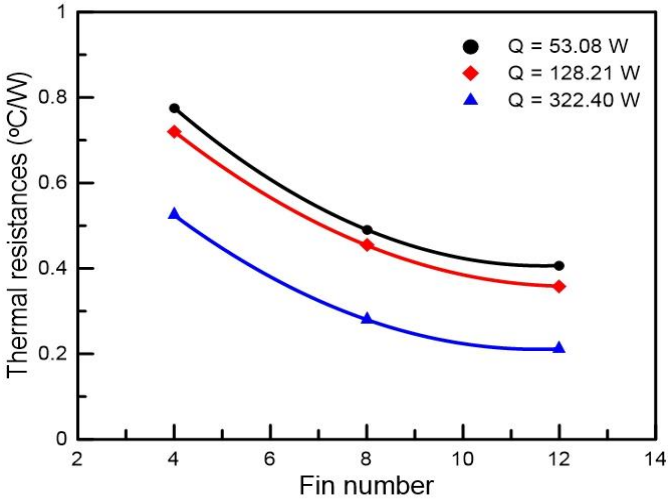

(c) case CS-50

Figure 4.12. Modulation in thermal conductivity under different input heat rates and research scenarios as a function of the Rayleigh number.

4.5. TEMPERATURE AND VELOCITY DISTRIBUTION

4.5.1 Temperature Contours

The temperature fields, or pattern plots of temperature contours (floods), are determined numerically from Figures 4.13 to 4.19. The isotherm floods were produced with eighteen levels, uniformly spaced from low (15 °C) to high (82 °C). The results showing heat flow's effect on temperature distribution at vertical fixed are displayed in Figure 4.13. Isotherms flood the temperature variations between hot (red) and cool (blue) airflow displayed in the figure. The low air temperature at the entrance, and the high air temperature that connects to the hot base cylinder surface. As expected, the cold air controller at the inlet and mid-region experiences a decrease in heat flows due to the high heat input flow in nearly all regions with high temperatures. Since heat is transferred by free convection, the same pattern may be observed in all input heat flow scenarios. The closely spaced isotherms on the fin base and cylinder surface show the maximum rate of heat transmission. The outermost layer forms along the surface, with high air temperature increasing vertically. The temperature distribution here is strongly influenced by the height along the surface, with high air temperature accumulating near the top.

Similarly, the design of the fins with different shapes as in Figures 4.14 to 4.16 had a clear effect on the increase in temperature. The figures show a side view of the resulting temperature level in the heat sink's bottom. The effect of fins design with different shapes on temperature distribution. The high temperature shows in the case SC-40, phenomenon because of the lower time air flow over fins and the heat sink base and low area contact. In the lower temperature shown in the case SC-0, This is due air flows over the material fins surface smoothly. Generally speaking, a larger heat transfer area and sufficient time for air to come into contact with fins increased the rate of heat transmission.

Figures 4.17 to 4.19 display the temperature distribution with orientation angles at 52, 128 and 322 W inlet heat flow, respectively. It is evident that as orientation angles grow, so does the temperature. At 12 fins, the temperature reaches its maximum at 30°.

This phenomenon is caused by the thermal boundary layer's prolonged contact with the fin faces and upper cylinder due to free convection heat transfer. An asymmetric temperature distribution results from the boundary layer forming at an angle when the system is tilted. The tilt angle determines the boundary layer's thickness. This behavior causes the heat transfer coefficient to rise in proportion to the orientation angle.; Figure 4.3 illustrates this outcome graphically.

Figure 4.20 displays the temperature distribution of the cylinder base with semi-circular fins with different input heat inputs at the 30-degree orientation for 12 fins. From the figure, it can be clearly seen that with the increase of input heat flow the temperature increases. The low temperature displayed in the end of semi-circular fin.

Using different fin numbers (4, 8, and 12) for the cases (SC-0, SC-40, and SC-50) at various input heat flow rates of 52, 128 and 322 W, respectively, Figures 4.21, 4.22, and 4.23 display the temperature profiles for cases (a, b, and c). Since the thermal boundary layer for case (a) in 4.21, 4.22, and 4.24 gradually expands from the base to the fins, the heat sink's midsection experiences the maximum thermal resistance, which raises the temperature in case (a). The small number of fins, or the small heat transfer area from the base to the fins, caused the maximum temperature for all figures to be at case (a). As a result, the temperature is excited at the base, raising the surface temperature, and then dissipating at the fin's end due to exposure to the surrounding air. In contrast, adding fins and mounting them on the heat sinks' bases for cases (b) and (c) of the three shapes helps to dissipate more heat, or more heat from the cylinder to the fins in a more efficient manner. As seen in Figures 4.21, 4.22, and 4.23, this has a favorable impact on the thermal profile and lowers the surface temperature in situations (b) and (c).

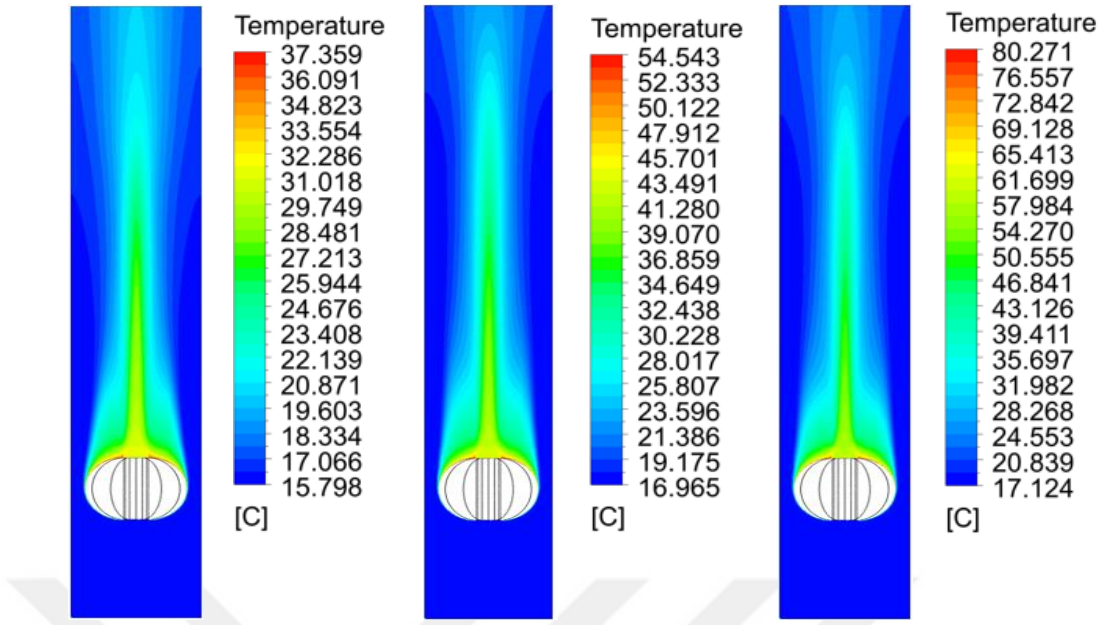

Figure 4.13. Temperature variation with different heat flow at the vertical system at 12 fins (a) 53 W, (b) 128 W, and (c) 322W

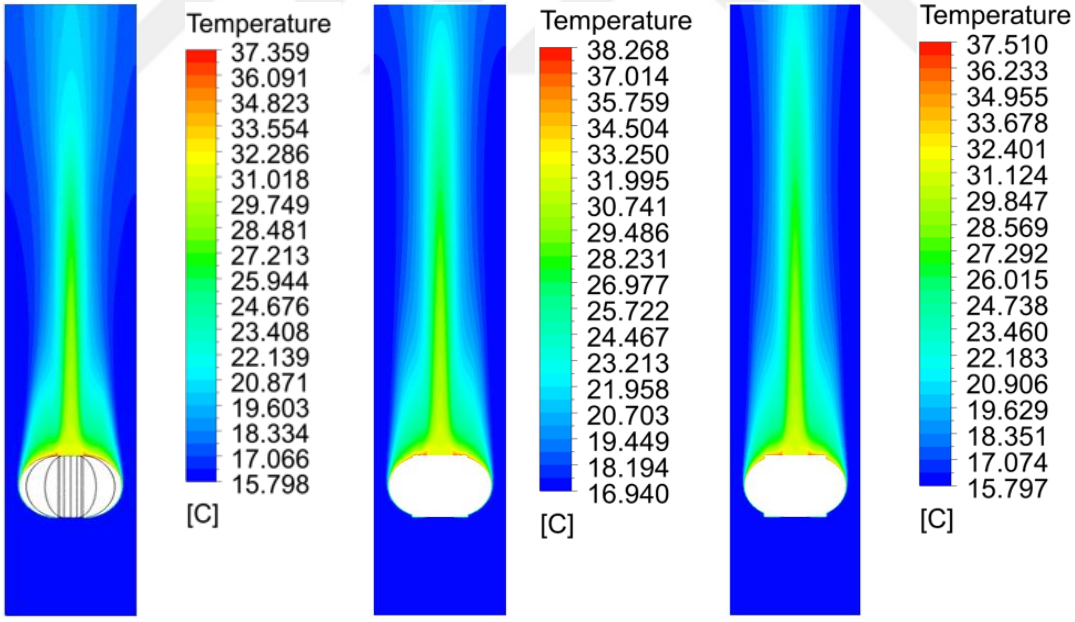

Figure 4.14. Temperature variation with different heat flow at vertical system at (angle zero for 53 W, 12 fins)

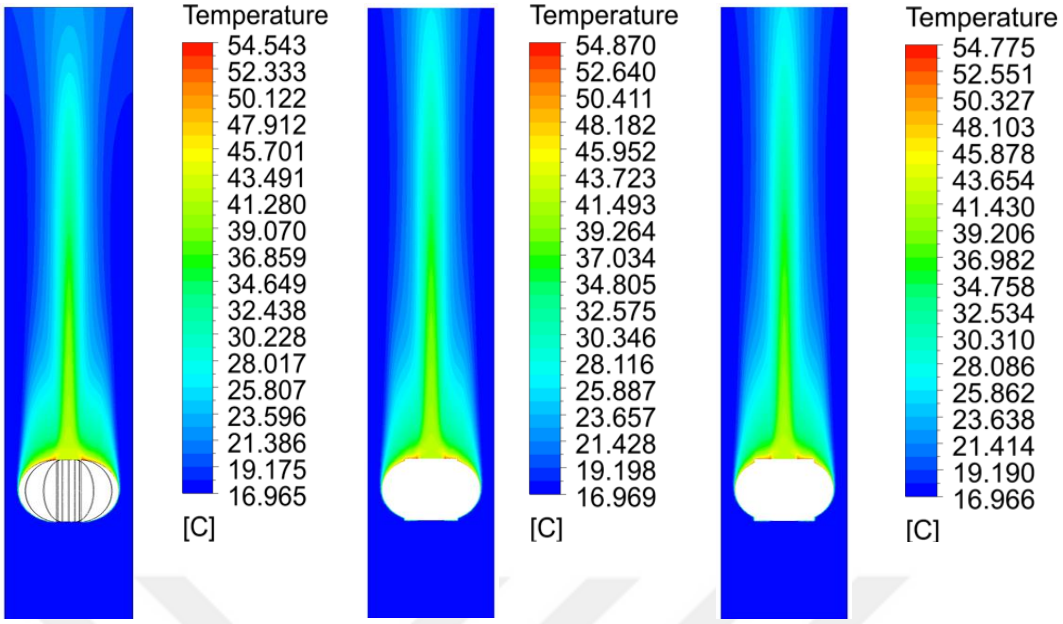

Case SC-0 Case SC-40 Case SC-50

Figure 4.15. Temperature variation with different heat flow at vertical system at (angle zero for 128 W, fin 12)

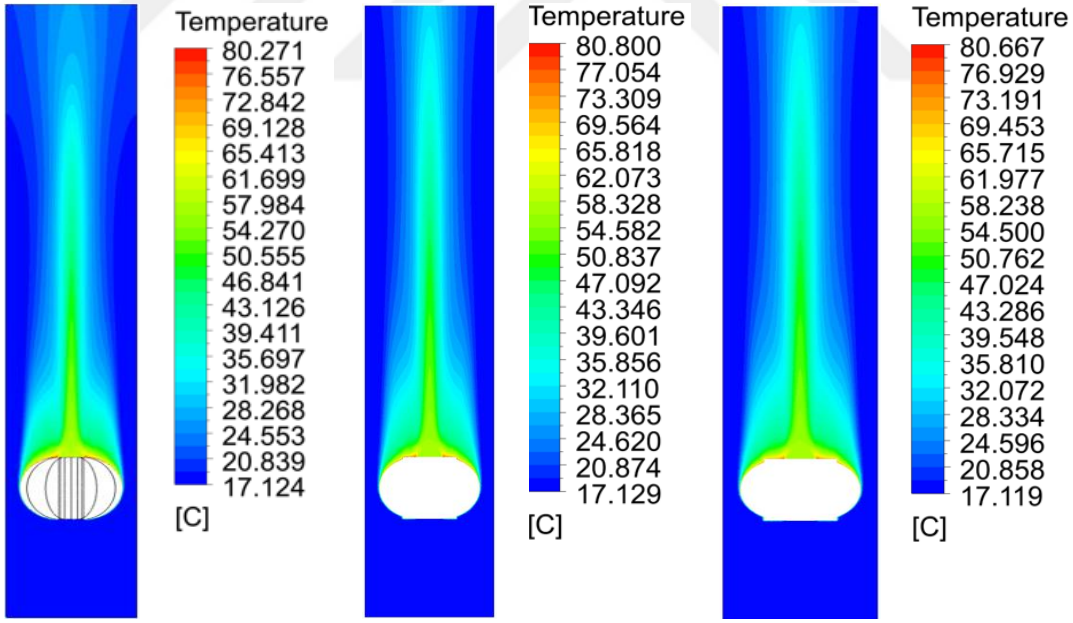

Case SC-0 Case SC-40 Case SC-50

Figure 4.16. Temperature variation with different heat flow at vertical system at (angle zero for 322 W, fin 12)

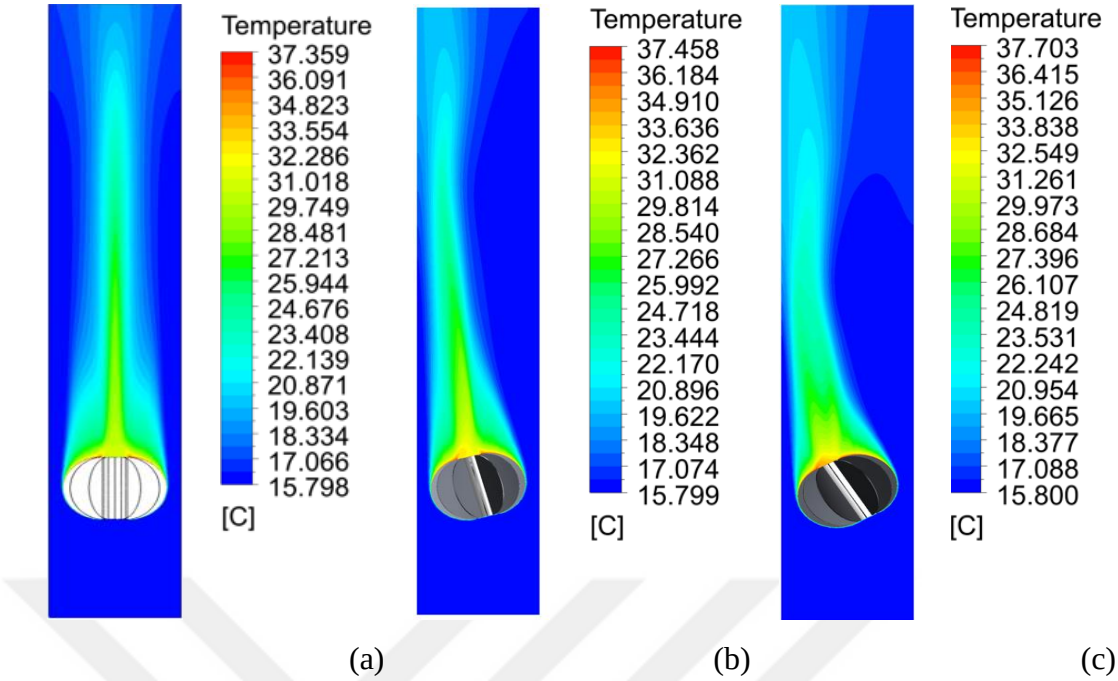

Figure 4.17. Temperature variation with different orientation at heat flow 52 W, (a) 0º, (b) 15º(c) 30º. (Case SC-0)

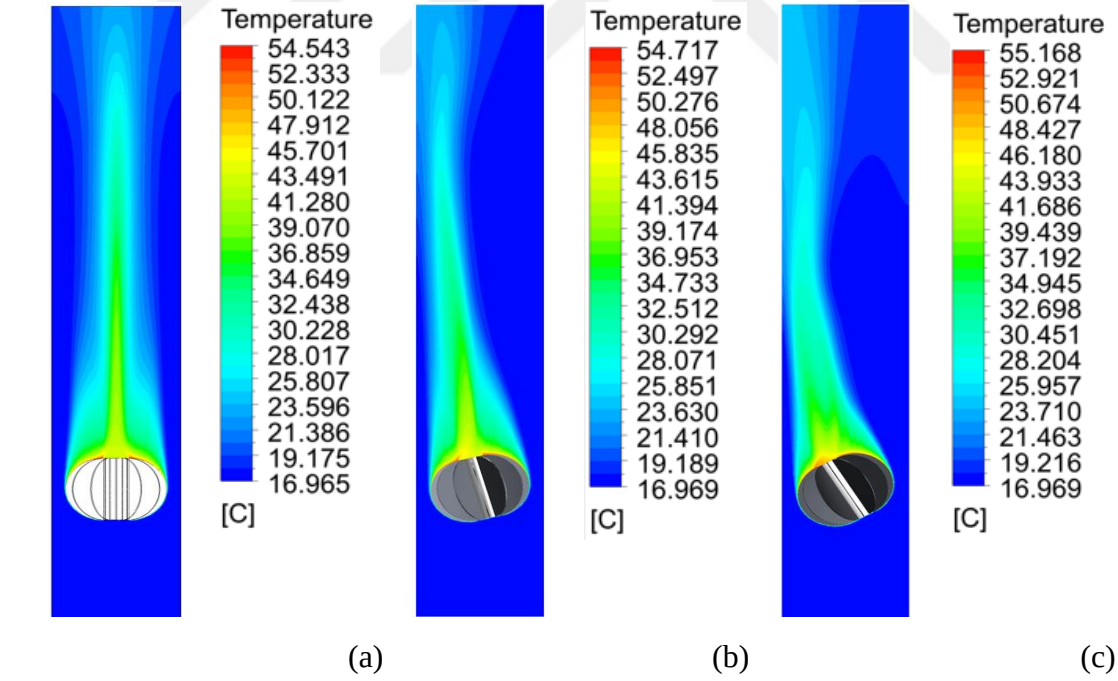

Figure 4.18. Temperature variation with different orientation at heat flow 128 W, (a) (a) 0º, (b) 15º and (c) 30º. (Case SC-0)

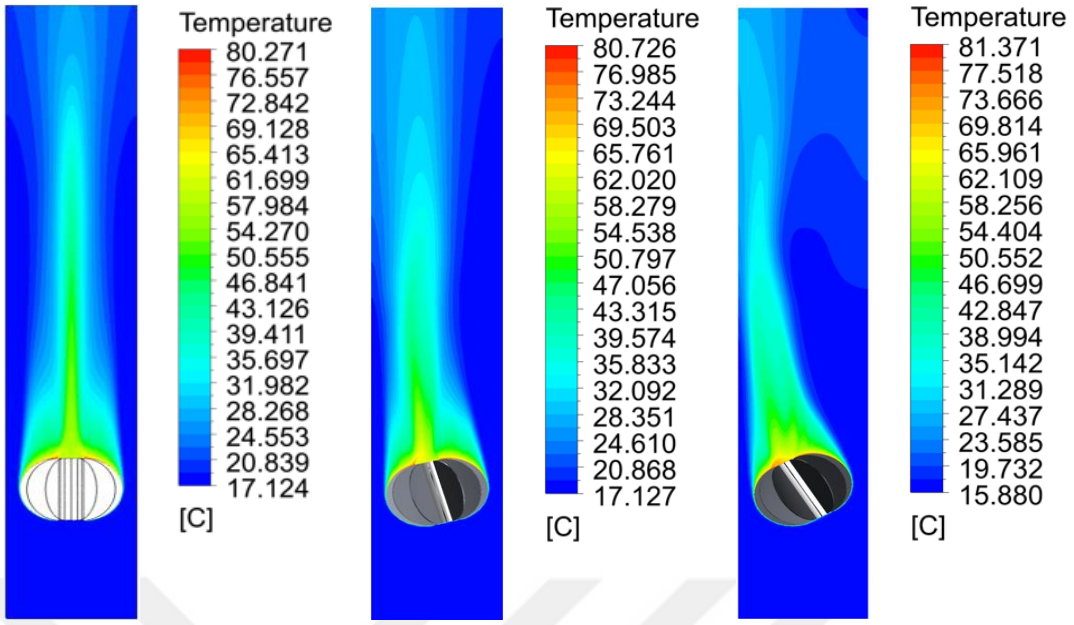

Figure 4.19. Temperature variation with different orientations at heat flow 322W, (a) 0º, (b) 15º and (c) 30º. (Case SC-0)

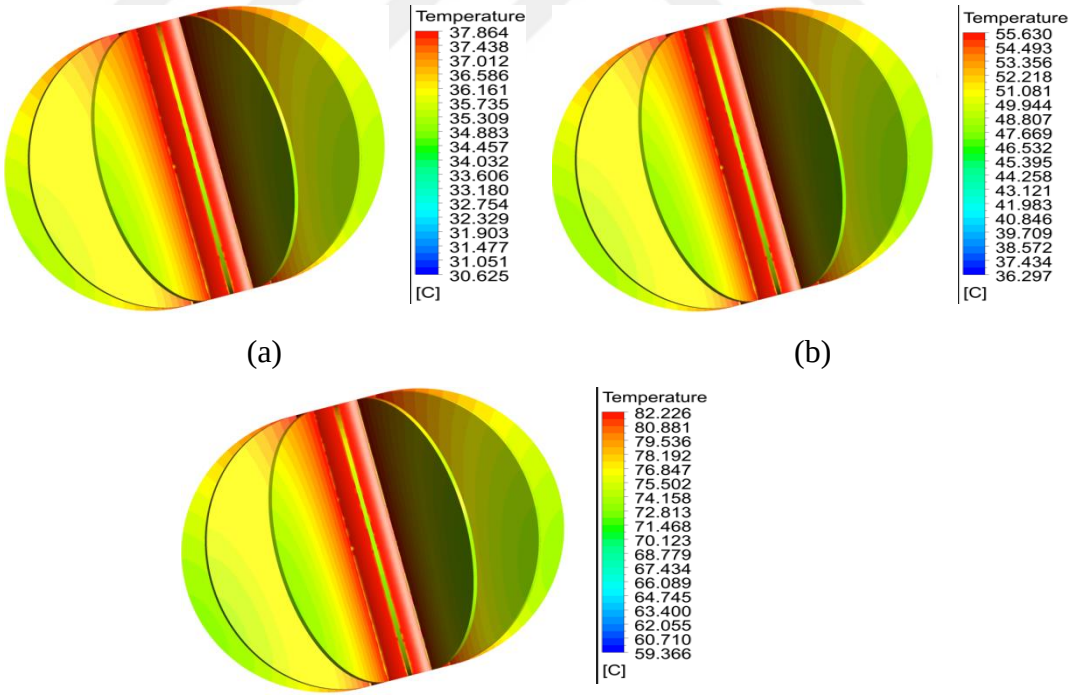

Figure 4.20. Temperature variation with different heat flow at 30-degree orientation (a) 53 W, (b) 128 W, and (c) 322W. (Case SC-0, for 12 Fins)

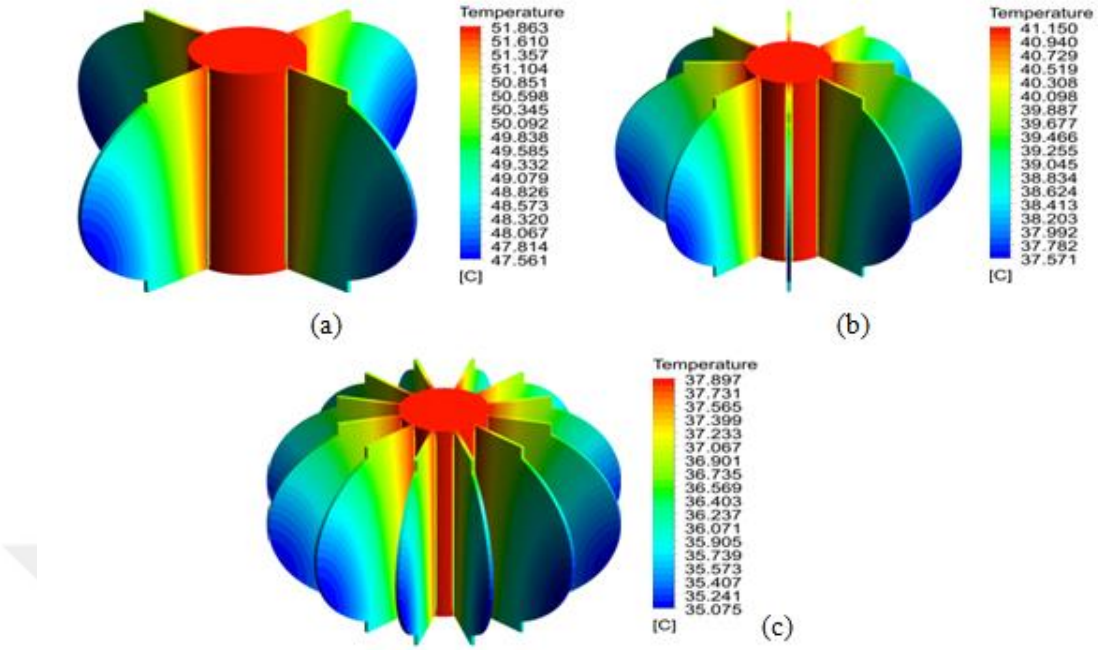

Figure 4.21. Temperature variation with different heat flow at at (0-degree, Q= 53 W). (a) 4 Fins (b) 8 Fins (c) 12 Fins. (Case SC-50)

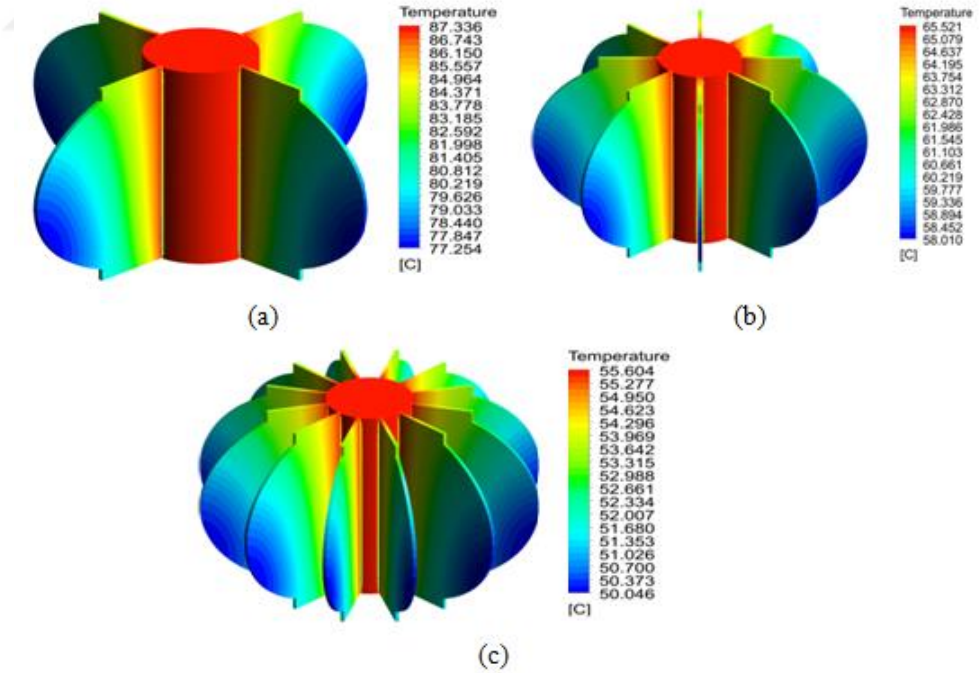

Figure 4.22 Temperature variation with different heat flow at at (0-degree, Q= 128 W). (a) 4 Fin (b) 8 Fin (c) 12 Fin. (Case SC-40)

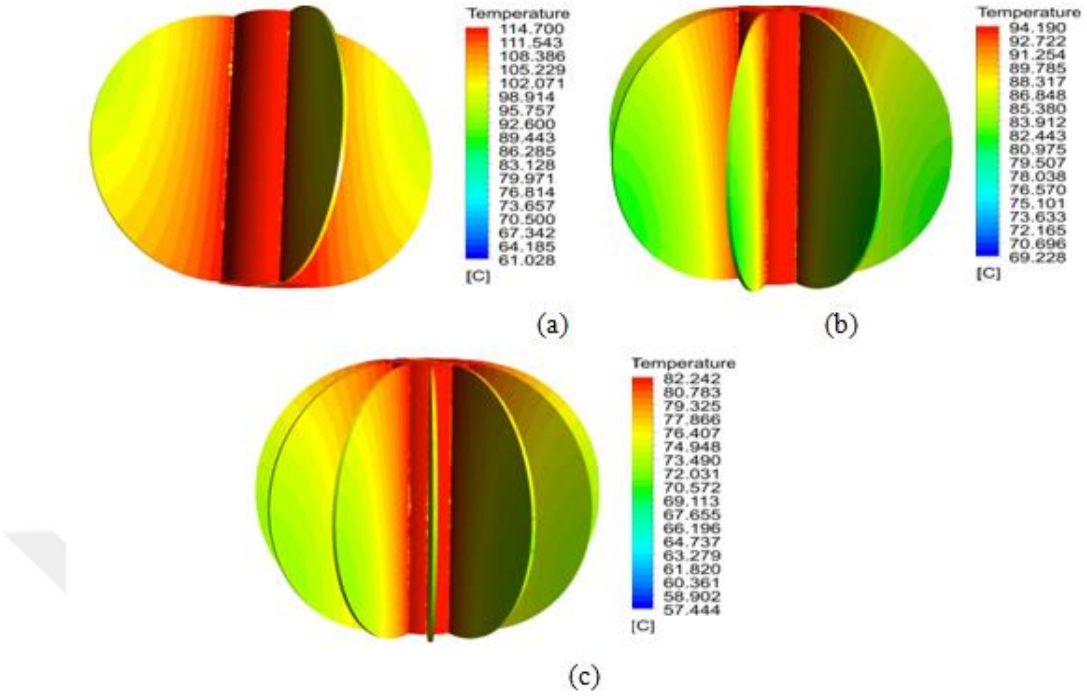

Figure 4.23. Temperature variation with different heat flow at (0-degree, Q= 322 W). (a) 4 Fins (b) 8 Fins (c) 12 Fins. (Case SC-0)

4.5.2. Velocity Contours

Figure 24 shows the velocity distribution and flow streamlines for the cases (Case SC-0, Case SC-40, Case SC-50) along with the flow directions on the middle plane x-y with input heat flow 332 W and 12 Fins. From the figures the high air velocity shows in case SC-50 the reasons because front air flow impact with fins for unstable of flow. in addition, the fins profile changes due to the increases in air velocity also the unstable of the air boundary layer with contact of a solid surface.

The airflow velocity with input heat flow for 0-degree orientation at 12 fins is shown in Figure 4.25. Additionally, it was observed that as the input heat flow increases, so does the temperature. The airflow velocity behavior was studied for the heat sink with three orientation angles (0, 15, 30 degrees) for input heat flow 332 W at 12 fins (case SC-0) as shown in Figure 4.26. It is clear that in any situation, the air velocity decreases as the orientation angle increases. The 0-orientation angle showed a greater airflow velocity value. The heat transfer coefficient increased in the heat sink examples of 15

and 30-degree orientations at 12 fins because the fins blocked the airflow. On the other hand, because the airflow flowed parallel to the fins at 0-degree orientation, there was little obstruction. In comparison to the 15 and 30-degree orientations, the heat transfer coefficient was found to be roughly 3.9% and 7.3% lower, respectively (see Figure 4.3).

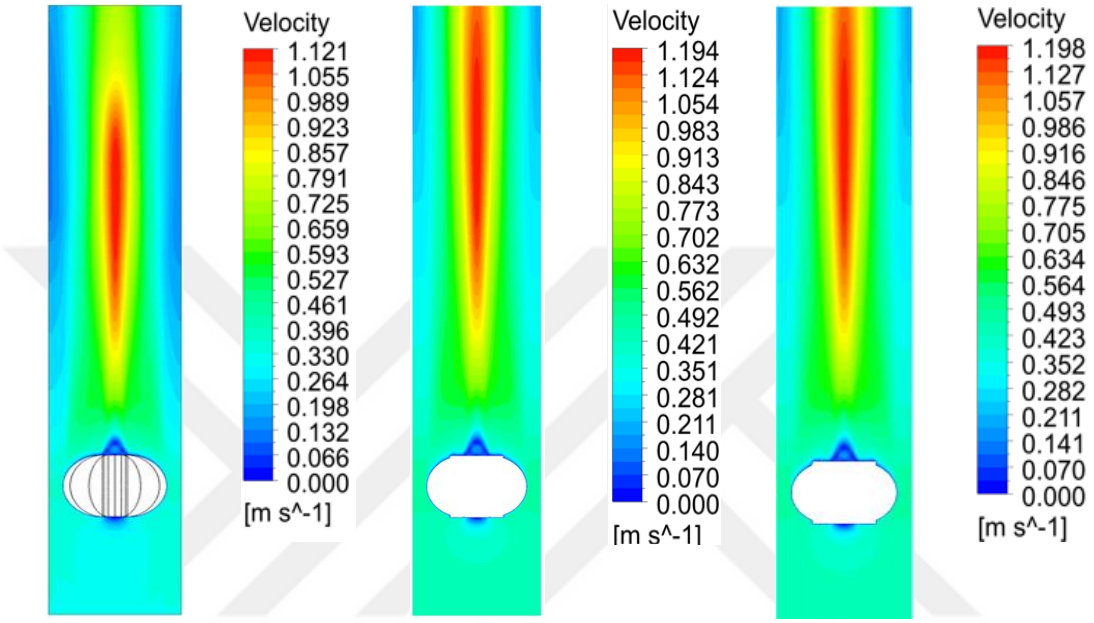

(a) (b) (c)

Figure 4.24. Velocity distribution with different orientation at input heat flow 332 W (a) zero degree, (b) 15 degree and (c) 30 degree. (Case SC- 0, Case SC - 40, Case SC-50)

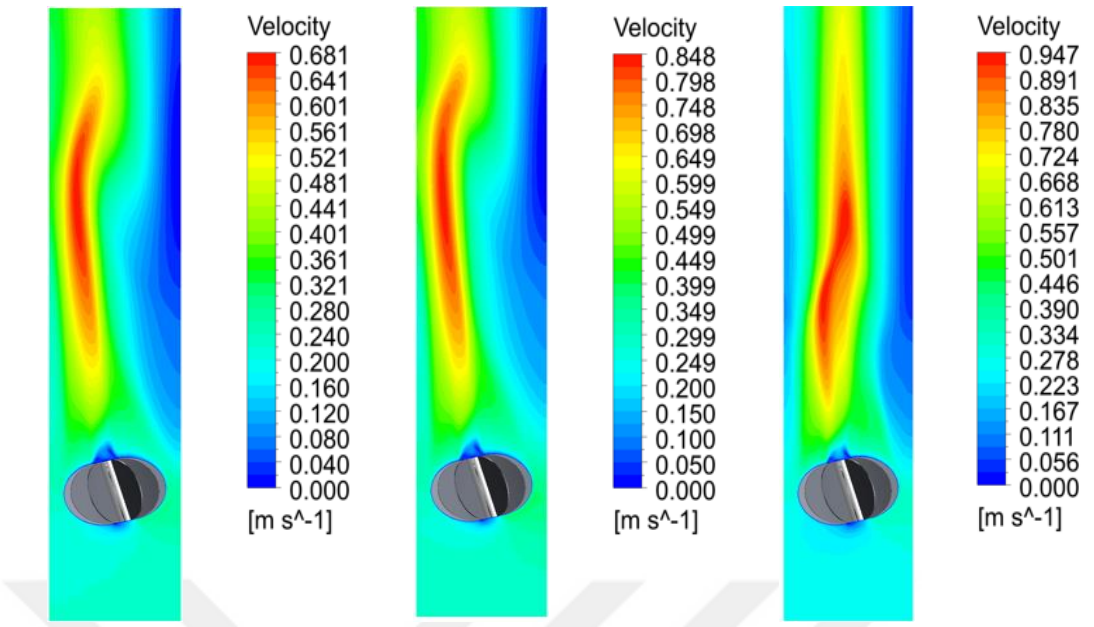

Figure 4.25. Velocity distribution with different heat flow at 15-degree (a) 53 W, (b) 128 W, and (c) 322W. (Case SC-0)

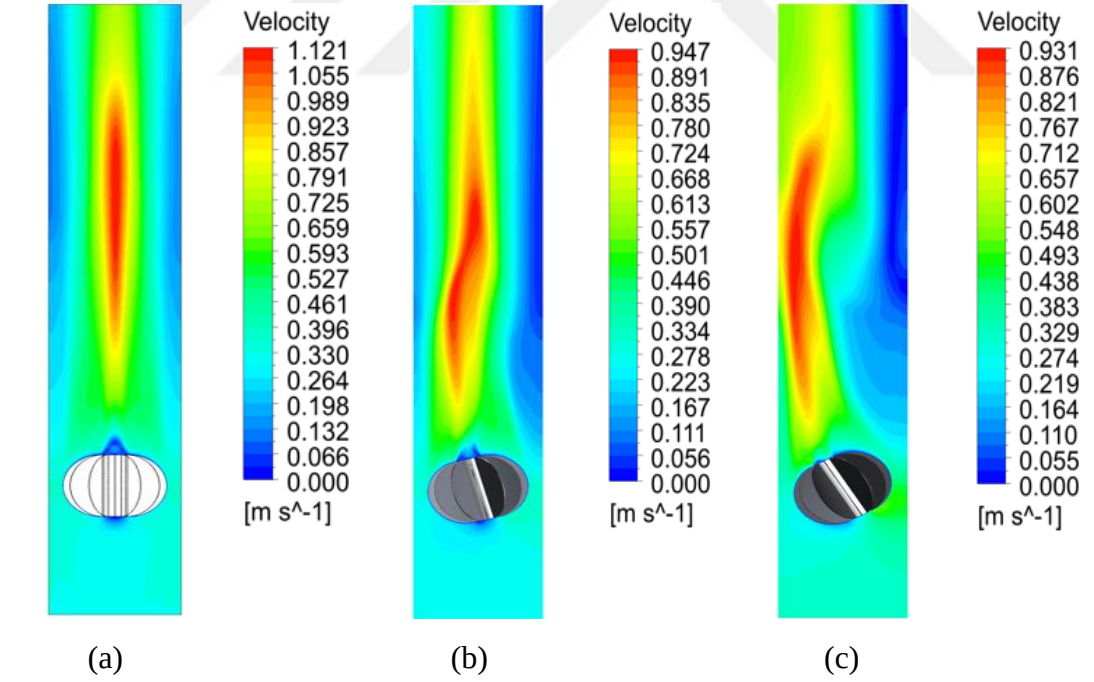

Figure 4.26. Velocity distribution with different orientation at input heat flow 332 W, (a) zero degree, (b) 15 degree and (c) 30 degree.(Case SC-0)

4.6. DESIGN OF EXPERIMENTAL RESULT

4.6.1. Experiment And Statistical Analysis

The output characteristics, including thermal resistance and Nu number, were recorded in Table 4.1. The results in Table 4.1 were then analyzed through the use of experimental design.

Table 4.1. The response data and the input parameter.

		Input factors		Response	
Std	**Run**	$Ra \times 10^6$	**Fin no.**	**Nu**	R_{th}
12	1	13.4	8	53.2	0.402
8	2	16.32	4	83.8	0.485
6	3	10.03	4	64.3	0.680
1	4	10.03	0	43.3	0.775
20	5	24.95	12	79.2	0.202
13	6	16.32	8	61.7	0.349
16	7	10.03	12	36.6	0.417
19	8	19.6	12	62.3	0.254
5	9	24.95	0	84.8	0.345
14	10	19.6	8	76.5	0.297
4	11	19.6	0	67.6	0.433
15	12	24.95	8	93.9	0.239
10	13	24.95	4	126.0	0.303
7	14	13.4	4	72.6	0.572
11	15	10.03	8	45.3	0.478
17	16	13.4	12	45.3	0.343
2	17	13.4	0	48.9	0.650
9	18	19.6	4	100.4	0.383
3	19	16.32	0	56.4	0.553
18	20	16.32	12	53.2	0.302

To determine the perfect conditions and get the highest heat transfer rates, a parametric experimental study in this work made use of the DOE technique's capabilities, particularly the GFD. The DOE suggested establishing a correlation between heat transport and important factors (Ra and fin numbers). These tests were designed and analyzed using Design-Expert-v.11 software, a well-used tool for various engineering purposes [100,101]. Analysis of variance (ANOVA), a statistical method frequently used in DOE, was used to assess the impact of input parameters on the experimental outcomes and investigate data variability. ANOVA takes into account a normal distribution of errors with constant variance and a zero mean. To use GFD models in this work, experimental data had to be gathered using a particular design. The D-optimal design generated a total of 20 tests using a minimum of 20 model points, five points that indicate lack of fit, five divides, and two-level factors (+1 for high and -1 for low). The practical ranges for the chosen parameters are shown in Table 4.2. The program was used to examine the computed thermal resistance and Nusselt number following the completion of 20 experiments.

Table 4.2. The identified parameters and their corresponding experimental ranges.

Parameter	**Ranges and levels**	
	-1	**1**
Rayleigh number (Ra)	$\mathbf{10.03 \times 10^6}$	$\mathbf{24.95 \times 10^6}$
Fins number	0	12

The residuals, or differences between the estimated and observed values, are examined in order to determine whether the model is adequate. First, as shown in Figure 4.27, the model adequacy check for the Nu number is shown in order to confirm the normality assumption. To provide a general idea of the normal distribution of errors, Figure 4.27a shows the normal % probability plot of residuals, in which the plotted dots generally align along a straight line. According to this ocular examination, the GFD shows no anomalies (R^2=98.15%). According to statistical research, the developed linear model based on GFD is statistically sound and appropriate for navigating the design space. Plotting studentized residuals against the run order, as illustrated in Figure 4.27b, solves the problem of externally studentized residuals, which is frequently encountered in conventional probability plots. The two lines above

and below the horizontal zero line represent the boundaries of an evenly distributed residual band. Outliers, or residuals outside of this range, are not shown in this representation, demonstrating that the experiments surrounding the zero residual line were appropriately randomized. This outcome demonstrates total error independence. The residuals' independence from other factors, including the expected response and run number, is also examined. The residuals' independence from a run number and an anticipated response is shown in Figure 4.27 (c) and (d), respectively. Interestingly, no observable trends support the residuals' independence. The correlation model for the empirical data is validated by these tests taken together.

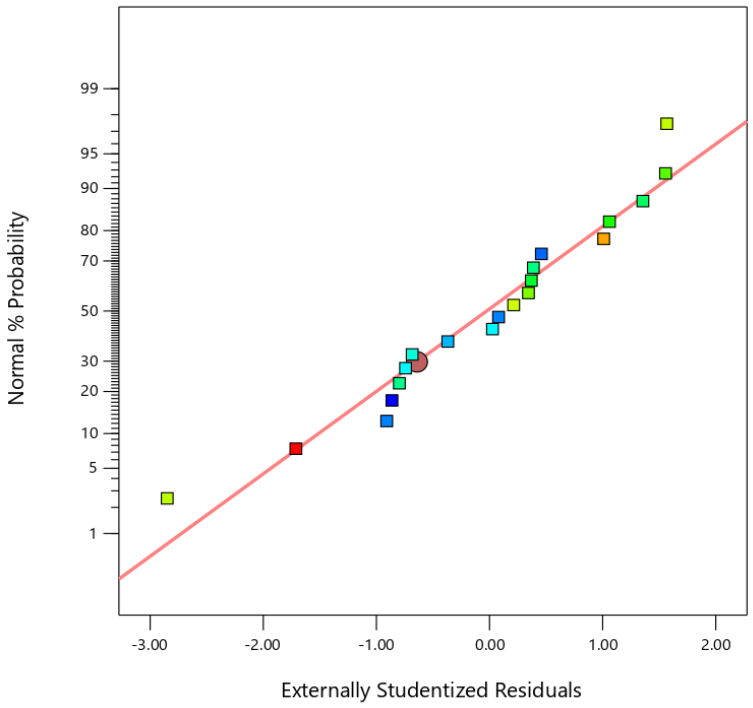

(a)

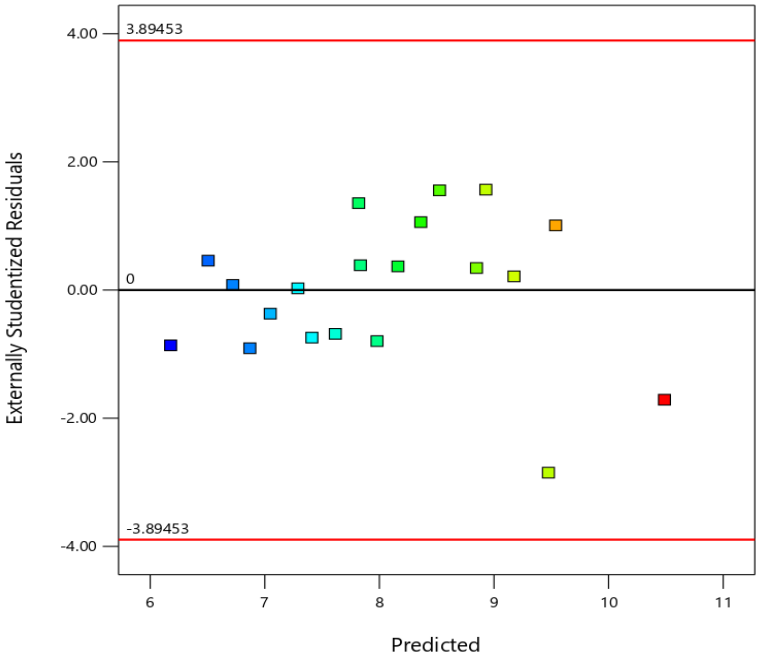
4.00
2.00
0.00
-2.00
-4.00
3.89453
0
-3.89453
Externally Studentized Residuals
6
7
8
9
10
11
Predicted

(b)

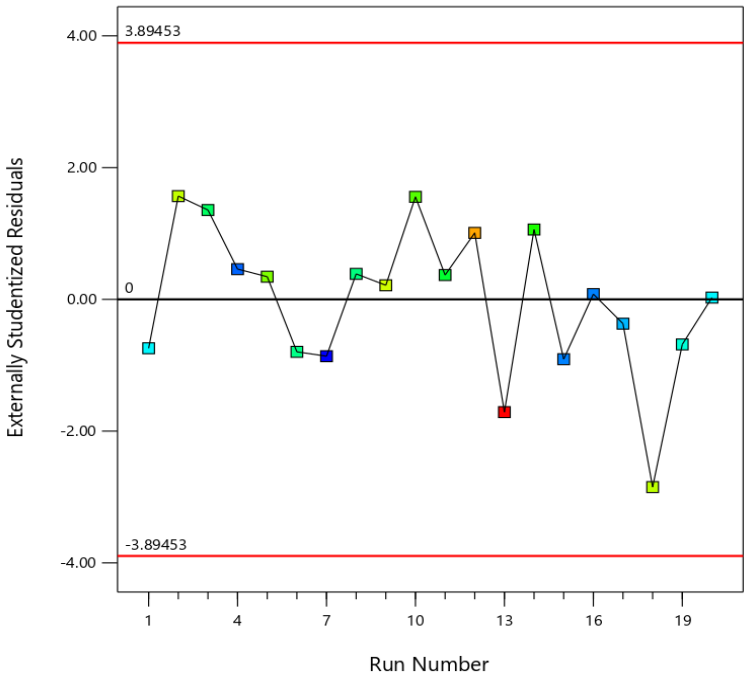
4.00
2.00
0.00
-2.00
-4.00
3.89453
0
-3.89453
Externally Studentized Residuals
1
4
7
10
13
16
19
Run Number

(c)

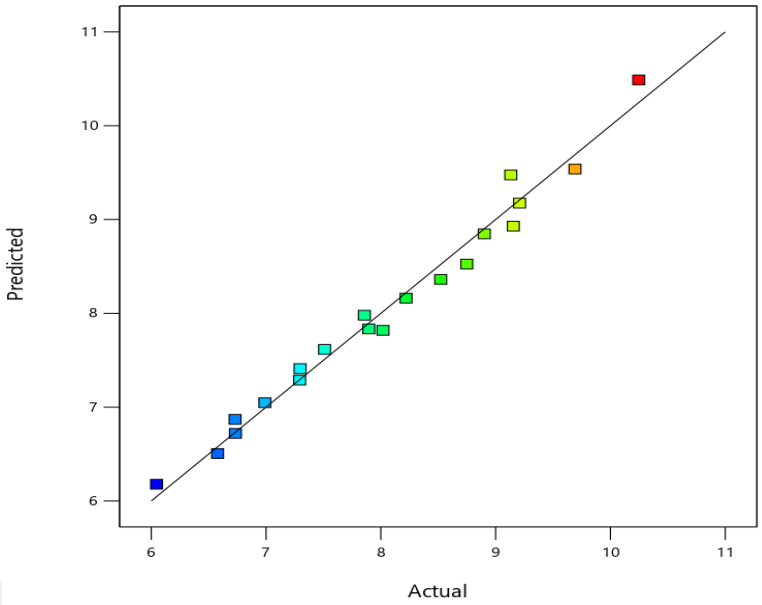

(d)

Figure 4.27. Tests of (a) the normal probability of residuals, (b) studentized residuals against expected, (c) the independence residuals on run, and (d) the actual value on predicted response are used to verify the model's appropriateness for Nu number.

Generated by the DOE goal. Through an examination of the actual value on the anticipated response, the studentized residuals vs. predicted, the independence residuals on run, and the normal probability of the residuals, Figure 4.28 illustrates the behavior of the model adequacy checking for Nu number.

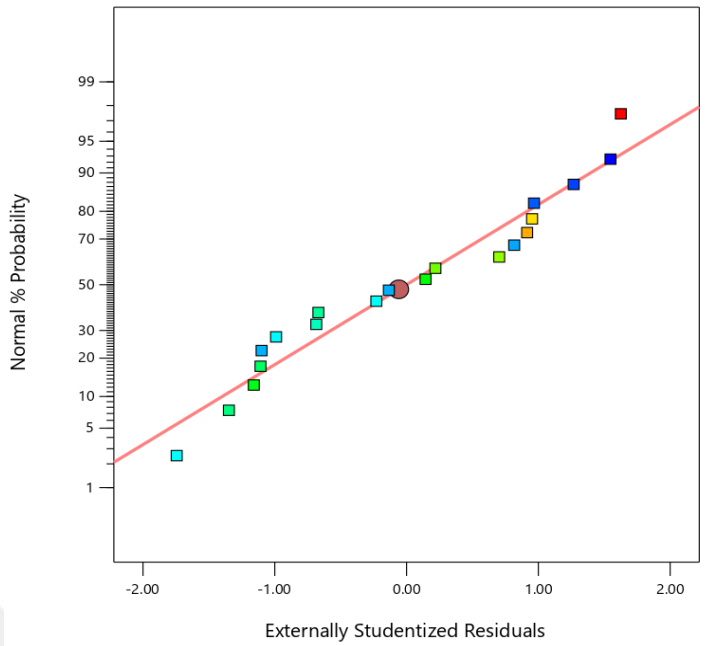
Normal % Probability
99
95
90
80
70
50
30
20
10
5
1
-2.00
-1.00
0.00
1.00
2.00
Externally Studentized Residuals

(a)

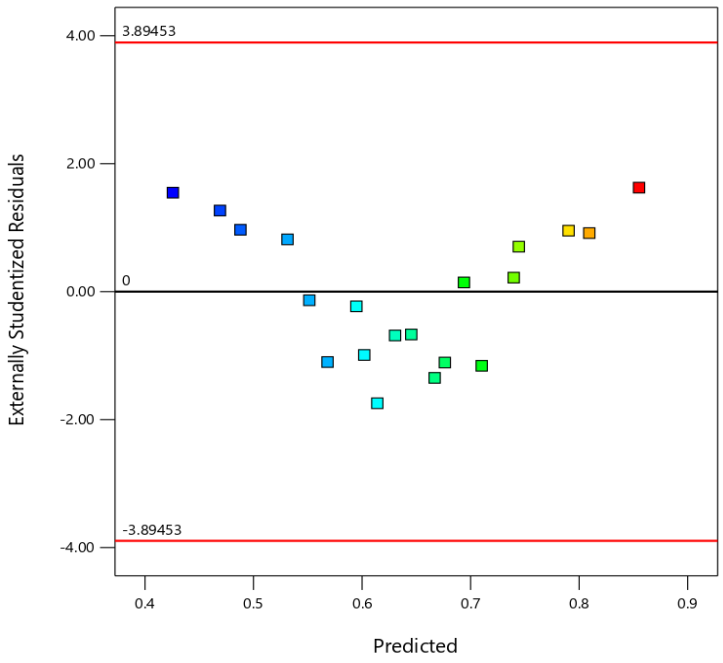
Externally Studentized Residuals
4.00
2.00
0.00
-2.00
-4.00
3.89453
0
-3.89453
0.4
0.5
0.6
0.7
0.8
0.9
Predicted

(b)

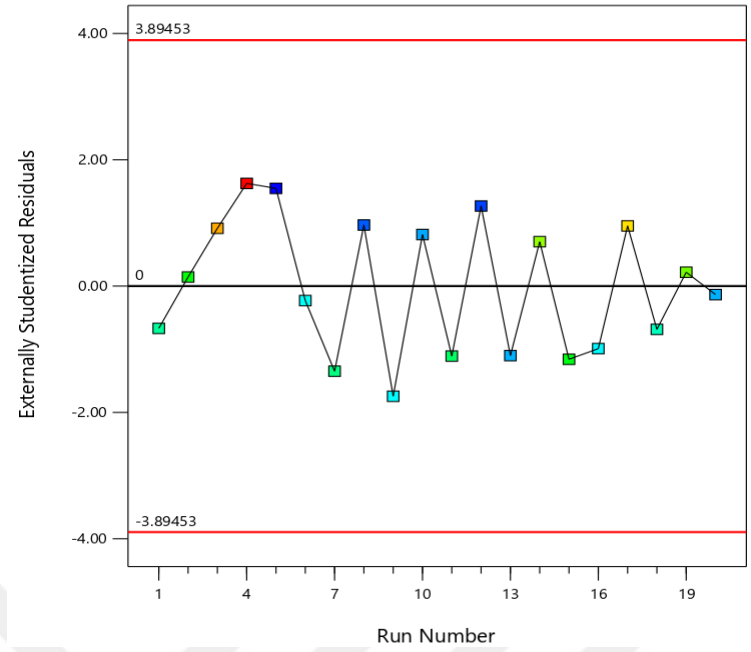

(c)

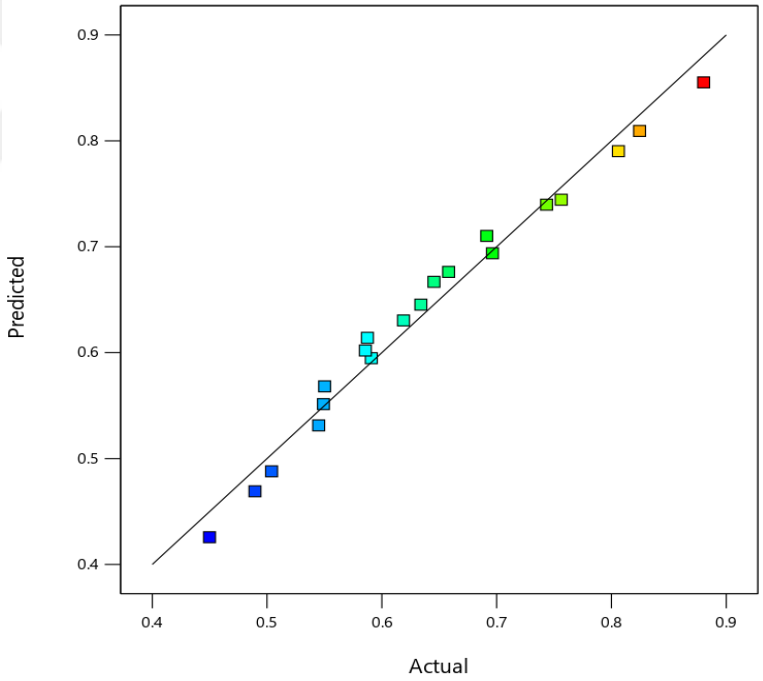

(d)

Figure 4.28. Testing (a) the normal probability of residuals, (b) studentized residuals versus expected, (c) the independence residuals on run, and (d) the actual value on predicted response are ways to verify the suitability of the model for thermal resistance.

The ANOVA results for radial semicircular fins using GFD are shown in Tables 4.3 and 4.4. The results, which were evaluated using a 95% confidence level or P-value of

0.05, show that any factor or their interactions with < 0.05 are significant, according to the ANOVA Table's rightmost column. Only the significant components and their interactions remained after the non-significant factors (defined as those with a P-value > 0.05) were eliminated from the study. A lack of fit with a P-value > 0.05 is not considered significant in the current model. All of the factors chosen for thermal resistance and Nu number, i.e., fins number and Ra number, are significant when the P-value is less than 0.05. The only meaningful association found in the semicircular radial fins model is between fins no., which is represented by heat flux, and Ra number. The quadratic terms of both components are also significant with a P-value <0.05 [100]. An ANOVA is used to calculate the F value, which is the ratio of the mean square error to the regression mean square. It is computed as the difference between the variation caused by mistake terms and the variance caused by factors influence and is sometimes referred to as the variance ratio. The influence of the variables looked at in the thermal resistance, Nu number, and investigations is also represented by the F value. A rise in the F value raises the significance of the components in the current study, as the ANOVA Tables show. The model's F-value of 91.12 indicates that it is significant. The likelihood that noise is the cause of this kind of large F-value is 0.01%. P-values less than 0.0500 indicate that the model's terms are significant. In this instance, the model terms A and B are important. If the value is more than 0.1000, the model terms are irrelevant. If a model has many unnecessary terms (aside from those required to preserve hierarchy), model reduction may improve the model. Furthermore, the Model F-value of 80.49 for thermal resistance suggests that the model is substantial. The value R^2 indicates that the variability of the wear model is 98.15% according to significant and non-significant factors. Since only major terms have an impact on adjusted-R^2, $R^2\geq$ adjusted-$R^2$is always influenced by adjusted R^2, and an appropriate model should have a difference between the two of less than 0.1, which also holds for the current analysis. Sufficient accuracy, which yields the signal-to-noise ratio, is another statistic used to evaluate the model. The ratio in this study is 34.7461, indicating that the model is sufficient; ideally, the ratio is more than 4. It demonstrates how accurate good modeling is. The following final equation, which was developed in terms of coded factors, was used to investigate how variables affected the Nusselt number.

$$[Nu]^{1/2} = 8.04 - 1.2A_1 - 0.6533A_2 - 0.0854A_3 + 0.4604A_4 - 0.3374B_1 + 0.9761B_2 - 0.026B_3 \quad (4\text{-}1)$$

The definitions of heat resistance formalized using the same process are as follows:

$$[R_{th}]^{1/2} = [0.6403 + 0.1201A_1 + 0.0552A_2 + 0.0046A_3 - 0.0588A_4 + 0.0948B_1 + 0.0489B_2 - 0.0502B_3]^2 \quad (4\text{-}2)$$

By applying the equation in terms of coded factors, it is possible to forecast the reaction for particular levels of each component in the aforementioned equations. Usually, the low values of the factors are generated as -1 and the high levels as +1. The relative influence of the components can be estimated using the coded equation by comparing the factor coefficients. Eq. (4.2) was taken into consideration for the examination of the various factors in the current study because all of the components in Eq. (4.1) are at the same level. The first constant, 8.04, represents the Nusselt number. Furthermore, the fins number-related negative value of -0.026 showed that the Nusselt number dropped as the fins number rose. The thermal resistance is represented by the first constant, 0.6403, in Eq. (4.2). Conversely, the fins number is shown by the negative data, -0.0502.

The value of λ for the models is 0.5. Figure 4.29(a) shows a plot of the Nusselt number, where λ is defined as 0.5. The optimum value for the case is 1.05, and the Nusselt number ranges from 0.34 to 1.67. For the thermal resistance, the optimum value is -0.33, with a range of approximately -0.47 to -0.19 as shown in Figure 4.29(b).

Table 4.3. Nu number pooled analysis of variance.

Source	Sum of squares	Degrees of freedom	Mean square	F-value	Prob.>F	
Model	24.530	7.0	3.500	91.120	< 0.00010	significant
Residual	0.46150	12.0	0.03850			
A-Ra	16.980	4.0	4.250	110.400	< 0.00010	
B-fin no.	7.540	3.0	2.510	65.400	< 0.00010	
Cor. total	24.990	19.0				
Standard deviation = 0.19610						
Mean = 8.04			$R^2 = 98.15\%$			
Coefficient of variation = 2.44%			R^2adjusted $= 97.08\%$			
Predict $R^2 = 94.87\%$			Adequate precision = 34.74610			

Table 4.4. Thermal resistance pooled analysis of variance.

Source	Sum of squares	Degrees of freedom	Mean square	F-value	Prob.>F	
Model	0.25570	7.0	0.03650	80.490	< 0.00010	signific
Residual	0.00540	12.0	0.00050	0		
A-Ra	0.14240	4.0	0.03560	78.480	< 0.00010	
B-Fin no.	0.11320	3.0	0.03770	83.170	< 0.00010	
Cor. total	0.26110	19.0				
Standard deviation = 0.02130						
Mean = 0.6403			$R^2 = 97.91\%$			
Coefficient of variation = 3.33%			R^2adjusted $= 96.70\%$			
Predict $R^2 = 94.21\%$			Adequate% = 31.8783			

The relationship between the Nu number, Ra number, and fins number is shown in Figure 4.30(a). As the fins number remains constant, it is evident that raising the Ra number also raises the Nu number. The greater temperature differential between the fin root and the surrounding air caused this trend. In addition, the thickness of the thermal boundary layer is reduced. Figure 4.30(b) shows the Nu number as a function of fins number. It is evident that when the fins number rises above four, the Nu number rises as well. This problem arises from a huge temperature differential between the fin and the sky, which causes the coefficient of heat transfer to drop for fin numbers more than four. The current thermal resistance, R_{th}, is shown in Figure 4.31(a) together with

the fins number and Ra number. Additionally, a downward trend is observed when the Ra number rises. The reduction in the temperature differential between the ambient and fin base is the reason. Figure 4.31(b) shows the corresponding profiles for R_{th} with fins no. As can be seen from the figure, R_{th} lowers as the fins number increases. This, in turn, causes the temperature differential to diminish as the base temperature drops.

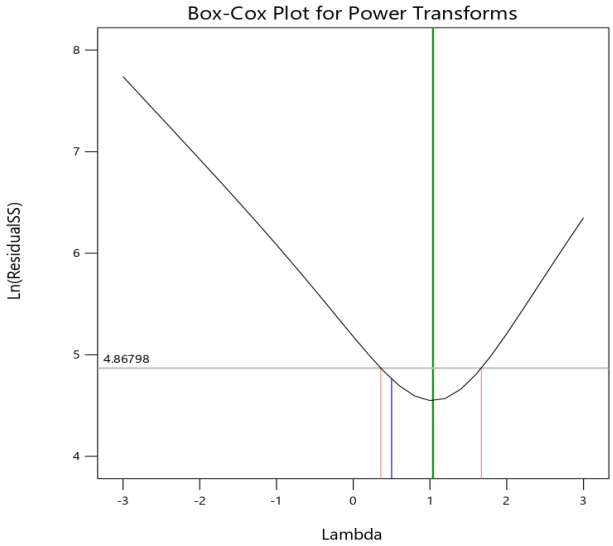

(a)

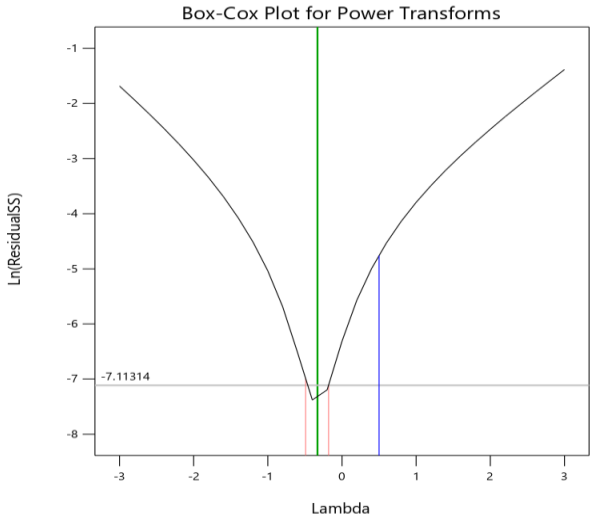

(b)

Figure 4.29. The box-cox diagram of the Log_{10} transfer function, (a) the Nusselt number, and (b) the thermal resistance.

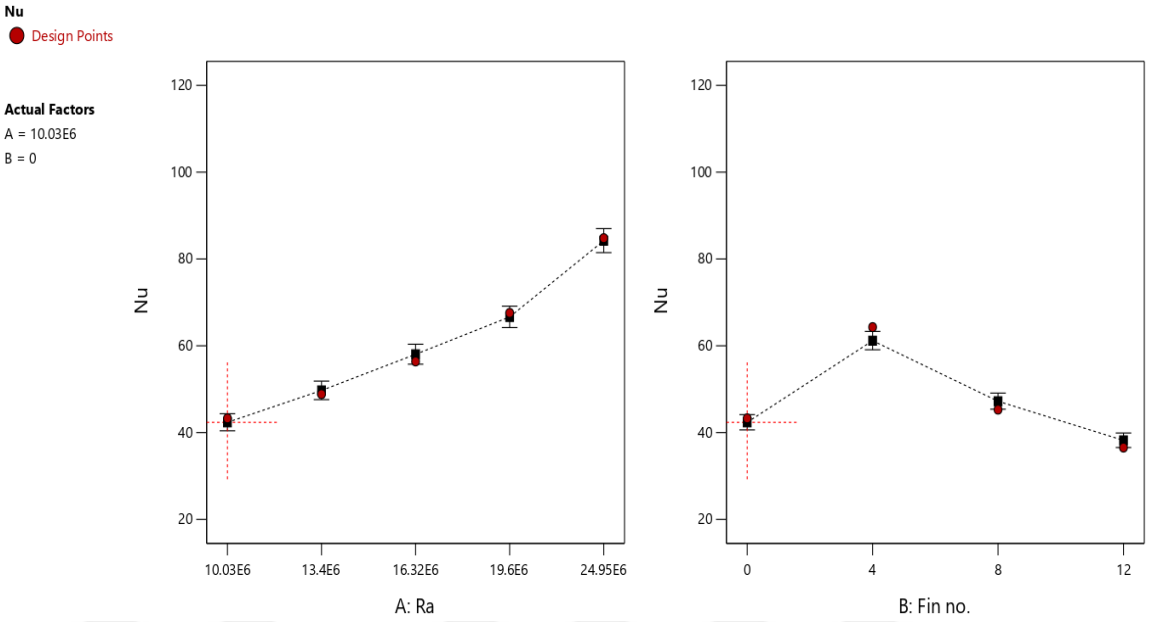

(a) (b)

Figure 4.30. Nu number fluctuation with (a) Ra number and (b) fin no.

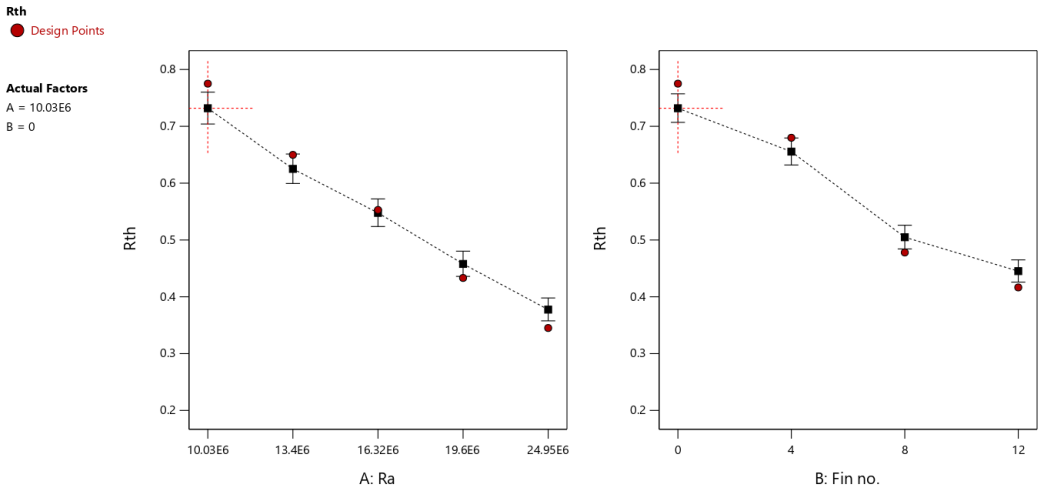

(a) (b)

Figure 4.31. The Ra number (a) and fins no (b) had an impact on the R_{th}.

The outcomes of the experimental tests and the predictions made by the current model are shown in Table 5.5. The slight inaccuracies found in the current model of the free convection heat transfer study in the semicircular fins—which range from 0.359 to 5.379% for thermal resistance and 5.89×10^{-4} to 1.52×10^{-2}% for Nusselt number—make it sufficient.

Table 4.5. There is an error between the experimentally determined value and the modelled value.

	(Nu) number				**(R_{th})**			
Run	**Act.**	**Pred.**	**Res.**	**Error (%)**	**Act.**	**Pred.**	**Res.**	**Error (%)**
1	7.30	7.410	-0.11490	0.015740	0.6340	0.64530	-0.01130	1.78230
2	9.150	8.930	0.22480	0.024570	0.69640	0.69390	0.00250	0.35890
3	8.020	7.820	0.19920	0.024840	0.82460	0.80940	0.01520	1.84330
4	6.580	6.510	0.07220	0.010970	0.88040	0.85520	0.02520	2.86230
5	8.90	8.850	0.05430	0.006100	0.44990	0.42570	0.02420	5.37890
6	7.860	7.980	-0.12290	0.015640	0.59080	0.59480	-0.00390	0.66010
7	6.050	6.180	-0.13230	0.021870	0.64540	0.66690	-0.02150	3.33120
8	7.90	7.830	0.06110	0.007730	0.5040	0.4880	0.0160	3.17460
9	9.210	9.170	0.03380	0.003670	0.58750	0.61410	-0.02660	4.52760
10	8.750	8.530	0.22350	0.025540	0.5450	0.53130	0.01370	2.51370
11	8.220	8.160	0.05830	0.007090	0.65820	0.67630	-0.01810	2.74990
12	9.690	9.540	0.15320	0.015810	0.48950	0.46910	0.02040	4.16750
13	10.250	10.490	-0.24130	0.023540	0.55020	0.56820	-0.0180	3.27150
14	8.520	8.360	0.16020	0.018800	0.75630	0.74450	0.01190	1.57340
15	6.730	6.870	-0.1390	0.020650	0.69140	0.71020	-0.01890	2.73350
16	6.730	6.720	0.01270	0.001890	0.58570	0.6020	-0.01630	2.78290
17	6.990	7.050	-0.05810	0.008310	0.80610	0.79030	0.01580	1.96000
18	9.130	9.480	-0.34290	0.037550	0.61890	0.63040	-0.01160	1.87420
19	7.510	7.620	-0.10620	0.014140	0.74350	0.73980	0.00380	0.51100
20	7.290	7.290	0.00430	0.000590	0.54910	0.55140	-0.00230	0.41880

$$E\% = \left|\frac{\text{Residu}}{\text{Actu}}\right| \times 100$$

4.7. THE EXPERIMENTAL MODIFIED CORRELATION

The functional form of the correlation is obtained from previous research in order to generate the correct Nu number correlation. The cylindrical heat sink is surrounded by both vertical and horizontal flows. In general, the vertical flow in an upward direction is produced by the buoyancy force in the heated fluid. The horizontal flow inward is

caused by fluid flowing from the surroundings to balance the vertical flow in the inner region. Consequently, the overall flow pattern seems to be horizontal surface fin array-like and is chimney-type [103]. The functional form of the (Nn) number correlation for the rectangular fin array on a horizontal surface serves as the first approximation in this investigation. According to [51], the Nn number correlation has the following functional form:

$$Nu_L = C\left(Ra_L \frac{A_{cross}}{LR}\right)^{n_1}\left(\frac{S_{ave}}{R}\right)^{n_2}\left(\frac{L}{R}\right)^{n_3} \quad (4\text{-}3)$$

where, $Ra_L A_{cross}/LR$, S_{ave}/R, and L/R represent the fin length, fin-to-fin distance, and dimensionless fluid velocity, respectively. This association holds for a rectangular fin array on a horizontal surface within the range of $2.63 \times 10^7 < Ra_L A_{cross}/LR < 1.11 \times 10^8$. Eq. (4.1) represents the average fin-to-fin separation (S_{ave}), the cross-section area of airflow (Across), and Rn number.The A_{cross}, and S_{ave} are given, accordingly, Regarding the vertically oriented cylindrical heat sink with a semi-cir fins.

$$\left.\begin{aligned} A_{\text{cross}} &= \pi(D/2+R)^2 - \pi(D/2)^2 \\ S_{ave} &= \pi(D+R)/N - t \end{aligned}\right\} \quad (4\text{-}4)$$

The empirical values of C, n_1, n_2, and n_3 that match the Nn number determined from the experimental data are produced using a least-squares fit and are displayed in Table 4.6.

Table 4.6. The coefficients that exist in Eq. (4-1).

Coefficien	**CS-0**	**CS-40**	**CS-50**
C	3.4830	2.1260	1.2520
$\boldsymbol{n_1}$	0.766	0.673	0.861
$\boldsymbol{n_2}$	0.394	0.120	0.128
$\boldsymbol{n_3}$	4.306	1.978	1.733
$\boldsymbol{R^2(\%)}$	97.234	94.917	91.818

While the former requirement is not met, Eq. (4.1) satisfies the latter. To meet both requirements, the correlation in the current study was changed as follows [98]:

$$Nu_L = C\left(Ra_L \frac{A_{cross}}{LR}\right)^{n_1}\left(0.5 + \frac{1000}{n_2}\left(\frac{S_{ave}}{R}\right)^{n_3}\right)^{-1}\left(\frac{L}{R}\right)^{n_4} \quad (4-5)$$

Using to the least-square fitting method, the updated correlation, as shown in Table 4.7, best fits the Nn number derived from the experimental data when the actual coefficients are provided as.

Table 4.7. The coefficients of the Eq. (4 - 3).

Coefficient	CS-0 case	CS-40 case	CS-50 case
c	12.5650	6.9630	6.6850
n_1	0.766	0.673	0.861
n_2	16.364	17.434	8.579
n_3	0.394	0.120	0.129
n_4	8.391	6.018	5.862
R^2(%)	98.015	95.581	93.553

The Nusselt values for the cylinders with semi-circular fins derived from the experimental data are compared with Eq. (4 - 5) in Figure 4.32. According to Figure 4.32, the adjusted Nn number correlation is in good agreement with the experimental data, with an error of ±5% in the CS-0 and CS-40 instances and approximately ±10% in the CS-50 case [104].

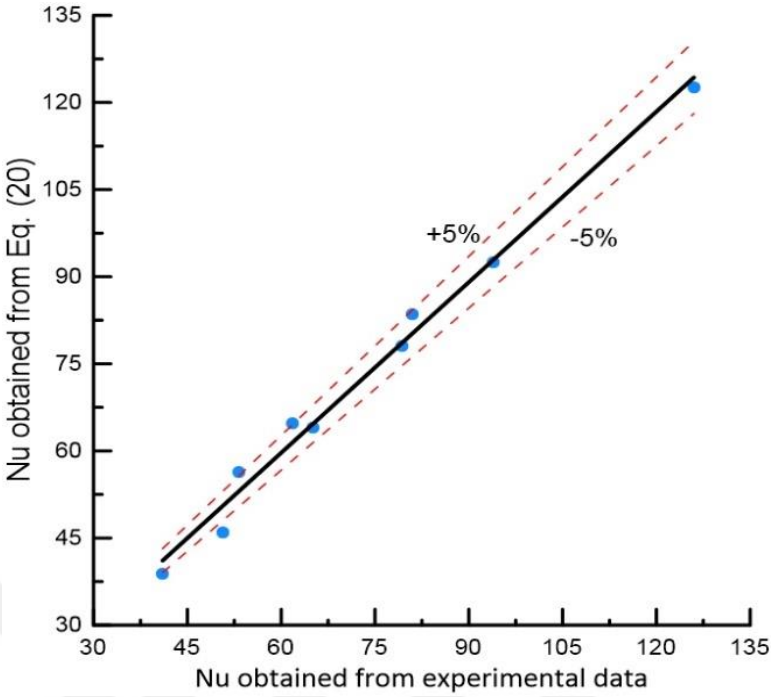

(a) case CS-0

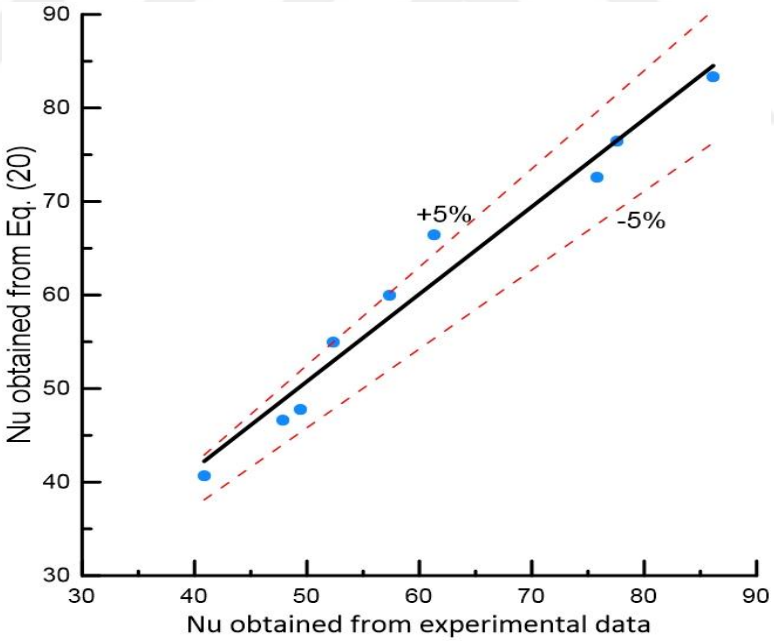

(b) case CS-40

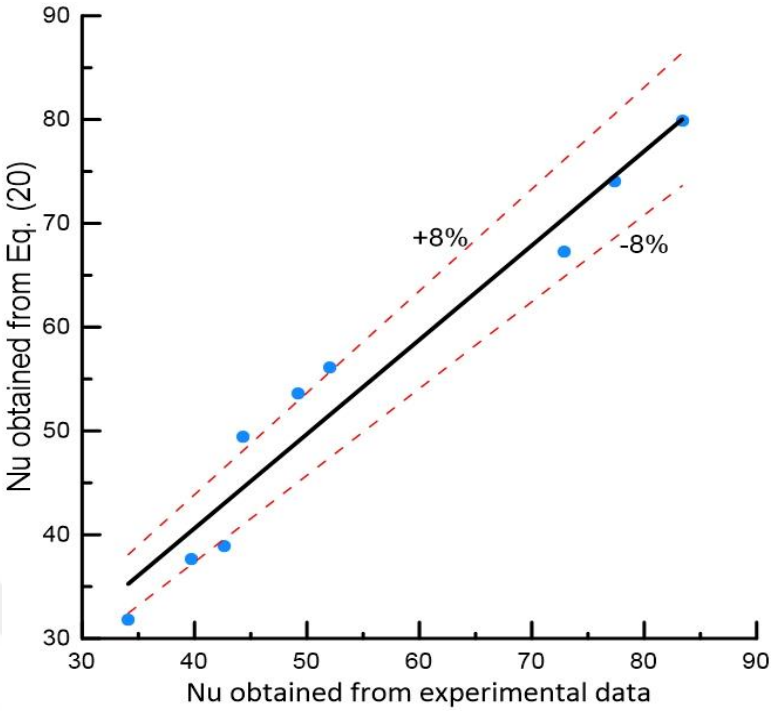

(c) case CS-50

Figure 4.32. Nn number computed using the improved correlation and those derived from the experimental data are compared.

CHAPTER FIVE

CONCLUSIONS AND RECOMMENDATION

The analysis of a semicircular finned heat sink under free convection was conducted using both computational and experimental techniques. The experimental work involved three circular fin shapes (CS-0, CS-40, and CS-50) with varying input heat while the system was positioned vertically. Furthermore, there were differences in the number of fins between the three conditions (4, 8, and 12). Preliminary results are described in this thesis, along with suggestions for further research to build on the current work.

5.1. CONCLUSIONS

The following conclusions are drawn:

- For every case studied the Nu number increased as the Ra number value climbed, and R_{th} fell as the Ra number increased.
- As the fins increase in height, there is a noticeable drop in temperature, which is always greater than with an increase in the number of fins.
- The 0^o orientation exhibited the highest airflow velocity but lower heat transfer efficiency due to minimal airflow obstruction. The 30^o orientation demonstrated the higher the fin height, the greater the drop in temperature., characterized by increased temperature and maximized Nu numbers.
- It was observed that the heat transfer coefficient at temperature 0^o orientation was 3.9% to 7.3% lower than at the 15^o and 30^o orientations due to reduced airflow obstruction.
- The most appropriate and applicable transfer function, i.e., 98.15%, 97.08%, 94.87%, and 2.44%, respectively, for Nu number and 97.91%, 96.70%,

94.21%, and 3.33%, respectively, for thermal resistance, was determined in this study using R^2, Adjusted-R^2, Predicted-R^2, and C.V(%) as selection criteria.

- The present model's predictions and the findings from the confirmation tests closely matched each other, with errors ranging around 0.00059% to 0.03755% for the Nu number. For the thermal resistance, the range was about 0.359% and 5.379%.
- The results of the validation tests corresponded to the predictions of the current model, with errors for the Nu number ranging from about 0.00059% to 0.03755%. The range for the R_{th} was somewhere between 0.359% and 5.379%.
- Variance analysis of variation (ANOVA) was used to estimate the performance-predicted parameters and calculate the coefficient of correlation.
- With an inaccuracy of less than ±5%, the correlation that was established for the Nu number based on experimental data demonstrated good agreement with actual experimental data.
- The temperature difference between CFD simulations and experiments was within ±4.9%, validating the numerical model.

5.2. RECOMMENDATIONS

Further study should carry out the following to build on the successes of the existing work:

- Investigate the heat transfer performance of the same design under forced convection.
- Examine the same fins with perforations.
- Analyze the effect of adding foam material to the fin surface.
- Study how altering the fin shape affects the efficiency of heat transfer.
- Evaluate the same fin design using different fin materials.

REFERENCES

1. Çengel, Y. A. and Ghajar, A. J., "Heat and mass transfer fundamentals & applications 5th ed"., *Mc Graw Hill*, New York (2015).

2. Shah, Ramesh K., "Extended surface heat transfer". *In Thermopedia*. Begel House Inc (2011).

3. Može, Matic, Aljaž Nemanič, and Primož Poredoš. "Experimental and numerical heat transfer analysis of heat-pipe-based CPU coolers and performance optimization methodology". *Applied Thermal Engineering*.,179: 115720 (2020). .

4. Bejan, Adrian. *Convection heat transfer*., John wiley & sons (2013).

5. Schnurr, N. and Cothran, C. "Radiation from an array of gray circular fins of trapezoidal profile". *AIAA Journal*., 12(11), 1476-1480 (1974).

6. Aziz, A. "Advanced heat conduction theory with a symbolic algebra package". *Computational methods.* Springer ., 829-48 (2006).

7. T. L. Bergman, A. S. Lavine, F. P. Incropera and D. P. Dewitt., "Introduction to heat transfer sixth ed"., New York, USA: John Wiley & Sons (2011).

8. Shariati, V., Ahmadian, M. H., and Roohi, E., "Direct simulation monte carlo investigation of fluid characteristics and gas transport in porous microchannels"., *Scientific reports.*, 9(1), 17183 (2019).

9. Kraus, A., "The efficiency of a transistor cap as a heat dissipater"., *The 2nd National Heat Transfer Conference*, ASME Chicago, IL., Pp. 1-15 (1958).

10. Webb, R. L. and Kim, N. H., Principle of enhanced heat transfer 2nd ed". New York, USA: *Taylor & Francis* (2005).

11. Garimella, S. V., Fleischer, A. S., Murthy, J. Y., Keshavarzi, A., Prasher, R., Patel, C, Bhavnani, SH, Venkatasubramanian, R. M., and Ravi Joshi, Y., "Thermal challenges in next-generation electronic systems"., *IEEE Transactions on Components and Packaging Technologies*, 31(4), 801-815 (2008).

12. Stellman, J. M., "Encyclopedia of occupational health and safety 4th ed"., *International Labour Organization*, Geneva, Switzerland (1998).

13. Lee, S., "Optimum design and selection of heat sinks"., *IEEE Transactions on Components, Packaging, and Manufacturing Technology A*, 18(4), 812-817 (1995).

14. Faghri, A., and Zhang, Y., "Transport phenomena in multiphase systems"., *Burlington*, USA: Elsevier Inc (2006).

15. Kraus, A. D., Aziz, A., Welty, J., and Sekulic, D. P., 'Extended surface heat transfer"., *Appl. Mech. Rev.*, 54(5), B92-B92 (2001).

16. Elshafei, E., "Natural convection heat transfer from a heat sink with hollow/perforated circular pin fins"., *Energy*, 35(7), 2870-2877 (2010).

17. Enescu, D., "Thermoelectric energy harvesting: basic principles and applications". *Green Energy Advances*, 1-20 (2019).

18. Bejan, A., and Kraus, A. D. "Heat transfer handbook"., *New Jersey*, USA: John Wiley & Sons, Inc (2003).

19. Bergles, A., "The implications and challenges of enhanced heat transfer for the chemical process industries"., *Chemical Engineering Research and Design*, 79(4), 437-444 (2001). .

20. Shaeri, M., and Yaghoubi, M., "Thermal enhancement from heat sinks by using perforated fins". *Energy Conversion and Management*, 50(5), 1264-1270 (2009).

21. Sahin, B., and Demir, A., "Performance analysis of a heat exchanger having perforated square fins". *Applied Thermal Engineering*, 28(5-6), 621-632 (2008).

22. Alam, M. W., Bhattacharyya, S., Souayeh, B., Dey, K., Hammami, F., Rahimi-Gorji, M., & Biswas, R., "CPU heat sink cooling by triangular shape micro-pin-fin: Numerical study"., *International Communications in Heat and Mass Transfer*, 112, 104455 (2020).

23. Umrao Sarwe, D., and Kulkarni, V. S., "Differential transformation method to determine heat transfer in annular fins"., *Heat Transfer*, 50(8), 7949-7971 (2021). .

24. Jang, D., Yu, S.-H., and Lee, K.-S., "Multidisciplinary optimization of a pin-fin radial heat sink for LED lighting applications". *International Journal of Heat and Mass Transfer*, 55(4), 515-521 (2012). .

25. Yu, S.-H., Lee, K.-S., and Yook, S.-J., "Optimum design of a radial heat sink under natural convection". *International Journal of Heat and Mass Transfer*, 54(11-12), 2499-2505 (2011).

26. Park, S.-J., Jang, D., Yook, S.-J., and Lee, K.-S., "Optimization of a staggered pin-fin for a radial heat sink under free convection"., *International Journal of Heat and Mass Transfer*, 87, 184-188 (2015).

27. Narendran, N., and Gu, Y., "Life of LED-based white light sources"., *IEEE/OSA Journal of Display Technology*, 1, 167–170 (2005).

28. Sadeghianjahromi, A., and Wang, C. C., “Heat transfer enhancement in fin-and-tube heat exchangers–A review on different mechanisms”. *Renewable and Sustainable Energy Reviews,* 137, 110470 (2021).

29. Varma, E., and Gautam, A. “A review of thermal analysis and heat transfer through fins”., *In AIP Conference Proceedings* (Vol. 2413, No. 1). AIP Publishing (2022). .

30. Johnston, E., Szabo, P. S., and Bennett, N. S., “Cooling silicon photovoltaic cells using finned heat sinks and the effect of inclination angle’., *Thermal Science and Engineering Progress,* 23, 100902 (2021).

31. Kazem, H. A., Al-Waeli, A. A., Chaichan, M. T., Sopian, K., and Al-Amiery, A. A., “Enhancement of photovoltaic module performance using passive cooling (Fins): A comprehensive review”., *Case Studies in Thermal Engineering,* 103316 (2023).

32. Lienhard, I., and John, H., “A heat transfer textbook (3rd ed.)”., *Cambridge, MA,* USA: Phlogiston Press (2005).

33. M. Arqam., L.S. Raffa., L. Clemon., M.S. Islam., M. Ryall., and N.S. Bennett., “Numerical and experimental investigation of a phase change material radial fin heat sink for electronics cooling”., *J. Energy Storage*. 98 (Part A) 113113 (2024).

34. Hussein, Y. H., Tahseen, T. A., Akroot, A., Mithu, M. A. H., and Abdulateef, A. M., “A multi-criteria optimization for a radial heat sink with semicircular fins based on the design of experiments approach”., *Case Studies in Thermal Engineering.*, 105727 (2024).

35. Bdaiwi M, Akroot A, Abdul Wahhab HA, Assaf YH, Nawaf MY, Talal W., “Enhancement heat exchanger performance by insert dimple surface ball inside tubes: A review”. *Results in Eng*., 19:101323 (2023).

36. J.B. Khaleel, M. Danışmaz, T.A. Tahseen, M.I.A. Tahseen, T.K. Salem., “Design of an axisymmetric triangular heatsink with radial arrangement: an experimental investigation of natural convection heat transfer”., *Tikrit J. Eng. Sci*. 31(4), 92-101 (2024).

37. De Almeida, B. Santos, B. Paolo, and M. Quicheron , “Solid state lighting review – Potential and challenges in Europe, Renew”., *Sustain. Energy Rev*. 34, 30-48 (2014).

38. Elenbaas, W., “Heat dissipation of parallel plates by free convection”. *Physical,* 9(1), 1-28 (1942).

39. Schuepp, P., “Model experiments on free-convection heat and mass transfer of leaves and plant elements”., *Boundary-Layer Meteorology*, 3(4), 454-467 (1973).

40. J.N Ojuro, G.M Sobamowo, and A.M. de Oliveira Siqueira., “Heat transfer management of thermal and electronics systems using convective-radiative porous fins with thermal contact resistance and diabatic tip”., *J. Eng. Exact Sci*. 10 (5), 18523-18523 (2024).

41. M.H. Mousa, C-M. Yang, K. Nawaz, and N. Miljkovic., “Review of heat transfer enhancement techniques in two-phase flows for highly efficient and sustainable cooling, Renew”., *Sustain. Energy Rev*. 155, 111896 (2022).

42. S. H. Yu, K. S. Lee, and S. J. Yook. Optimum design of a radial heat sink under natural convection, Int. J. *Heat Mass Tran*. 54 (11–12) 2499–2505 (2011).

43. Assaf YH, Akroot A, Abdul Wahhab HA, Talal W, Bdaiwi M, and Nawaf MY., “Impact of nano additives in heat exchangers with twisted tapes and rings to increase efficiency: A review”., *Sustainability*.,15(10):7867 (2023).

44. O. Karimi, and N. M. Nouri., “Optimization of wavy geometries for enhanced condensation heat transfer on vertical plates: an experimental study, Case Stud”., *Therm. Eng*. 36, 105276 (2024).

45. J. Xiang, Z. Liu, C. Zhang, C. Zhou, and C. Chen., “Finite element simulation of the machining process of boiling structures in a novel radial heat sink for high-power LEDs”, *Materials,* 13, (18) (2020).

46. K.T. Chiang, C.C. Chou, and N.M. Liu., “Application of response surface methodology in describing the thermal performances of a pin-fin heat sink”, *Int. J. Therm*. Sci. 48(6) 1196–1205 (2009).

47. T.A. Tahseen, M. Ishak, and M.M. Rahman. “An overview on thermal and fluid flow characteristics in a plain plate finned and un-finned tube banks heat exchanger, Renew”., *Sustain. Energy Rev*. 43, 363-380 (2015).

48. S. Wiriyasart, and P. Naphon., “Heat spreading of liquid jet impingement cooling of cold plate heat sink with different fin shapes”*., Case Stud. Therm. Eng*. 20, 100638 (2020).

49. Z. Tang, Q. Liu, H. Li, and X. Min., “Numerical simulation of heat transfer characteristics of jet impingement with a novel single cone heat sink”., *Appl. Therm. Eng*. 127, 906–914 (2017).

50. Elshafei, E. A. M. “Thermal Issues in Emerging Technologies”. *Paper presented at the ThETA 3,* Cairo, Egypt (2010).

51. Yu, S.-H., Lee, K.-S., and Yook, S.-J., “Optimum design of a radial heat sink under natural convection”. *International Journal of Heat and Mass Transfer*., 54(11-12), 2499-2505 (2011).

52. B. Freegah, A.A. Hussain, A.H. Falih, and H. Towsyfyan., “CFD analysis of heat transfer enhancement in plate-fin heat sinks with fillet profile: Investigation of new designs”., *Therm. Sci. Eng*. Prog. 17 (2020).

53. H.A. Mohamed, and T.A. Tahseen., “Free convection heat transfer from radial heat sink with wing fins shape: An experimental investigation”., *Edelweiss App. Sci. Tech*. 8 (6), 9425-9437 (2024)

54. D. Kim, and D.K. Kim., “Experimental study of natural convection from vertical cylinders with branched pin fins”., *Int. J. Heat Mass Tran*. 177, 121545 (2021) .

55. I.T. Nazzal, T.K. Salem, S. Farhan, and T.A. Tahseen., “Investigation into the heat sink performance of the inline and cut cross fins types using different aluminum alloys”., *J. Therm. Eng*. 10 (1) ,10-20 (2021).

56. T.A. Tahseen, M. Ishak, and M.M. Rahman., “Performance predictions of laminar heat transfer and pressure drop in an in-line flat tube bundle using an adaptive neuro-fuzzy inference system (ANFIS) model”., *Int. Commun. Heat Mass Tran*. 50, 85-97 (2014).

57. Zahid, M. Farooq, M. Farhan, M. Usman, A. Qamar, M. Imran, M.A. Alqahtani, S. Anwar, M. Sultan, and M.Y. Javaid., “Thermal performance analysis of various heat sinks based on alumina NePCM for passive cooling of electronic components: an experimental study”., *Energies*, 15 (22), 8416 (2022)

58. C. Ma, J. Hu, M. Li, X. Deng, J. Yang, J. He, C. Hua, L. Wang, J. Liu, K. Liu, Y. Zhou, M. Li, J. Zhou, X. Deng, and S. Weng., “Multi-objective topology optimization for cooling element of precision gear grinding machine tool”., *Int. Commun. Heat Mass Tran*. 160,108356 (2025).

59. Qamar, A. Kanwal, M. Amjad, M. Farooq, A. Munir, S. Ahmad, and M. Abdollahian., “Advancing sustainable cooling: Performance analysis of a solar-driven thermoelectric refrigeration system for eco-friendly solutions”., *Case Stud. Therm. Eng*. 60, 104781 (2024).

60. Li, B., Baik, Y. J., and Byon, C., “Enhanced natural convection heat transfer of a chimney-based radial heat sink”. *Energy conversion and management*., 108, 422-428 (2016).

61. Y. Jain, V. Kurkute, S.M. Deshmukh, K.A. Pathan, A.R. Attar, and S.A. Khan., “The influence of plate fin heat sink orientation under natural convection on thermal performance: an experimental and numerical study”., *J. Adv. Res. Fluid Mech. Therm. Sci*. 114 (2), 118-129 (2024).

62. M. Baldry, V. Timchenko, and C. Menictas., “The Effect of orientation on the performance of small free-convection heat sinks for use with a thermoelectric cryotherapy device”, *J. Therm. Sci. Eng. Appl*. 13 (4), 041001 (2021).

63. A.M. Elsaid, G.B. Abdelaziz, S.W. Sharshir, and E.M.S. El-Said., “Orientation effects on mixed convective performance of twisted pin fin heat sink: Experimental investigation”., *Appl. Therm. Eng*. 250, 123490 (2024).

64. R. Almuzaiqer, M.E. Ali, and K. Al-Salem., “Tilt angle’s effects on free convection heat transfer coefficient inside a water-filled rectangular parallelepiped enclosure”., *Processes*, 10(2), (2022).

65. H. Daghab, M. Kaddiri, M. Lamsaadi, S. Raghay, I. Arroub, and I. Erritali., “Free convection of thermodependent non-Newtonian fluids in a square enclosure partially heated at one side”., *Num. Heat Tran., Part A: Appl*.1-24, 2284337 (2023).

66. Lee, G., and Kim, S. J., “Thermal optimization of radial plate-fin heat sinks under an L-shaped flow”., *Applied Thermal Engineering*., 133, 580-587 (2018).

67. Li, J., and Yang, L., “Recent Development of Heat Sink and Related Design Methods”., *Energies*., 16(20), 7133 (2023).

68. Khan, W. A., Culham, J. R., and Yovanovich, M. M., “The role of fin geometry in heat sink performance”. *Journal of Electronic Packaging, ASME*, 128, 324-330 (2006).

69. R. Mauri., “Transport phenomena in multiphase flows”., *Springer*, New York, USA, 2015.

70. Sundar, S., Song, G., Zahir, M. Z., Jayakumar, J., and Yook, S.-J., “Performance investigation of radial heat sink with circular base and perforated staggered fins”. *International Journal of Heat and Mass Transfer*, 143, 118526 (2019).

71. Kwak, D.-B., Noh, J.-H., Lee, K.-S., & Yook, S.-J., “Cooling performance of a radial heat sink with triangular fins on a circular base at various installation angles”., *International Journal of Thermal Sciences*., 120, 377-385 (2017).

72. Kwak, D.-B., Kwak, H.-P., Noh, J.-H., and Yook, S.-J., “Optimization of the radial heat sink with a concentric cylinder and triangular fins installed on a circular base”. *Journal of Mechanical Science and Technology*., 32(1), 505-512 (2018).

73. Li, B., and Byon, C., “Experimental and numerical study on the heat sink with radial fins and a concentric ring subject to natural convection”. *Applied Thermal Engineering*, 90, 345-351 (2015).

74. El Ghandouri, I., El Maakoul, A., Saadeddine, S., and Meziane, M., “Design and numerical investigations of natural convection heat transfer of a new rippling fin shape”. *Applied Thermal Engineering*., 178, 115670 (2020).

75. Pua, S., Ong, K, Lai, K., and Naghavi, M., “Natural and forced convection heat transfer coefficients of various finned heat sinks for miniature electronic systems”.

Proceedings of the Institution of Mechanical Engineers, Part A: *Journal of Power and Energy*., 233(2), 249-261 (2019).

76. Yildiz, Ş, and Yüncü, H., "An experimental investigation on performance of annular fins on a horizontal cylinder in free convection heat transfer"., *Heat and Mass Transfer*., 40, 239-251 (2004).

77. Walunj, A., Daund, V., and Palande, D., "Review of Performance of Rectangular Fins under Natural Convection at Different Orientation of Heat Sink"., *International Journal of Innovation and Applied Studies*., 6(2), 232-240 (2014).

78. E. Sparrow and P. Bahrami, "Experiments on natural convection heat transfer on the fins of a finned horizontal tube", *Int. J. Heat Mass Transf.*, vo 23, no. 11, pp. 1555-1560, Nov. 2008.

79. S.W. Churchill and H. H. Chu., "Correlating equations for laminar and turbulent free convection from a horizontal cylinder", *Int. J. Heat Mass Transf.*, vo 18, no. 9, pp. 1049-1053, Sept. 1975.

80. V.T. Morgan, "The overall convective heat transfer from smooth circular cylinders"., *Adv. Heat Transf*., vo. 11, 199-264. 1975.

81. Muneeshwaran, M., Tsai, M. K., and Wang, C. C., "Heat transfer augmentation of natural convection heat sink through notched fin design"., I*nternational Communications in Heat and Mass Transfer*, 142, 106676 (2023).

82. Rao, A.K., and Somkuwar, V., "Heat transfer of a tapered fin heat sink under natural convection. Materials Today"., *Proceedings*, 46, 7886–7891(2021).

83. Dhumne, A. B., and Farkade, H. S., "Heat transfer analysis of cylindrical perforated fins in staggered arrangement"., *International Journal of Innovative Technology and Exploring Engineering*, 2(5), 225-230 (2013).

84. M. S. Hassan, T. A. Tahseen and M. M. Weis, "Natural convection from a radial heat sink with triangular fins," *NTU J. Eng. Tech*., vo. 1, no. 2, pp. 40-49, Feb. 2022.

85. Dhanadhya, R. V., Nilawar, A. S., and Yenarkar, Y. L., "Theoretical study and finite element analysis of convective heat transfer augmentation from horizontal rectangular fin with circular perforation"., *International Journal of Mechanical and Production Engineering Research and Development*, 3(2), 187-192 (2013).

86. Huang, C.-H., and Chen, L., "An optimized natural convection Y-shape-shifted heat sink design problem". *Case Studies in Thermal Engineering*, 28, 101520 (2021).

87. Baobaid, N.; Ali, M.I.; Khan, K.A., and Al-Rub, R.K.A. "Fluid flow and heat transfer of porous TPMS architected heat sinks in free convection environment"., *Case Studies in Thermal Engineering*, 33, 101944 (2022).

88. Feng, S., Shi, M., Yan, H., Sun, S., Li, F., and Lu, T. J., “Natural convection in a cross-fin heat sink”., *Applied Thermal Engineering*, 132, 30-37 (2018).

89. Noda, H., Ikeda, M., Kimura, Y., and Kawabata, K. ., “Development of High-Performance Heatsink “Crimped fin”., *Furukawa Review*, 27, 14-19 (2005).

90. Iyengar, M., and Bar-Cohen, A., “Least-material optimization of vertical pin-fin, plate-fin, and triangular-fin heat sinks in natural convective heat transfer”. *ITherm'98. 6th Intersociety Conference on Thermal and Thermomechanical Phenomena in Electronic Systems*: p. 295-302 (1998).

91. Aziz, A., Torabi, M., and Zhang, K., “Convective–radiative radial fins with convective base heating and convective–radiative tip cooling: homogeneous and functionally graded materials”., *Energy Conversion and Management*, 74, 366-376 (2013).

92. Incropera, F. P., Dewitt, D. P., Bergman, T. L., and Lavine, A. S., *Fundamentals of heat and mass transfer*. (6th ed.) USA: John Wiley & Sons, Inc.(2011).

93. Hoffmann, K. A., and Chiang, S. T., Computational fluid dynamics. (3rd ed.), vol. *I, Engineering Education System*, Wichita, KS.(1998).

94. ANSYS, Inc., ANSYS 2021 R2: *User’s Guide*, Canonsburg, PA, 2021.

95. Figliola, R. S. and Beasley, D. E., *Theory and design for mechanical measurements*., (Fifth ed.), New York, USA: John Wiley & Son. (2011).

96. Li, B., and Byon, C., “Investigation of natural convection heat transfer around a radial heat sink with a concentric ring”., *International Journal of Heat and Mass Transfer*, 89, 159-164 (2015).

97. Rogers, G. F. C. and Mayhew, Y. R., *Thermodynamic and transport properties of fluids*, 5th ed., UK: Blackwell Publishing.(2004).

98. Lee, M., Kim, H. J., and Kim, D.-K. “Nusselt number correlation for natural convection from vertical cylinders with triangular fins”., *Applied Thermal Engineering*, 93, 1238-1247 (2016).

99. Holman, J. P. *Experimental methods for engineers*. (8th ed.), New York: *McGraw-Hill*. (2012).

100. Singh, G., and Goyal, S., “Dry sliding wear behaviour of AA6082-T6/SiC/B4C hybrid metal matrix composites using response surface methodology”., The Institution of Mechanical Engineers, Part L: *Journal of Materials: Design and Applications*. 232(11):952-964 (2018).

101. Azizi, Z., Barzegarian, R., and Behvandi, M., “Design-expert aided thermohydraulic assessment of a nanofluid-cooled cylindrical microchannel heat

sink: Possible application for thermal management of electric vehicle batteries. *Sustainable Energy Technologies and Assessments*, 50, 101876 (2022).
102. Myers, R. H., Montgomery, D. C., and Anderson-Cook, C. M., *Response surface methodology: process and product optimization using designed experiments*. USA: John Wiley & Sons (2016).

103. Harahap, F., and McManus, H. N., "Natural convection heat transfer from horizontal rectangular fin arrays"., *Journal of Heat Transfer*, 89(1), 32-38 (1967).

104. Raithby, G. D., and K. G. T. Hollands., "Natural convection"., *Handbook of heat transfer,* 3 (1998).
105. Tahseen, T. A. (2014). Optimal geometric arrangement of unfinned and finned flat tube heat exchangers under laminar forced convection. (Ph. D. Thesis), *Universiti Malaysia Pahang, UMP*, Pahang, Malaysia.

APPENDIX (A)

A SAMPLE OF CALCULATION

Case: SC-0-12fins

The voltage (Φ) of 98.3 volt

The current (I) of 0. 54 A

The input electric power is:

$$Q_{\text{in}} = \Phi \times I \qquad (A\text{-}1)$$

$$Q_{\text{in}} = 98.3 \times 0.54 = 53 \text{ W}$$

Average temperature of cylinder surface is:

$$\bar{T}_b = \frac{1}{3}\sum_{i=1}^{3} T_{b,\text{i}} \qquad (\text{A-}2)$$

$$\bar{T}_b = \frac{1}{3}(52.2 + 51.65 + 51.75) = 51.9\ ℃$$

The cylinder base area is:

$$A_b = \left(\frac{\pi}{4}D^2\right) + \pi DL - NLt - 5\left(\frac{\pi}{4}d_{\text{heater}}^2\right) \qquad (\text{A-}3)$$

$$A_b = \left[\frac{\pi}{4}\left(\frac{70}{1000}\right)^2\right] + \pi\frac{70}{1000}\times\frac{210}{1000} - 12\frac{210}{1000}\times\frac{3}{1000} - 5\left[\frac{\pi}{4}\left(\frac{8}{1000}\right)^2\right]$$

$$= 0.045334286 \text{ m}^2$$

The heat flux is:

$$\dot{Q}_{\text{net}} = \frac{Q_{\text{in}}}{A_b} \qquad \text{(A - 4)}$$

$$\dot{Q}_{\text{net}} = \frac{53}{0.041484} = 1277.6 \ \frac{\text{W}}{\text{m}^2}$$

The fin area can be estimated as:

$$A_{\text{fin}} = \frac{\pi}{4} L^2 + \frac{1}{2} \pi L t \qquad \text{(A - 5)}$$

$$A_{\text{fin}} = \frac{\pi}{4} \times \left(\frac{210}{1000}\right)^2 + \frac{\pi}{2} \times \frac{210}{1000} \times \frac{3}{1000}$$

$$= 0.03564 \ \text{m}^2$$

the net heat transfer area is:

$$A_{\text{net}} = A_b + N A_{\text{fin}} \qquad \text{(A - 6)}$$

$$A_{\text{net}} = 0.045334286 \ + 12 \times 0.03564 \ = 0.473014286 \ \text{m}^2$$

The following equation yields the average free heat transfer coefficient:

$$h = \frac{\text{Q}_{\text{net}}}{A_{\text{net}}(\bar{T}_b - T_\infty)} \qquad \text{(A - 7)}$$

$$h = \frac{53}{0.473014286 \times (51.9 - 15.8)} = \ 3.11 \ \frac{\text{W}}{\text{m}^2\text{K}}$$

The appropriate air properties are calculated using the engineering equation solver (EES) program.

The air thermal conductivity is:

$$k_{\text{air}} = 0.026713 \ \frac{\text{W}}{\text{m K}}$$

The air kinematic viscosity is:

$$\nu_{\text{air}} = 1.56 \times 10^{-5} \frac{\text{m}^2}{\text{s}}$$

The air thermal diffusivity:

$$\alpha_{\text{air}} = 2.21 \times 10^{-5} \frac{\text{m}^2}{\text{s}}$$

The Nusselt number (Nu) is:

$$Nu = \frac{hL}{k_{\text{air}}} \qquad \text{(A - 8)}$$

$$Nu = \frac{3.11}{0.026713} \times \frac{210}{1000} = 24.4$$

Rayleigh number is found by:

$$Ra = \frac{g\beta_{\text{air}}(\bar{T}_b - T_\infty)L^3}{\nu_{\text{air}}\alpha_{\text{air}}} \qquad \text{(A - 9)}$$

The coefficient of thermal expansion:

$$\beta_{\text{air}} = \frac{1}{\frac{[(\bar{T}_b + 273) + (T_\infty + 273)]}{2}} \qquad \text{(A - 10)}$$

$$\beta_{\text{air}} = \frac{2}{[(51.9 + 273) + (15.8 + 273)]} = 0.001629$$

Rayleigh number equation will be:

$$Ra = \frac{9.81 \times 0.001629 \times (51.9 - 15.8) \times \left(\frac{210}{1000}\right)^3}{1.56 \times 10^{-5} \times 2.21 \times 10^{-5}} = 15.5199 \times 10^6$$

Thermal resistance is estimated by:

$$R_{th} = \frac{(\bar{T}_b - T_\infty)}{Q_{net}} \qquad \text{(A - 11)}$$

$$R_{th} = \frac{51.9 - 15.8}{53} = 0.679891489$$

APPENDIX (B)

EXPERIMENTAL ERROR ANALYSIS

The experimental error analysis was conducted based on what was presented by the researcher [100]. The sources of errors are broadly divided into three groups of errors, including calibration, data collection and data analysis, and each group has many sources and elements of errors. The manufacturers of measuring equipment or instruments include different information about the specifications such as: linearity, accuracy, deviations.

The independent parameters (such as temperature, dimensions, etc.) were found to be bias error (B) and precision limit (P) using the root-sum-squares (RSS) method:

The bias error is calculated from the following equation [90]:

$$B = \pm\left[\left(\frac{1}{2}\text{Resolution}\right)^2 + (\text{Accuracy})^2\right]^{1/2} \quad \text{(B-1)}$$

The average measured value is calculated as follows:

$$\bar{\chi} = \frac{1}{n}\sum_{i=1}^{n}\chi_i \quad \text{(B-2)}$$

The standard deviation (σ) of the sampling distribution is calculated as follows:

$$\sigma_\chi = \left[\frac{1}{n-1}\sum_{i=1}^{n}(\chi_i - \bar{\chi})^2\right]^{1/2} \quad \text{(B-3)}$$

Thus, the average standard deviation $\sigma_{\bar{\chi}}$ of the values can be derived using the following relationship:

$$\sigma_{\bar{\chi}} = \frac{\sigma_\chi}{\sqrt{N}} \quad \text{(B-4)}$$

Using the (student–t) distribution at the 95% confidence limit with degrees of freedom (N-1) and the total accuracy limits are as follows:

By integrating between the initial error limits at 95% and being an absolute value, the following relationship is used [96]:

$$P_{\chi} = t_{(N-1),95\%} \times \sigma_{\bar{\chi}} \quad \text{(B - 5)}$$

$$U_{\chi} = \pm \left[B^2 + P_{\chi}{}^2\right]^{1/2} \quad \text{(B - 6)}$$

Accordingly, the experimental error rate (percentage) is calculated from the following relationship:

$$\frac{U_{\chi}}{\chi}\% = \pm \left(\frac{U_{\chi}}{\chi}\right) \times 100 \quad \text{(B - 7)}$$

In equations (C.1) – (C.7) (χ) is any independent coefficient.

Estimation of experimental error in thermocouple (temperature)

Calibration itself does not eliminate system errors, but it may help in estimating experimental error in a particular part of the equipment used. Calibration errors contain the initial errors that enter into the measurement system. Calibration errors consist of three sources, which are: the calibration process, the system or device used in calibration, and the third is the reference or standard value used in calibration. In addition, the calibration curve has a significant effect on the error ratio [90].

The error ratio in thermocouple is defined as follows:

$$U_{\text{Temp}} = \pm \left[(U_{\text{Std}})^2 + (U_{\text{Fitting-curve}})^2\right]^{1/2} \quad \text{(B - 8)}$$

Where:

U_{Temp}= represents the experimental error of the thermocouple

U_{Std} = the error in the standard device used in the calibration

$U_{\text{Fitting-curve}}$= the error in the calibration curve

Temperature data logger Pico TC-08 error

Accuracy = (0.2% + 0.1) ℃

Resolution = 0.1 ℃

Thus, the error percentage of the deviation is

$$B_{\text{Temp}(T_b)} = \pm \left[\left(\frac{1}{2} \times 0.1\right)^2 + \left(114.727 \times \frac{0.2}{100} + 0.1\right)^2\right]^{1/2} = \pm 0.333\ ℃$$

$$B_{\text{Temp(Ta)}} = \pm \left[\left(\frac{1}{2} \times 0.1\right)^2 + \left(17.13 \times \frac{0.2}{100} + 0.1\right)^2\right]^{1/2} = \pm 0.143\ ℃$$

A number of thermocouples are installed according to the locations mentioned in Chapter 3 and can be viewed in Figure 3.9. Accordingly, the average temperature and standard deviation of a number of thermocouple readings are determined according to equations (C.2) to (C.5). The limits of overall accuracy in measuring temperature (P_T) are as follows:

$$\left.\begin{aligned} P_{T_b} &= \sigma_{T_b} \times t_{(N-1),95\%} = 0.243 \times 2.776 = 0.675\ ℃ \\ P_{\text{Ta}} &= \sigma_{\text{Ta}} \times t_{(N-1),95\%} = 0.100 \times 4.271 = 0.427\ ℃ \end{aligned}\right\}$$

$$\left.\begin{aligned} U_{\text{Std}} &= \pm \left[\left(B_{\text{Temp}}\right)^2 + \left(P_{\text{Temp}}\right)^2\right]^{1/2} \\ U_{T_b} &= \pm \left[(0.333)^2 + (0.675)^2\right]^{1/2} = \pm 0.752\ ℃ \\ U_{\text{Ta}} &= \pm \left[(0.143)^2 + (0.427)^2\right]^{1/2} = \pm 0.450\ ℃ \end{aligned}\right\} \quad \text{(B - 9)}$$

The thermocouple calibration process was carried out as in item (3.5) and thus the experimental error generated from this process is somewhat the same as the experimental error associated with the fitting curve between the thermocouple reading and the mercury thermometer (standard points). Therefore, the experimental error can be determined from the fitting curve using the average standard deviation according to the following equation [104]:

$$U_{\text{Fitting-curve}} = \sigma_{\bar{\chi}} \times t_{(N-1),95\%} \quad \text{(B - 10)}$$

Since B_(Fitting-curve) = 0

Then the relative experimental error (in percentage) can be obtained as follows:

$$\left.\begin{aligned} \left(\frac{U_{T_b}}{T_b}\right) &= \pm \frac{0.752}{114.727} \times 100 = \pm\ 0.657\ \% \\ \left(\frac{U_{\text{Ta}}}{T_a}\right) &= \pm \frac{0.450}{17.13} \times 100 = \pm\ 2.626\ \% \end{aligned}\right\}$$

Experimental error of physical properties of air

The rationale for estimating the experimental error of these properties can be written as follows:

$$U_{\psi} = \pm\frac{1}{2}\left|\psi_{\mathrm{T,max}} - \psi_{\mathrm{T,min}}\right| \quad \text{(B - 11)}$$

Where (ψ) represents any property of air

Air density (ρ_a):

$$U_{\rho_a} = \pm\frac{1}{2}\left|\rho_{\overline{T_{\max}}} - \rho_{\overline{T_{\min}}}\right| = \pm\frac{1}{2}|1.0518 - 1.1614| = \pm 0.0548 \ \text{kg/m}^3 \quad \text{(B - 12)}$$

$$\left(\frac{U_{\rho_a}}{\rho_a}\right) = \pm\frac{0.0548}{1.1614} \times 100 = \pm 4.178\%$$

Specific heat (c_{Pa}):

$$U_{c_{p_a}} = \pm\frac{1}{2}\left|c_{p\,\overline{T_{\max}}} - c_{p\,\overline{T_{\min}}}\right| = \pm\frac{1}{2}|1009.84 - 1006.53| = \pm 1.6542 \ \text{J/(kg°C)} \quad \text{(B - 13)}$$

$$\left(\frac{U_{c_{p_a}}}{c_{p_a}}\right) = \pm\frac{1.6542}{1009.84} \times 100 = \pm 0.1638\,\% \quad \text{(B - 14)}$$

Thermal conductivity (k_a):

$$U_{k_a} = \pm\frac{1}{2}\left|k_{\overline{T_{\max}}} - k_{\overline{T_{\min}}}\right| = \pm\frac{1}{2}|0.0245 - 0.0272| = \pm 0.0014 \ \text{W/(m℃)} \quad \text{(B - 15)}$$

$$\left(\frac{U_{k_a}}{k_a}\right) = \pm\frac{0.0014}{0.0272} \times 100 = \pm 5.1470\,\% \quad \text{(B - 16)}$$

Viscosity (μ_a):

$$U_{\mu_a} = \pm\frac{1}{2}\left|\mu_{\overline{T_{\max}}} - \mu_{\overline{T_{\min}}}\right| = \pm\frac{1}{2}|2.1105 - 1.9039| \times 10^{-5} = \pm 1.033 \times 10^{-6} \ \text{kg/(m s)} \quad \text{(B - 17)}$$

$$\left(\frac{U_{\mu_a}}{\mu_a}\right) = \pm\frac{1.033 \times 10^{-6}}{2.1105 \times 10^{-5}} \times 100 = \pm 4.894\,\% \quad \text{(B - 18)}$$

Experimental error of input power (Q_{in})

$$Q_{\mathrm{in}} = \Phi \times I \quad \text{(B - 19)}$$

Potential difference

Accuracy = (± (1.2%+ 5))

Resolution = (0.01 V)

Electric current

Accuracy = ± (3%+15)

Measurement period (Resolution) = 0.1 A

Thus, the deviations are as follows:

$$\left.\begin{aligned} B_{\Phi} &= \pm \left[\left(\frac{1}{2} \times 0.01\right)^2 + \left(208 \times \frac{1.2}{100} + 1 \times 10^{-5}\right)^2\right]^{1/2} = \pm\, 2.496 \text{ V} \\ B_I &= \pm \left[\left(\frac{1}{2} \times 0.1\right)^2 + \left(1.55 \times \frac{3}{100} + 1 \times 10^{-15}\right)^2\right]^{1/2} = \pm\, 0.0682 \text{ A} \end{aligned}\right\}$$

The standard deviation rate of the voltage and current difference after taking (7) seven special readings and using equations (C.2) to (C.5) we get:

$$\left.\begin{aligned} P_{\Phi} &= \sigma_{\bar{E}} \times t_{(N-1),95\%} = 2.496 \times 2.447 = 6.1077 \text{ V} \\ P_I &= \sigma_{\bar{I}} \times t_{(N-1),95\%} = 0.0682 \times 2.447 = 0.1668 \text{ A} \end{aligned}\right\} \quad \text{(B - 20)}$$

The absolute value of the experimental error is

$$\left.\begin{aligned} U_{\Phi} &= \pm\, [(B_E)^2 + (P_E)^2]^{1/2} = \pm\, [(2.496)^2 + (6.1077)^2]^{1/2} = \pm\, 6.597 \text{ V} \\ U_I &= \pm\, [(B_I)^2 + (P_I)^2]^{1/2} = \pm\, [(0.0682)^2 + (0.1668)^2]^{1/2} = \pm\, 0.1802 \text{ A} \end{aligned}\right\} \quad \text{(B - 21)}$$

The relative value of the experimental error is

$$\left.\begin{aligned} \left(\frac{U_{\Phi}}{\Phi}\right) &= \pm\, \frac{6.597}{208} \times 100 = \pm\, 3.171\,\% \\ \left(\frac{U_E}{I}\right) &= \pm\, \frac{0.1802}{1.55} \times 100 = \pm\, 11.625\,\% \end{aligned}\right\} \quad \text{(B - 22)}$$

$$\left(\frac{U_{Q_{in}}}{Q_{in}}\right) = \pm \left[\left(\frac{U_{\Phi}}{\Phi}\right)^2 + \left(\frac{U_I}{I}\right)^2\right]^{1/2} \times 100$$

$$= \pm \left[\left(\frac{6.597}{208}\right)^2 + \left(\frac{0.1802}{1.55}\right)^2\right]^{1/2} \times 100 \quad \text{(B - 23)}$$

= ±0.1205%

RESUME

Yousef Hashim HUSSEIN, obtained a bachelor's degree in mechanical engineering from the College of Engineering, Tikrit University, Tikrit, Iraq in 2017. He obtained a master's degree in mechanical engineering from the College of Engineering, Tikrit University, Tikrit, Iraq in 2020. I am seeking to obtain a doctorate degree in the Department of Mechanical Engineering at Karabuk University, Turkey. He participated in many academic conferences in many countries such as Egypt, the Emirates, Jordan, the Sultanate of Oman, and also in Iraq. I have more than four years of research in the field of mechanical engineering and more than three in the first quarter in Scopus and Clarivate. He is a referee for many prestigious scientific journals. He supervised graduation projects and scientific research. He participated in developing curricula and practical training for students. Al-Rifai's research interests revolve around the fields of heat transfer in thermal systems, LED lighting systems, and computers by finding the best way to transfer heat.